

ABSTRACT

Title of dissertation: ORGANIC ELECTRONICS WITH POLYMER
 DIELECTRICS ON PLASTIC SUBSTRATES
 FABRICATED VIA TRANSFER PRINTING

Daniel R. Hines, Doctor of Philosophy, 2007

Dissertation directed by: Professor Ellen Williams
 Department of Physics

Printing methods are fast becoming important processing techniques for the fabrication of flexible electronics. Some goals for flexible electronics are to produce cheap, lightweight, disposable radio frequency identification (RFID) tags, very large flexible displays that can be produced in a roll-to-roll process and wearable electronics for both the clothing and medical industries. Such applications will require fabrication processes for the assembly of dissimilar materials onto a common substrate in ways that are compatible with organic and polymeric materials as well as traditional solid-state electronic materials. A transfer printing method has been developed with these goals and application in mind. This printing method relies primarily on differential adhesion where no chemical processing is performed on the device substrate. It is compatible with a wide variety of materials with each component printed in exactly the same way, thus avoiding any mixed processing

steps on the device substrate. The adhesion requirements of one material printed onto a second are studied by measuring the surface energy of both materials and by surface treatments such as plasma exposure or the application of self-assembled monolayers (SAM). Transfer printing has been developed within the context of fabricating organic electronics onto plastic substrates because these materials introduce unique opportunities associated with processing conditions not typically required for traditional semiconducting materials. Compared to silicon, organic semiconductors are soft materials that require low temperature processing and are extremely sensitive to chemical processing and environmental contamination. The transfer printing process has been developed for the important and commonly used organic semiconducting materials, pentacene (Pn) and poly(3-hexylthiophene) (P3HT). A three-step printing process has been developed by which these materials are printed onto an electrode subassembly consisting of previously printed electrodes separated by a polymer dielectric layer all on a plastic substrate. These bottom contact, flexible organic thin-film transistors (OTFT) have been compared to unprinted (reference) devices consisting of top contact electrodes and a silicon dioxide dielectric layer on a silicon substrate. Printed Pn and P3HT TFTs have been shown to out-perform the reference devices. This enhancement has been attributed to an annealing under pressure of the organic semiconducting material.

ORGANIC ELECTRONICS
WITH POLYMER DIELECTRICS ON PLASTIC SUBSTRATES
FABRICATED VIA TRANSFER PRINTING

by

Daniel R. Hines

Dissertation submitted to the Faculty of the Graduate school of the
University of Maryland, College Park in partial fulfillment
of the requirements for the degree of
Doctor of Philosophy
2007

Advisory Committee:
Professor Ellen D. Williams, Chair/Advisor
Professor Robert M. Briber
Professor John T. Fourkas
Professor Michael S. Fuhrer
Professor Gottlieb S. Oehrlein

TABLE OF CONTENTS

List of Tables	iv
List of Figures	v
1 Introduction	1
1.1 Motivation	1
1.2 Description of Transfer Printing	2
1.3 Adhesion Issues and Devices Fabrication	6
1.4 Conclusion	13
2 Organic Semiconductor Materials and Devices	14
2.1 Introduction	14
2.2 Classes of Nontraditional Semiconductors	15
2.3 Electronic Properties of Organic Semiconductors	23
2.4 Determination of Mobility	27
2.5 Determination of Threshold Voltage, On/Off Ratio and Subthreshold Slope	29
2.6 Determination of Contact Resistance	29
2.7 Growth Properties of Organic Films	30
2.8 Toward Flexible Circuits	32
3 Printing	35
3.1 Introduction	35
3.2 Traditional Printing	38
3.3 Electrophotographic Printing	41
3.4 Inkjet Printing	41
3.5 Soft Lithography	43
3.6 Nanoimprint Lithography	45
4 Transfer Printing Methods	50
4.1 Introduction	50
4.2 Transfer Printing Procedure	52
4.3 Gold Printing onto Plastic	54
4.4 Pentacene Printing onto Plastic	56
4.5 Inorganic Features Printed onto Plastic	57
4.6 Carbon Nanotubes Printed onto Plastic	59
4.7 Metallic Nanowires Printed onto Plastic	62
4.8 Single Atomic Layers Printed onto Plastic	62
5 Flexible OTFT Devices Transfer Printed onto Plastic Substrates	65
5.1 Introduction	65
5.2 Fabrication of Au Electrodes onto Si Transfer Substrates	66
5.3 Dielectric Polymers Spin Coated onto Si Transfer Substrates	67
5.4 Organic Film Deposition onto SiO ₂ /Si Transfer Substrates	68

5.5	Issues and Requirements for both Single and Multi- Layer Transfer Printing	69
5.5.1	Differential Adhesion	70
5.5.2	Assembly of Model System using Transfer Printing	78
5.6	Conclusion	80
6	Electronic Characteristics of Transfer Printed Pn TFTs	81
6.1	Introduction	81
6.2	Proof-of-Concept of Printed Pn TFTs	81
6.3	Optimization of Printed Pn TFTs	83
6.4	X-ray Measurements of Transfer Printed Pn Films	89
6.5	Conclusion	92
7	Electronic Characteristics of Transfer Printed P3HT OTFTs	93
7.1	Proof-of-Concept of printed P3HT TFT	93
7.2	Optimization of Printed P3HT TFTs	93
7.3	Fabrication of P3HT Reference Devices	94
7.4	Optimized Printed P3HT Device Characteristics	95
7.5	Dielectric Effects	100
7.6	Conclusion	101
8	<i>In-Situ</i> Transport Measurements of Transfer Printed Pn Thin-Films	103
8.1	Introduction	103
8.2	Experimental Setup	107
8.3	<i>In-situ</i> Transport Data and Discussion	107
8.4	Conclusion	113
9	Concluding Remarks and Suggestions for Future Work	115
9.1	Introduction	115
9.2	CNT CTFTs on Flexible Substrates	116
9.3	Graphene CTFTs on Flexible Substrates	117
9.4	Surface Modifications to Control Adhesion	118
9.5	Submicron Scale Devices	126
9.6	Circuit Fabrication	127
9.7	Self-Aligned Electrode Subbassemblies	130
9.8	Summary	132
	Appendix A Chemical Structures of Polymers	133
	References	137

LIST OF TABLES

1.1	List of specification for several fabrication methods. Photolithography (PL), micro-contact printing (μ CP), Inkjet printing, nanoimprint lithography (NIL) and transfer printing (TP). Other synonyms include polydimethylsiloxane (PDMS) and self-assembled monolayers (SAM).	3
1.2	List of surface energies for five standard liquids commonly used for contact angle measurements.	9
1.3	Surface energy of a Si transfer substrate after photolithographic processing of Au electrodes followed by, as noted, surface treatments. Right most column indicates polymer dielectrics which could be spin coated onto these surfaces and used in transfer printing.	12
3.1	Non-photolithographic methods for micro- and nanofabrication. ¹⁰	37
5.1	For each sequential printing step, the adhesion rule is that for all interfaces between the surface of the transfer substrate and the (possibly mixed) surface of the device substrate, the work of adhesion must be less than both the works of cohesion for all materials above and below that interface and the works of adhesion for all interfaces above and below that interface. This is illustrated here for the model OTFT discussed in Section 5.2.2. Note that the (before printing) top surface of the Au electrodes is treated with a thiol compound causing the two Au surfaces to have different works of adhesion. In addition, the SiO_2 transfer substrate surfaces with Au electrodes were treated with a release layer (RL) <i>after</i> fabrication of the electrodes, as noted in the text. ²²	72
6.1	Pn OTFT device parameters for Pn layer printed at 600 PSI and 120 °C. Note: μ is mobility ¹ , V_T is threshold voltage ¹ , S is sub-threshold slope ¹ and R_p is the parasitic (contact) resistance. ^{39,22}	89
7.1	Parameter associated with the fabrication and printed of the S/D electrodes and polymer dielectric layers onto plastic substrates. ²⁵	97
7.2	Device properties of reference and flexible P3HT OTFTs. ²⁵	99
9.1	Materials that have been successfully transfer printed and incorporated into high-quality OTFTs are shown in bold (green). Materials that have been successfully transfer printed but not incorporated into high-quality devices are shown in underline (blue). Materials that have not been successfully transfer printed are shown in italics (red).	122

LIST OF FIGURES

1.1	Illustration of the transfer printing method showing the printable layer being printed from the transfer substrate over to the device substrate.	4
1.2	Photograph of the Nanonex 2500 imprint machine.	5
1.3	Transfer printing assembly process for the fabrication of organic thin-film transistors onto plastic substrate. The components are listed in the top panel and the printing steps with a description of the printable layer are listed in the bottom panel.	7
1.4	Surface energy components for a liquid drop on a flat substrate.	9
1.5	List of adhesion requirement for the transfer printing of an electrode subassembly.	10
1.6	Optical and AFM images of an electrode subassembly transfer printed under non-optimized conditions. The AFM image on the left highlights the stress flow pattern visible in the surface of the polymer dielectric layer and the AFM image on the right highlights the protrusion of the source/drain electrodes above the polymer surface.	11
2.1	Chemical structure of (a) a benzene molecule and (b) a thiophene molecule.	15
2.2	Structure of Oligophenylenes and (n)-Acenes with examples of several acene molecules. [Adapted from Gamota ¹ Figs. 2.2.1 and 2.2.2]	17
2.3	AFM image (left panel) of Pn thin film deposited onto an untreated SiO ₂ /Si substrate. The panel on the right illustrates the crystal structure of Pn.	18
2.4	Structure of several heterocyclic rings with an example of a sexithiophene molecule and two related derivatives. [Adapted from Gamota ¹ Figs. 2.2.5 and 2.2.6]	19
2.5	: Structure of the 2-D fused ring molecule naphthalene carbodianhydride (NTCDA) and the related naphthalene carbodiimide (NTCDI). [Adapted from Gamota ¹ Figs. 2.2.18]	20
2.6	Structures of several types of polymeric semiconductor materials. Poly(p-phenylenevinylene) (PPV), poly(thiophenol) (PTP), poly(p,p'-biphenol) (PBP), poly(thienylene vinylene) (PTV), poly(pyrrole) (PPy), poly(thiophene) (PT) and poly(aniline) (PANI). [Adapted from Gamota ¹ Figs. 2.3.2]	22

2.7	: Structure of regioregular poly(3-substituted thiophene) and an example of regioregular P3HT. [Adapted from Gamota ¹ Figs. 2.3.4]	23
2.8	Thin-film transistor geometries showing the relative orientation between electrodes and semiconductor components. Top-left panel illustrates a top-gate/bottom-S/D configuration. Top-right panel illustrates a bottom-gate/bottom-S/D configuration. Bottom-left panel illustrates a top-gate/top-S/D configuration. Bottom-right panel illustrates a bottom-gate/top-S/D configuration.	24
2.9	(a) Output (I_D vs. V_D) and (b) transfer (I_D vs. V_G) characteristics of a Pn reference device with $L = 100\ \mu\text{m}$ and $W = 3\ \text{mm}$. (An optical image of an associated Pn reference device can be found in Fig. 5.2)	26
3.1	Diamond Sutra. One of the oldest known examples of a printed document. [By permission of the ©British Library Board. All Rights Reserved]	36
3.2	Examples of different types of traditional printing. a) gravure printing, b) pad printing, c) screen printing and d) flexography printing. [Adapted from Gamota ¹ Figs 3.4.2, 3.5.1, 3.6.1 and 3.3.1]	40
3.3	Illustration of a) Nanoimprint Lithography (NIL) and b) the transfer printing method. ²²	48
4.1	Illustration of the transfer printing method for simultaneous printing of multiple layers and for sequential printing of layers. ²²	52
4.2	Schematic illustration of the transfer print configuration. The top and bottom sections of the chamber seal against the sample tray. The solenoids engage the ring against the sample tray to vacuum seal the sample (transfer substrate/printable layer/device substrate stack) between two silicone rubber sheets. The chamber is pressurized using N_2 gas and heated using three, 500 Watt lamps. The temperature is measured with a thermocouple (T/C) in contact with a Si wafer piece. ²²	53
4.3	Optical image of 200 nm Au lines transfer printed onto a PET substrate. ²¹	55
4.4	Optical image of a 200 μm Au line transfer printed onto a PET substrate. Prior to printing, the Au was used as an etch mask and the Si substrate was etched to a depth of 700 nm. The profilometer scan shows that the Au line is embedded below the surface of the PET substrate by the depth of the transfer substrate etch. ¹⁴⁶	55

4.5	Optical image of a Au serpentine line transfer printed onto a Kapton substrate. The profilometer scan shows that the Au lines protrude above the surface of the kapton. ¹⁴⁶	56
4.6	Optical images of Pn films transfer printed onto (a) PVC, (b) PET and (c) latex substrates. ¹⁴⁶	57
4.7	Optical image of a 4 μ m line patterned into a Pn film. As shown in the before and after illustrations, the Pn was patterned by transfer printing against a patterned layer of photoresist. ¹⁴⁶	58
4.8	Optical image of a Pn/Au bilayer transfer printed onto a PET substrate. ²¹	58
4.9	Optical image of InP bars transfer printed onto a PET substrate containing previously printed electrodes. The top left image shows the InP substrate containing the bars prior to printing. The top right image shows the InP substrate after printing. The bottom right image shows the InP bars after having been printed onto the PET substrate. ¹⁴⁶	59
4.10	SEM image of CNT network transfer printed onto a PET substrate containing previously printed Au electrodes. ¹⁴⁶	61
4.11	Optical images of spray coated CNT films after having been transfer printed onto (a) Kapton and (b) polycarbonate substrates. The profilometer scan shows the roughness of the polymer/CNT surface after printing. Courtesy of A. Southard, UMD. ¹⁴⁶	61
4.12	Optical image of Ag nanowires printed onto a PET substrate. ¹⁴⁶	62
4.13	Optical image of a graphene sheet (a) before printing and (b) after transfer printing onto a PET substrate containing previously printed S/D electrodes. ¹⁵²	63
5.1	Illustration of the cross-sectional structure of a bottom-contact transfer printed OTFT device. ²²	76
5.2	Profilometer scan of (a) 100 nm and (b) 20 nm thick S/D electrodes (100 μ m wide) printed onto a PMMA coated PET substrate with corresponding optical image of electrodes after printing the Pn. Also shown are optical images of the Pn transfer substrate after printing showing the residual Pn. Note: the magnification is the same for all the optical images. ²²	77

5.3	Illustration of the transfer printing recipe for the fabrication of bottom gate/ bottom S/D OTFT devices onto flexible substrates. (a) illustrates the printing of the gate electrode, (b) illustrates the printing of the dielectric and S/D electrodes and (c) illustrates the printing of the semiconductor.	79
5.4	An optical image of a typical transfer printed device. Note that the Pn layer is visible on the right half of the image. The faint vertical line over the electrodes in the center of the image is the edge of the patterned Pn layer. This device has a 200 μm wide gate electrode, a channel length $L = 9 \mu\text{m}$ and a channel width $W = 100 \mu\text{m}$. ²²	79
6.1	Output characteristics (I_D vs. V_D) for a proof-of-concept Pn TFT device fabricated on a PET substrate via transfer printing. ²¹	82
6.2	Optical image of a Pn reference device with $L = 100 \mu\text{m}$ and $W = 3 \text{ mm}$. The two large squares are the Au S/D electrodes. The continuous Pn film in the center of the image is visible only where covered by the Au electrodes. The bright spots are dots of Ag paint used to connect Au wires to the electrodes. The dark background is the SiO_2 surface of the substrate.	83
6.3	Mobility of transfer printed Pn devices with PMMA (circles) and PHS (diamond) dielectric layers as a function of printing conditions compared with mobility range of Pn reference devices, shaded area. ²²	85
6.4	(a) Output (I_D vs. V_D) and (b) transfer (I_D vs. V_G) characteristics of a transfer printed Pn TFT with a PMMA dielectric layer, a channel length $L = 15 \mu\text{m}$ and a channel width $W = 100 \mu\text{m}$. ²²	86
6.5	(a) Output (I_D vs. V_D) and (b) transfer (I_D vs. V_G) characteristics of a transfer printed Pn TFT with a PHS dielectric layer, a channel length $L = 12 \mu\text{m}$ and a channel width $W = 100 \mu\text{m}$. ²²	87
6.6	Resistance vs Channel length for Pn OTFTs with a (a) PMMA and (b) PHS dielectric layer. Straight lines represent linear fits for each gate voltage that is extrapolated to $L = 0 \mu\text{m}$. ²²	88
6.7	(00 l) x-ray diffraction patterns of 50 nm Pn films (upper panel) after having been transfer printed onto a PMMA coated PET substrate and (lower panel) as deposited (i.e. unprinted) on a Si wafer with a 500 nm thick thermally oxidized surface. The first three (00 l) reflections are visible along with, as labeled, reflections from the associated substrate. ²²	91

6.8	Percent increase (compared to Pn on SiO ₂ before printing) of basal spacing correlation length as a function of Pn printing conditions. ²²	92
7.1	Output characteristics (I_D vs. V_D) for a Proof-of-concept P3HT TFT device fabricated onto a PET substrate with a PMMA dielectric layer using the transfer printing method. ²¹	94
7.2	(a) Output (I_D vs. V_D) and (b) transfer (I_D vs. V_G) characteristics of a transfer printed P3HT TFT with a PMMA dielectric layer, a channel length $L = 15 \mu\text{m}$ and a channel width $W = 100 \mu\text{m}$. ²⁵	98
7.3	Resistance vs Channel length for P3HT TFTs with a PMMA dielectric layer. Straight lines represent linear fits for each gate voltage. ²⁵	99
7.4	Plot of Threshold voltage vs polar component of the surface energy for P3HT devices fabricated with PMMA, PS, PC and PHS dielectric layers. Note: the threshold voltage is estimated for the devices fabricated with PHS. ²⁵	101
8.1	: (a) Cross-section illustration of the OTFT reference device geometry with thermally evaporated electrodes highlighting the as-grown pentacene bottom surface as the active device interface. (b) Cross-section illustration of the OTFT flexible device geometry highlighting the as-grown pentacene top surface as the active device interface. ²⁴	106
8.2	(a) Cross-section illustration of the typical geometry for transfer printing pentacene to a flexible electrode subassembly, which can be thought of as a reference device and flexible device sharing the same semiconducting layer. (b) Cross-section illustration of the OTFT control device geometry using the as-grown pentacene bottom surface as the active device interface. (c) Cross-section illustration of the OTFT plastic device geometry using the as-grown pentacene top surface as the active device interface.	106
8.3	<i>In-situ</i> I_D vs. V_D transport measurements of the flexible device for thermocouple temperatures of (a) 30 °C before heating, (b) 170 °C during heating and (c) 30 °C after heating, and of the reference device for thermocouple temperatures of (d) 30 °C before heating, (e) 170 °C during heating and (f) 30 °C after heating. All data correspond to a pressure of 600 PSI. ²⁴	109
8.4	Mobility of the (a) flexible device and (b) reference device during the heating and cooling phases of the transfer printing process with pressure held at 600 PSI. The red dots in (b) correspond to the calculated mobility due only to thermal excitation. The second (light gray) bar in	

(b) for 30 °C corresponds to the mobility of a reference device with thermally deposited top electrodes. ²⁴	111
9.1 Transfer characteristics (I_D vs. V_G) at fixed drain voltages of 1.0 V (top curve) and 0.5V (bottom curve) for CNT TFT. Inset shows SEM and AFM images of the CNT film in the source-drain region after transfer printing onto a PMMA-coated PET substrate containing previously printed Au electrodes. ²¹	117
9.2 Transfer Characteristics of a top gate graphene CTFT printed onto a PET substrate with a PMMA dielectric layer. ¹⁵²	118
9.3 Transfer printing results, in percent printed, for six polymer dielectric materials and a Au feature printed against thirteen plastic substrates.	123
9.4 Glass transition temperature for plastic substrates that appear in Fig. 9.3.	124
9.5 Surface energy for plastic substrates that appear in Fig. 9.3.	125
9.6 Dispersive (red) and polar (blue) componentd of the surface energy for the treated and untreated PET and FEP substrates that appear in Fig. 9.3.	126
9.7 Optical images of a set of 36 OTFTs transfer printed onto a 1” square PET substrate. ¹⁴⁶	128
9.8 Optical image of two transfer printed OTFTs devices on the same PET substrate. These devices can be electrically connected to make an inverter circuit.	129
9.9 Optical image of a solenoid fabricated using sequential transfer printing steps onto a PET substrate. The bottom set of Au lines are connected to the top set of Au lines by printed vias. ¹⁴⁶	129
9.10 Optical image of transformer printed onto PET substrate. The device was constructed from the sequential printing of Au lines and vias. (Courtesy of A. Tunnell, UMD)	130
9.11 Conceptual illustration of a self-aligned electrode subassembly created using a two-photo polymerization technique.	131

Chapter 1 Introduction

1.1 Motivation

Predominately based on silicon (Si) technology, solid-state electronics have dominated the revolution in information technology over the past several decades. Progress has been rapid; from the first semiconductor transistor in 1947, advances have followed Moore's Law to the point where, in 2005, an Intel Pentium 4 processor contains approximately 42 million transistors in a two inch square package. The modern era has seen juke boxes be replaced by iPods and pay phones be replaced by cell phones. Today we can carry around laptop computers that operate at 2 GHz, have 100 GB storage capacity, are approximately one inch thick and weight only a few pounds!

In addition to computer chips based on single crystal Si substrates, a flat panel display technology based on amorphous Si has emerged. This has been an enabling technology for the proliferation of laptop computers, although the display still accounts for a large fraction of the weight of a laptop. In the last five years, this technology has advanced to the point where flat panel displays are becoming ubiquitous as desktop computer monitors and televisions. For example, 50 inch flat panel displays are commercially available and 103 inch displays have been showcased.

What Si does, it does very well. However, fabrication processes for these two Si technologies are complex, costly and require high processing temperatures. Hence, they are not compatible with visions of disposable electronics, very large area displays, biocompatible electronics or wearable electronics. To address these issues,

a new era of lightweight, flexible, biocompatible electronics that are as easy to produce as magazines or newspapers has been envisioned and is just beyond the horizon in development. Two areas of rapid growth aimed at ushering in such an era are organic electronics and printing techniques for the fabrication of electronics on plastic substrates.

Developing practical and effective methods for printing electronic circuits onto flexible substrates involves serious research issues in materials science.¹ Efforts to address these issues are being driven by, among other things, the desire to manufacture large-area, flexible displays² and large volumes of inexpensive radio frequency identification (RFID) tags.³ Other applications for which flexible electronics may also have a large impact are wearable electronics,⁴ chemical sensors⁵ and medical testing.⁶ In order to meet the needs of these emerging technologies, fabrication methods that are compatible with organic and polymeric materials, as well as traditional solid-state electronic materials, are being developed.⁷⁻¹² The broad goal is to develop methods for assembling dissimilar materials onto a common substrate in a way that is cost effective and scalable to large areas, similar to roll-to-roll printing.¹

1.2 Description of Transfer Printing

Table 1.1 shows a comparison between five types of materials processing methods. The list includes photolithography (PL), micro-contact printing (μ CP),^{13,14} inkjet printing,¹⁵ nano-imprint lithography (NIL)¹⁶ and transfer printing (TP). Photolithography represents the benchmark by which all new device fabrication methods will be compared. It has been the work horse for the fabrication of Si based

electronics for close to fifty years. In its current form, PL is an expensive fabrication method that requires chemical processing in a batch mode of operation and is largely restricted to photoresist chemistry and inorganic semiconducting materials. The other processes are potentially less expensive and scaleable to continuous processing. However, μ CP, inkjet printing and NIL all require chemical processing which may not be compatible with a wide range of materials suitable for flexible electronics.

Specifications	PL	μCP	Inkjet	NIL	TP
Resolution	32 nm	35 nm	20 μ m	5-10 nm	5-10 nm
Price	\$\$\$	\$	\$	\$	\$
Materials	Resist on Inorganic Wafer	PDMS w/ SAM	Solution processible Inks	Resist on Inorganic Wafer	Wide Range of Materials
Processing	Batch	Continuous	Continuous	Continuous	Continuous
Requires Chemical Processing	Yes	Yes	Yes	Yes	No

Table 1.1: List of specification for several fabrication methods. Photolithography (PL), micro-contact printing (μ CP), Inkjet printing, nanoimprint lithography (NIL) and transfer printing (TP). Other synonyms include polydimethylsiloxane (PDMS) and self-assembled monolayers (SAM).

By comparison, transfer printing is potentially an inexpensive process, scaleable to continuous processing and does not rely on chemical processing. As will be demonstrated in this thesis, transfer printing is compatible with a wide variety of materials and will be developed for the use of lightweight, flexible transparent substrates. An added attraction of the transfer printing method is that it can be combined with NIL for simultaneous patterning of and printing onto a flexible substrate. The transfer printing process, while expected to be compatible with high resolution printing at the scale of 5 – 10 nm, is primarily an assembly process by

which a printable layer can be transferred from one substrate (the transfer substrate) to a second substrate (the device substrate). The transfer is complete if the printable layer adheres more strongly to the device substrate than to the transfer substrate as illustrated in Fig 1.1.

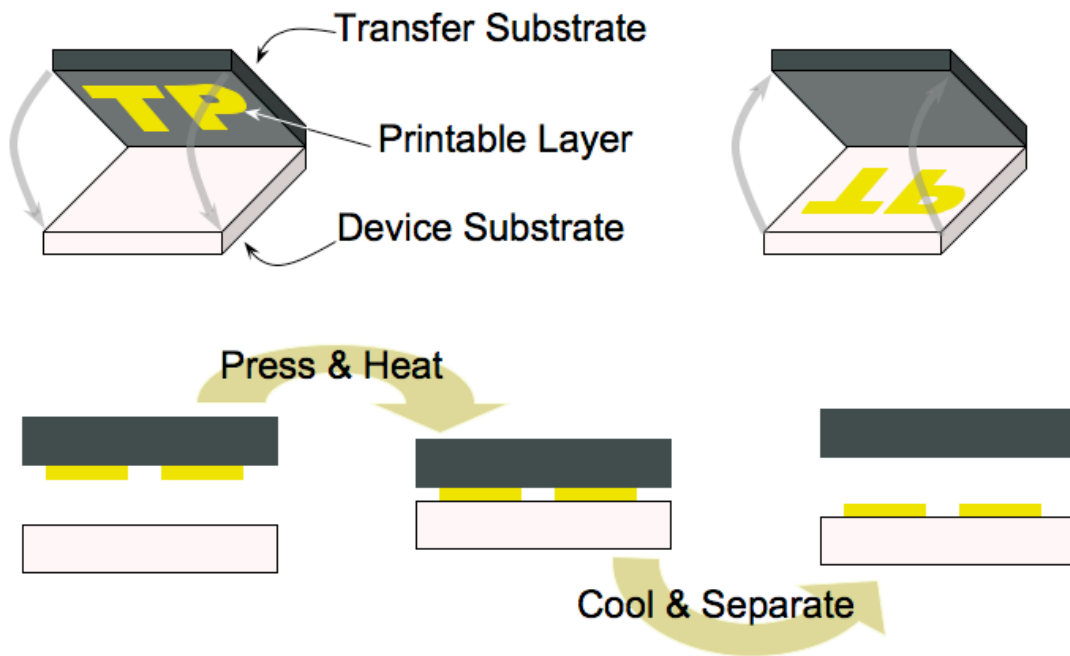


Figure 1.1: Illustration of the transfer printing method showing the printable layer being printed from the transfer substrate over to the device substrate.

The transfer printing process, as developed here, has been performed using a Nanonex 2500 imprint machine. This machine was originally designed for NIL and is shown in Fig. 1.2. Transfer printing is in no way restricted to such a machine. In general, all that is needed is for the printable layer to be brought into contact with the surface of the device substrate under the proper differential adhesion conditions. However, the Nanonex machine is convenient because it does not rely on a parallel plate configuration and will therefore allow printing onto non-flat substrates. The

imprint machine has a split chamber with a sample tray that permits the printable layer to be vacuum sealed in contact with the two substrates. The chamber can then be back filled with N_2 gas as the pressure medium and is equipped with three 500 Watt lamps for temperature control.



Figure 1.2: Photograph of the Nanonex 2500 imprint machine.

The imprint machine has been used to print Au features onto PET and Kapton substrates; to print pentacene onto PVC, PET, latex and photoresist surfaces; to print InP bars onto a mixed PMMA/Au surface; to print carbon nanotubes onto a mixed PET/Au surface and onto Kapton and PC substrates; to print Ag nanowires onto a


PET substrate and to print graphene onto a PET substrate. All of these examples will be discussed in Chapter 4.

1.3 Adhesion Issues and Devices Fabrication

With the transfer printing process demonstrated for a wide variety of materials, it is desirable to sequentially print all the components necessary for the fabrication of a thin-film transistor onto a plastic substrate. Figure 1.3 highlights this assembly process for thermoplastic substrates, Au electrodes, polymer dielectric layers and organic semiconducting thin-films. Thermoplastic substrates were chosen because they are lightweight, flexible and generally transparent. Adhesion of a printable layer to the surface of a thermoplastic can be increased by heating to a temperature above the glass transition temperature of the thermoplastic material. This promotes both physical and chemical adhesion by increasing the mobility of polymer chains so that they can move across the interface and/or move into intimate contact with chemically active site at the interface. Gold electrodes were chosen because they are excellent conductors with a work function reasonably well matched with organic materials¹⁷ and can be easily fabricated on Si transfer substrates using photolithography. Thermoplastic polymer dielectric layers were chosen because they have good dielectric properties and are easily processed by spin coating onto transfer substrates. As with thermoplastic substrates, adhesion to polymer dielectric layers can be promoted by heating to a temperature above the polymer glass transition temperature. Furthermore, they are generally flexible and transparent. Organic semiconducting materials were chosen because they are lightweight and flexible.

Thin-films of these materials are essentially transparent and can be processed more cheaply than can inorganic semiconducting materials. Since organic semiconducting materials are generally more sensitive to chemical, temperature and processing conditions than their inorganic counterparts, they are ideal materials for testing the robustness and limitations of the transfer printing method.

Organic Thin-Film Transistor Assembly

	Components	Materials
	1. Organic Semiconductor Layer	- Pn & P3HT
	2. Source/ Drain Electrodes	- Au
	3. Gate Dielectric Layer	- PMMA, PHS, PS, PC
	4. Gate Electrode	- Au
	5. Substrate	- PET, PC

Transfer Printing Recipe:

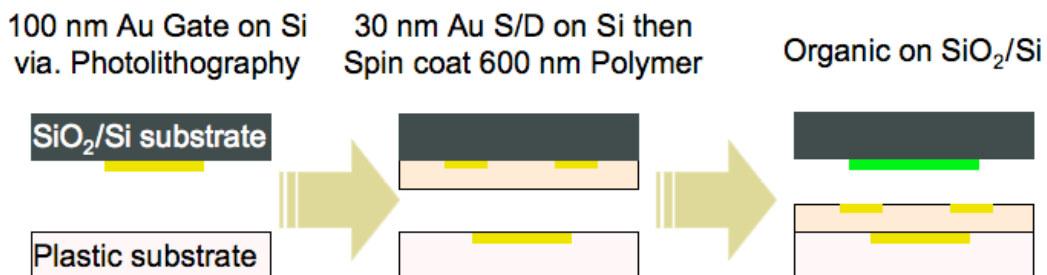


Figure 1.3: Transfer printing assembly process for the fabrication of organic thin-film transistors onto plastic substrate. The components are listed in the top panel and the printing steps with a description of the printable layer are listed in the bottom panel.

The fabrication of organic thin-film transistors requires the assembly of dissimilar materials onto a common substrate. During sequential transfer prints, the adhesion at previously printed interfaces and the cohesion of previously printed layers

must be larger than adhesion to the transfer substrate. The works of adhesion and cohesion¹⁸ can be expressed as

$$W_C(i) = 2\gamma_i \quad (1.1)$$

$$W_A(i/j) = \gamma_i + \gamma_j - \gamma_{ij} \quad (1.2)$$

where γ_i is the surface energy of surface i and γ_{ij} in the interfacial energy. Equation 1.2 is referred to as the Dupré equation.¹⁸ The total surface energy can be represented as a sum of components encompassing dispersive interactions and polar (non-dispersive) interactions such that $\gamma_i = \gamma_i^D + \gamma_i^P$. As shown in Fig 1.4, the surface energy of a flat surface (S) is related to the contact angle (θ) of a liquid (L) on that surface by

$$\gamma_S = \gamma_{SL} + \gamma_L \cos\theta \quad (1.3)$$

which is referred to as Young's equation.¹⁹ By expressing the work of adhesion as a geometric mean of the works of cohesion¹⁹ $W_A(i/j) = 2[W_C(i) W_C(j)]^{1/2}$ and by including the dispersive and polar terms, Eqs. 1, 2 and 3 can be combined to give

$$\gamma_L(1 + \cos\theta) = 2[\gamma_S^D \gamma_L^D]^{1/2} + 2[\gamma_S^P \gamma_L^P]^{1/2} \quad (1.4)$$

Using this equation along with standard liquids with known dispersive and polar surface energy components, such as the five listed in Table 1.2, values for γ_S^D and γ_S^P can be calculated for a given surface.

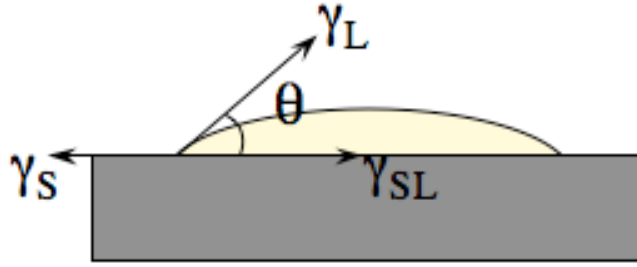


Figure 1.4: Surface energy components for a liquid drop on a flat substrate.

Liquid	γ	γ^D	γ^P
Water	72.8	21.8	51.0
Glycerol	64.0	34.0	30.0
Ethylene Glycol	48.0	29.0	19.0
Formamide	58.0	39.0	19.0
Diiodomethane	50.8	50.8	0.0

Table 1.2: List of surface energies for five standard liquids commonly used for contact angle measurements.

In a practical sense, the adhesion requirements for successful assembly of a transfer printed electrode subassembly using photolithographically patterned Au electrodes on a Si transfer substrate are enumerated in Fig 1.5. This list includes (1) the Au electrodes must survive lift-off during fabrication and yet have a low enough adhesion to transfer off the Si transfer substrate. (2) The Au electrodes must have a high adhesion to the plastic substrate and (3) to the polymer dielectric layer. (4) The polymer dielectric layer must have a high adhesion to the plastic substrate. (5) The Si transfer substrate must have a low adhesion to both the polymer dielectric layer and to the plastic substrate. (6) The top surface of the electrode subassembly must be flat with the electrodes in the same plane as the top surface of the dielectric layer.

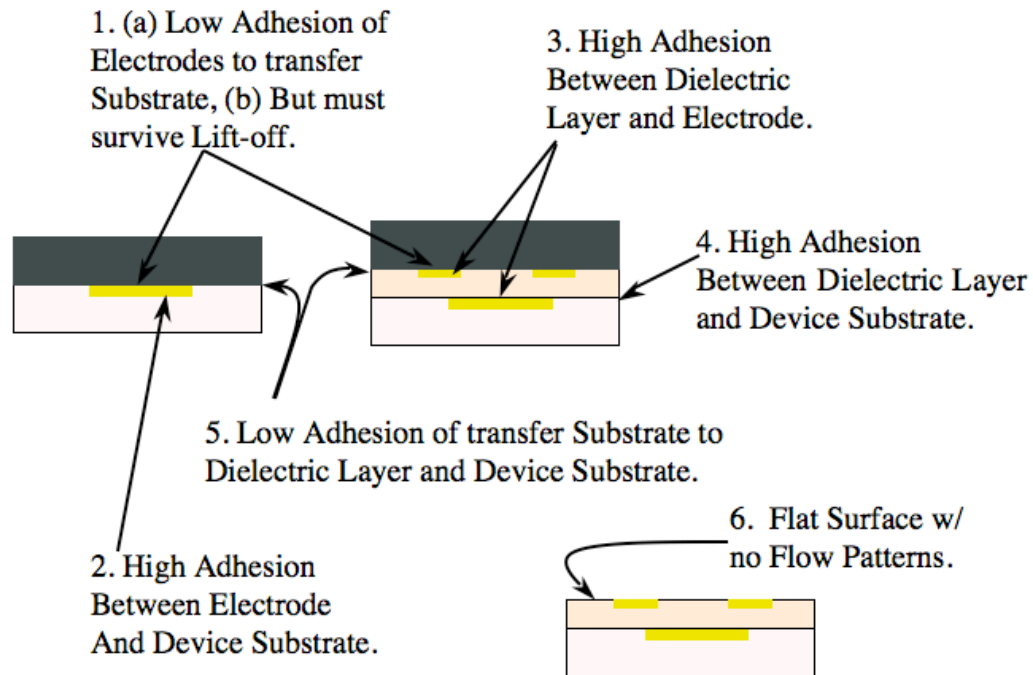


Figure 1.5: List of adhesion requirement for the transfer printing of an electrode subassembly.

The results of a non-optimized transfer printed electrode subassembly are shown in Fig. 1.6. Stress flow patterns in the polymer dielectric layer can be seen in both the optical and AFM images. Also the Au source/drain electrodes are seen to protrude above the surface. The stress flow patterns can be alleviated by printing at a higher temperature and pressure.²⁰ However, this also increases adhesion between the device substrate and the Si transfer substrate. It was found that decreasing the surface energy of the Si transfer substrate allowed for good transfer printing results at the higher temperature and pressure printing conditions. The surface energy of a Si transfer substrate after photolithographic processing is shown in Table 1.3 along with surface energies after both an O₂ plasma treatment and a vapor phase exposure to (tridecafluoro-1,1,2,2-tetrahydrooctyl) trichlorosilane (FDTS). It was determined that

PMMA and PHS could be spin coated onto and cleanly printed off a Si transfer substrate that was exposed to FTDS vapors for 2 min. In contrast, PS and PC could be spin coated onto and cleanly printed off an as processed substrates.

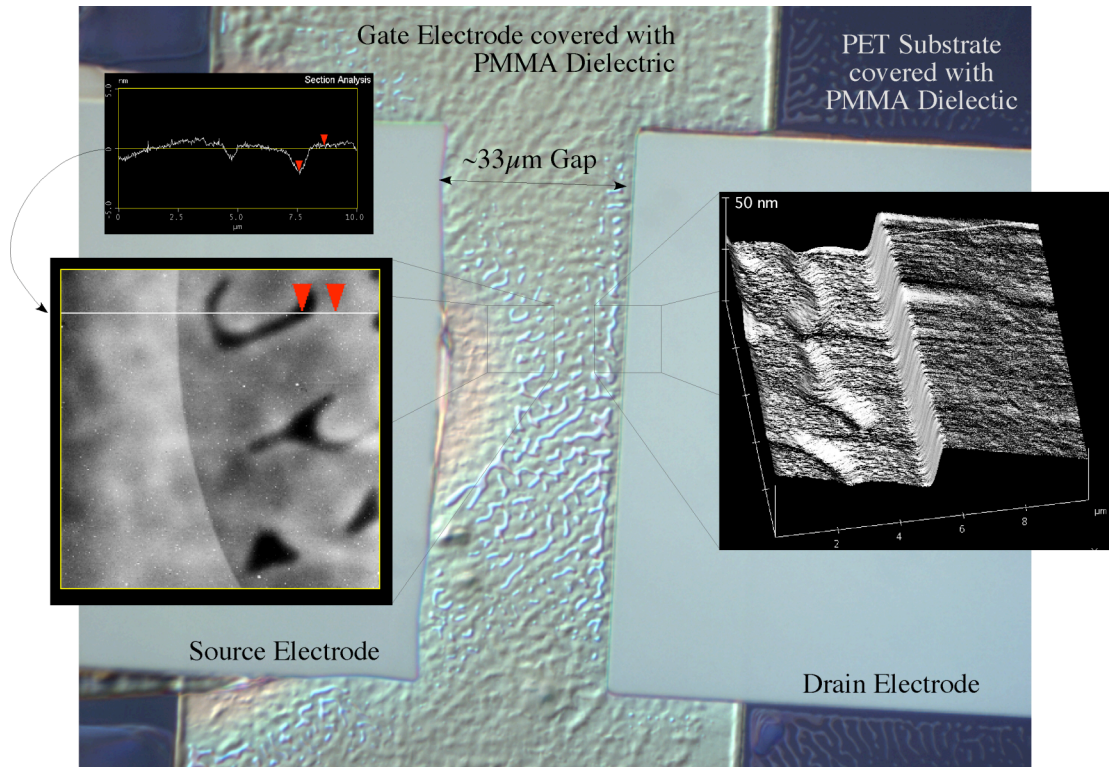


Figure 1.6: Optical and AFM images of an electrode subassembly transfer printed under non-optimized conditions. The AFM image on the left highlights the stress flow pattern visible in the surface of the polymer dielectric layer and the AFM image on the right highlights the protrusion of the source/drain electrodes above the polymer surface.

Processing of Si Wafer	Surface Energy, mJ/m²	Spin Coatable and Transfer Printable Polymer Dielectrics
Photolithography and O ₂ Plasma Etch	63	–
Photolithography	61	PC, PS
Photolithography and 2 min. FDTs exposure	23	PMMA, PHS
Photolithography and 2 hr FDTs exposure	15	–

Table 1.3: Surface energy of a Si transfer substrate after photolithographic processing of Au electrodes followed by, as noted, surface treatments. Right most column indicates polymer dielectrics which could be spin coated onto these surfaces and used in transfer printing.

Specific details of the transfer printing process have been developed and will be discussed through out this thesis. As an example of what is possible using the transfer printing method as an assembly tool for fabricating organic thin-film transistors onto plastic substrates, devices based on pentacene and P3HT were fabricated and characterized. Their performance will be compared to that of reference devices fabricated by depositing the organic material onto the oxidized surface of a highly doped Si wafer. Here the thermal oxide is the dielectric layer and the doped Si wafer is a global gate electrode. Source/drain electrodes were evaporated either before or after the deposition of the organic material onto the oxide surface. Details of the fabrication of these reference devices are found at the relevant places throughout the thesis.

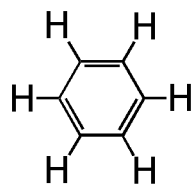
1.4 Conclusion

The body of work presented in this thesis has been designed to address research issues at the interface between organic semiconductor materials and the printing of active materials onto flexible substrates. Emphasis will be placed on both the development of printing techniques to fabricate organic electronics onto plastic substrates and on the electronic characteristics for these fabricated devices. Many of the results of this research have been published,²¹⁻²⁵ as will be noted with references to the published work in the figures and text. To begin with, in Chapters 2 and 3 a review of the state-of-the-art of organic semiconductor materials and printing technologies respectively will be presented. In Chapter 4 details of the transfer printing process will be introduced. The process will be discussed in detail in Chapter 5 in terms of the development of the transfer printing method for the fabrication of organic thin-film transistors. The electronic characteristics of the fabricated OTFT devices will be presented and discussed for pentacene (Pn) devices in Chapter 6 and for poly(3-hexylthiophene) (P3HT) devices in Chapter 7. The effect of transfer printing on the morphology of the organic film and device mobility will be presented and discussed in Chapter 8. Concluding remarks and suggestions for future work will be discussed in Chapter 9.

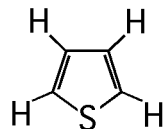
Chapter 2 Organic Semiconductor Materials and Devices

2.1 Introduction

In general, organic semiconductor materials are composed of conjugated chains (containing two or more double bonds each separated by a single bond) of carbon atoms or two-dimensional structures of aromatic ring units. As illustrated in Fig. 2.1, the benzene molecule containing six carbon atoms and the thiophene molecule containing four carbon atoms and one sulfur atom are common examples of such aromatic ring structures. The semiconductor properties of organic molecules arise from a combination of the HOMO-LUMO gap and the overlap of the π orbitals of neighboring molecules. Since the interaction between neighboring molecules is weak, the π orbital-overlap between neighboring molecules is sensitive to molecular alignment. In a thin-film of organic material, larger overlap between molecules generally leads to a larger electron mobility in the film. For electronics based on organic semiconductor materials, larger mobility typically translates into better device performance. Therefore, mobility is an important metric by which organic materials will be judged and the goal is to develop organic thin films with higher mobility.



(a) Benzene



(b) Thiophene

Figure 2.1: Chemical structure of (a) a benzene molecule and (b) a thiophene molecule.

2.2 Classes of Nontraditional Semiconductors

Organic semiconductor materials can be classified into four categories:

- 1) small molecules, 2) conjugated polymers, 3) “geometrical molecules” and 4) inorganic/organic hybrids.

The small molecule category consists of three subcategories: 1) acenes and oligophenylenes, 2) heterocycle-based linear oligomers and 3) two-dimensional fused rings. The general structures of acenes and oligophenylenes are shown in Fig. 2.2 along with well-known examples. The most famous example of these types of small molecule materials is pentacene (Pn) which consists of five ring units. Pn molecules crystallize in a triclinic crystal structure with two molecules per unit cell that are packed to form a herringbone motif as shown in the right panel in Fig. 2.3. There are at least four unique crystal polymorphs for Pn that are defined by their layer spacing.²³ When deposited as a thin film on a flat substrate, terraced grains form as illustrated in the left panel of Fig. 2.3. Both the deposition conditions and the substrate surface properties affect the grain size of the Pn film.²⁶

The structures of several heterocyclic rings are shown in Fig. 2.4 along with examples of molecules from the thiophene sub-category. The best known of these

molecules is sexithiophene (6T) which consists of six thiophene rings connected to form a planar molecule. The molecules are arranged in a monoclinic crystal structure. There are four molecules per unit cell forming a layered structure with two molecules per layer arranged in a herringbone motif.²⁷ Hexyl groups can be substituted, for example, at the α and ω sites to produce the molecule α, ω -dihexylsexithiophene (α, ω DH6T). Additionally, the hydrogen atoms of the hexyl group can be replaced by fluorine atoms to produce an n-type semiconductor α, ω -diperfluorohexylsexithiophene (α, ω DFH-6T).

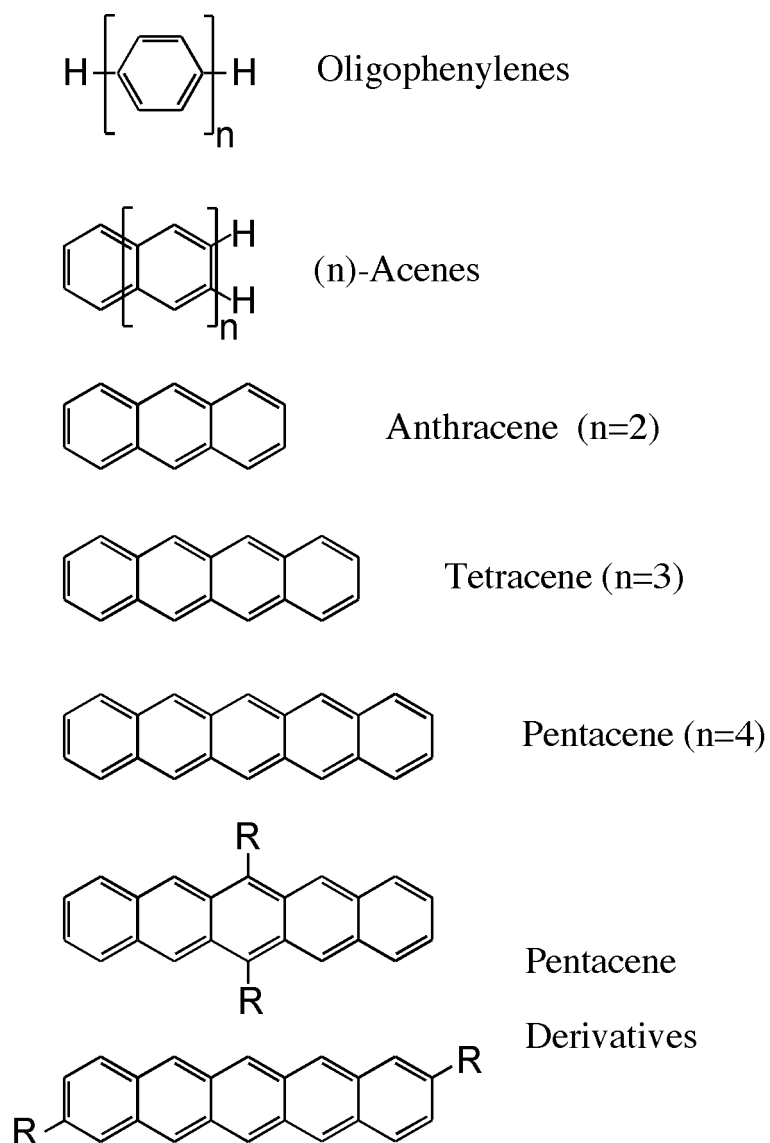


Figure 2.2: Structure of Oligophenylenes and (n)-Acenes with examples of several acene molecules. [Adapted from Gamota¹ Figs. 2.2.1 and 2.2.2]

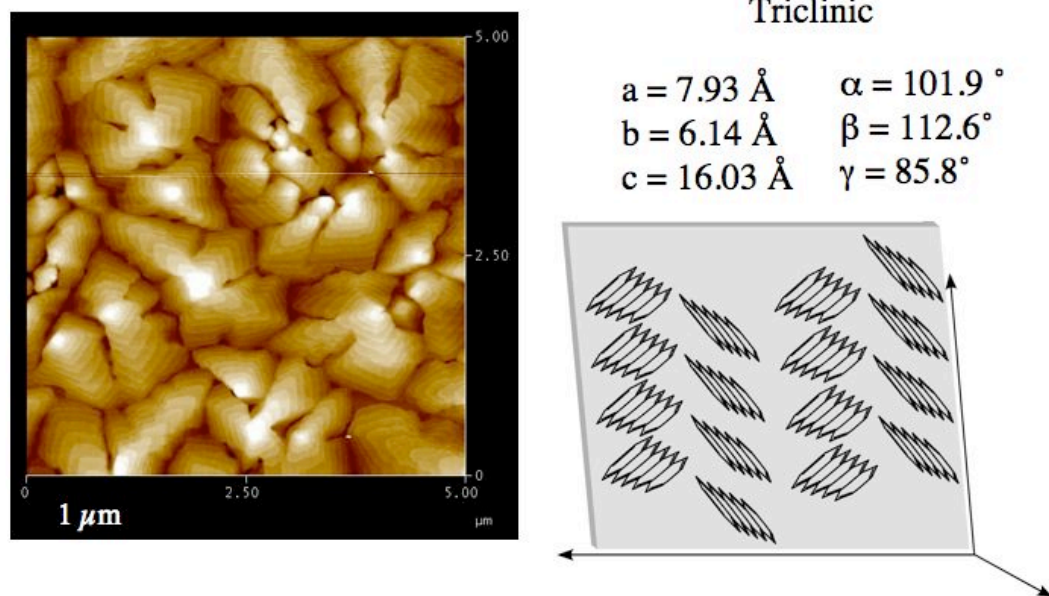
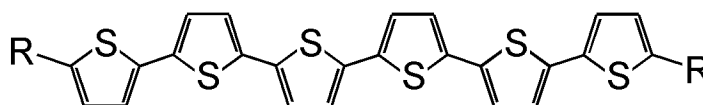
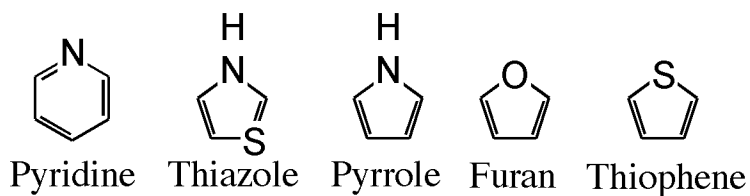


Figure 2.3: AFM image (left panel) of Pn thin film deposited onto an untreated SiO_2/Si substrate. The panel on the right illustrates the crystal structure of Pn.



$R = H$; sexithiophene (6T)

$R = C_6H_{13}$; α,ω -dihexylsexithiophene (α,ω -DH-6T)

$R = C_6F_{13}$; α,ω -diperfluorohexylsexithiophene (α,ω -DFH-6T)

Figure 2.4: Structure of several heterocyclic rings with an example of a sexithiophene molecule and two related derivatives. [Adapted from Gamota¹ Figs. 2.2.5 and 2.2.6]

In addition to linear chains of heterocyclic ring units, molecules built up from two-dimensional fused rings can also be synthesized and constitute the third subcategory of small molecule materials. Two examples of such materials are shown in Fig. 2.5. Naphthalene carbodianhydride (NTCDA) and the related imide-substituted naphthalene carbodiimide (NTCDI) are well studied examples of n-type semiconductor materials.²⁸ NTCDI forms a triclinic crystal structure with parallel planes of molecules with an interplane spacing of 0.3 nm. In the plane, each molecule is canted by 13° to maximize the hydrogen bonding between the imide and carbonyl groups of neighboring molecules.²⁹

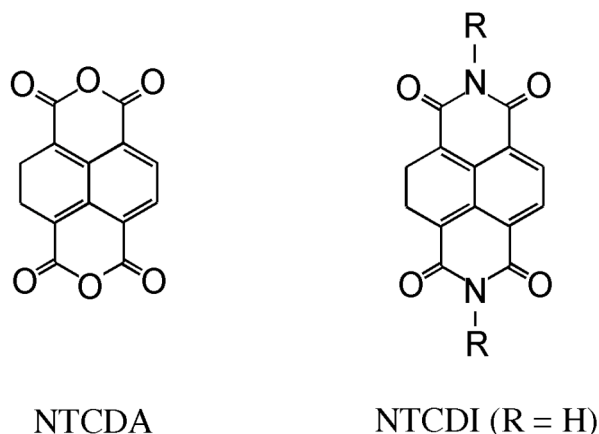


Figure 2.5: Structure of the 2-D fused ring molecule naphthalene carbodianhydride (NTCDA) and the related naphthalene carbodiimide (NTCDI). [Adapted from Gamota¹ Figs. 2.2.18]

The polymeric class of semiconductor materials is represented in Fig. 2.6 by several structures of materials. The polythiophene (PT) structure has shown a rich behavior with poly (3-hexylthiophene) (P3HT) emerging as a highly studied material and the related poly(3,4-ethylenedioxythiophene)/poly(styrene sulfonate) (PEDOT/PSS) material having been synthesized as a conducting organic material compatible with solution processing. As shown in Fig. 2.7, P3HT consists of a polymer chain of thiophene molecules with a hexyl group substituted at one of the carbon sites not neighboring the sulfur atom. The polymer is referred to as regioregular if neighboring molecules exhibit head-to-tail oriented hexyl groups. P3HT molecules order in a lamellar semi-crystal with the molecular stacking direction dependent on the degree of regioregularity.³⁰ PEDOT/PSS is a conducting polymer material synthesized from a thiophene backbone.³¹ The addition of poly(styrene sulfonic acid) renders the molecule water soluble and results in a good film-forming material with high conductivity (10 S/cm). PEDOT/PSS has been used with inkjet³² and micro-contact³³ printing methods to form electrodes for thin-film

transistor (TFT) devices. Another example of an important polymeric organic material is polyaniline (PANI), which has also been used as a conducting polymer for the fabrication of all-polymer electronic devices.³⁴ The conductivity of PANI is controllable through oxidation/reduction and acid/base reactions and can be varied from 10^{-9} to 10^2 S/cm.

The “geometrical molecule” category consists primarily of fullerenes and carbon nanotubes (CNTs). These carbon-based materials are, in fact, not organic because they lack hydrogen; however, they do represent an important category of nontraditional semiconductor material. CNTs have shown great promise as semiconductors with individual tubes exhibiting mobilities up to $80,000 \text{ cm}^2/\text{Vs}$.³⁵ Although plagued with the existence of intermixed metallic tubes, CNT mats have recently been studied as an easily processible material for active semiconductor layers.²¹ Although the aspect ratio is much larger (i.e. the diameter of the CNT is many more times smaller than its length in comparison to spaghetti) CNT mats can be loosely thought of as cooked spaghetti noodles randomly deposited onto a surface, where both the length of individual tubes and the number of tubes in the mat can be controlled.

The organic/inorganic category consists of a layered inorganic material intercalated with an organic material. These materials are of interest because they have the potential to be processed in the same manner as organic materials but have electronic properties similar to inorganic materials. An example of this type of hybrid material is tin iodide perovskite intercalated with m-fluorophenethylammonium ions $(\text{C}_6\text{H}_4\text{FC}_2\text{H}_4\text{NH}_3)_2\text{SnI}_4$. The material forms a monoclinic crystal structure that

consists of sheets of corner-sharing distorted SnI_6 octahedra separated by bilayers of fluorophenethylammonium cations.³⁶

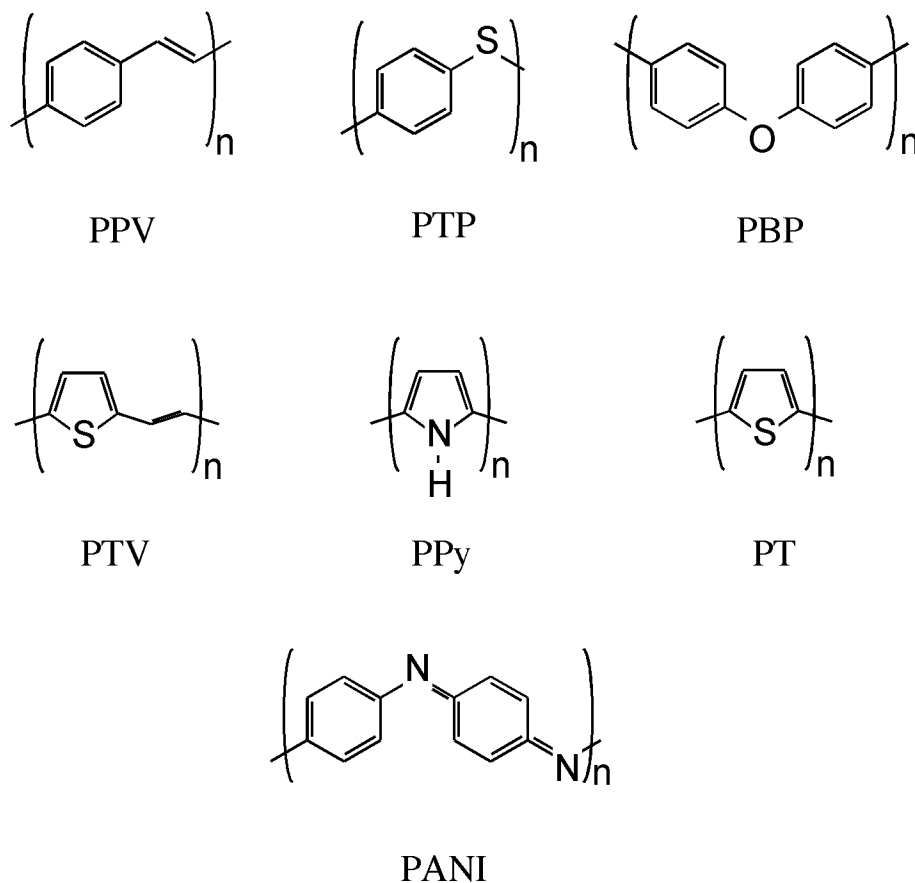
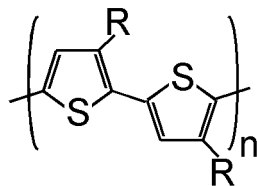
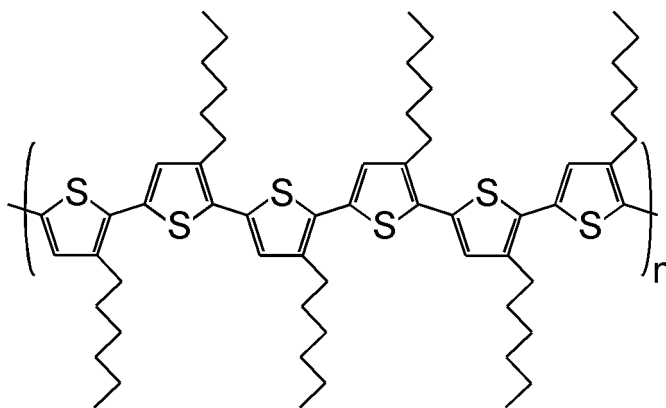


Figure 2.6: Structures of several types of polymeric semiconductor materials. Poly(p-phenylenevinylene) (PPV), poly(thiophenol) (PTP), poly(p,p'-biphenol) (PBP), poly(thienylene vinylene) (PTV), poly(pyrrole) (PPy), poly(thiophene) (PT) and poly(aniline) (PANI). [Adapted from Gamota¹ Figs. 2.3.2]



Regioregular Poly(3-substituted thiophene)



Regioregular Poly(3-hexylthiophene) (P3HT)

Figure 2.7: Structure of regioregular poly(3-substituted thiophene) and an example of regioregular P3HT. [Adapted from Gamota¹ Figs. 2.3.4]

2.3 Electronic Properties of Organic Semiconductors

Throughout the last half of the twentieth century and into the beginning of the twenty-first century, much work has been done in the area of organic semiconductor materials. Typically, organic devices are constructed as thin-film transistors (TFTs). The geometries of such devices are shown in Fig. 2.8 and are referred to as a) bottom gate - bottom source/drain (S/D), b) bottom gate - top S/D, c) top gate – top S/D and d) top gate – bottom S/D. Historically (as a platform for testing the electronic properties of organic semiconductor materials) OTFTs have been fabricated on thermally oxidized silicon (SiO_2/Si) substrates in the bottom gate configurations with

either top or bottom S/D electrodes. For these devices the Si substrate is highly doped and used as a global gate with the SiO₂ as the dielectric layer. Throughout this thesis, such devices on SiO₂/Si substrates will be referred to as reference devices and will be a benchmark against which the performance of the flexible devices fabricated using transfer printing methods will be judged.

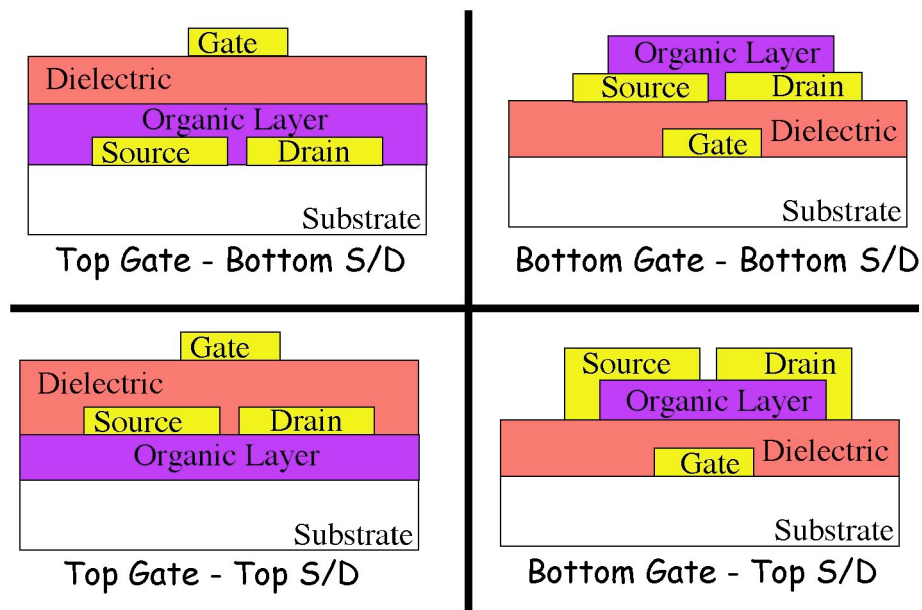


Figure 2.8: Thin-film transistor geometries showing the relative orientation between electrodes and semiconductor components. Top-left panel illustrates a top-gate/bottom-S/D configuration. Top-right panel illustrates a bottom-gate/bottom-S/D configuration. Bottom-left panel illustrates a top-gate/top-S/D configuration. Bottom-right panel illustrates a bottom-gate/top-S/D configuration.

It has been determined that the semiconductor properties of an organic thin-film transistor (OTFT) are confined to the first few monolayers at the interface near the dielectric layer and that they are limited by charge trapping at this interface.^{37,38} The chemistry and roughness of the substrate surface has also been shown to affect the measured mobility of a OTFT device.²⁶

The electronic transport properties of OTFTs are typically studied by measuring the current flow (I_D) from the source to the drain electrodes as a function of bias voltages applied between the S/D electrodes (V_D) and between the Gate/Source electrodes (V_G). Figure 2.9a shows the output characteristics of a Pn reference device, which is a plot of I_D vs V_D for various values of V_G . Figure 2.9b shows the transfer characteristics (transconductance) of a Pn reference device, which is a plot of I_D vs V_G for a fixed value of V_D . Important macroscopic parameters such as mobility, threshold voltage (V_T), On/Off ratio, subthreshold slope and contact resistance can be determined from these current-voltage characteristics as will be discussed in the Sections 2.4, 2.5 and 2.6.

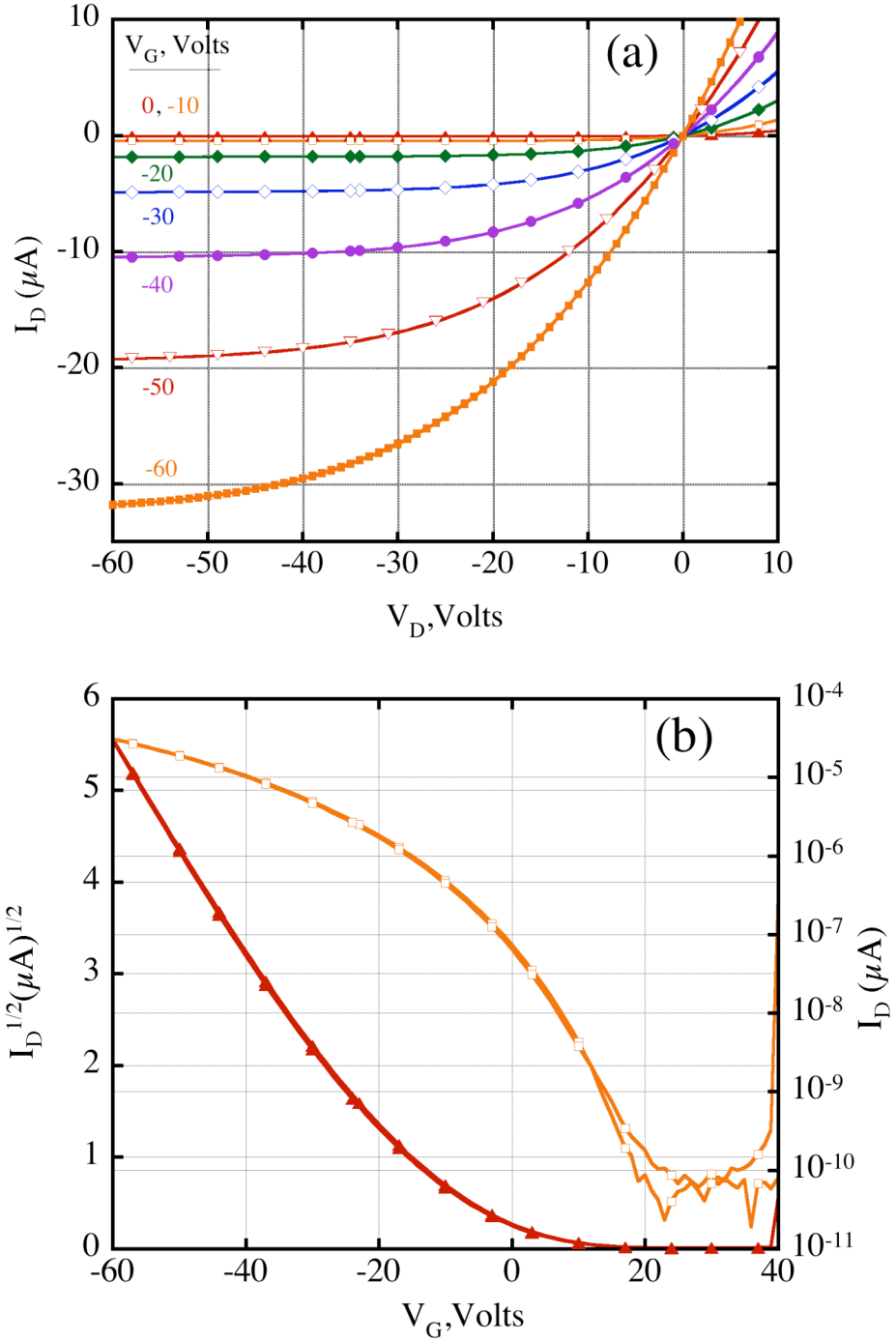


Figure 2.9: (a) Output (I_D vs. V_D) and (b) transfer (I_D vs. V_G) characteristics of a Pn reference device with $L = 100 \mu\text{m}$ and $W = 3 \text{ mm}$. (An optical image of an associated Pn reference device can be found in Fig. 5.2)

2.4 Determination of Mobility

The following discussion has been adapted from Gamota¹ section 4.2.3.1. For the analysis of OTFTs, it is standard practice to utilize current-voltage models developed from the gradual channel approximation for inorganic MOSFET devices. Here, the current density can be expressed as

$$J(x) = \sigma d\Phi/dx \quad (2.1)$$

where $J(x)$ is the current density in the semiconductor channel, σ is the conductance and $d\Phi/dx$ is the gradient of the potential in the channel. For a semiconductor material

$$\sigma = n e \mu \quad (2.2)$$

where n is the number density of charge carriers, e is the charge per carrier and μ is the mobility of the carrier. The current in the semiconductor channel (I_D) can be expressed as

$$I_D(x) = - \iint J(x) dy dz = - \mu d\Phi/dx \iint n e dy dz = - \mu d\Phi/dx W Q(x) \quad (2.3)$$

where W is the width of the channel and $Q(x)$ is the 2D charge density in the channel.

The charge in the semiconductor channel can be expressed as a function of applied voltages and internal potentials (such as the difference in work function of the metal contacts to the semiconductor channel, the depletion charge and the potential difference between the Fermi level and the intrinsic level) such that

$$Q(x) = -C(V_G - V_{SC}(x) - V_T) \quad (2.4)$$

where C is the capacitance of the gate dielectric layer per unit area and $V_{SC}(x)$ is the voltage across the semiconductor channel.

Equations 2.3 and 2.4 can be combined to give

$$I_D(x) = \mu W C (V_G - V_T - V_{SC}(x)) d\Phi/dx \quad (2.5)$$

With the current through the channel a constant, then

$$I_D = 1/L \int I_D(x) dx \quad (2.6)$$

Inserting Eq. 2.5 into Eq 2.6 and integrating for $x = 0$ to L (with the assumption V_{SC} varies linearly between the source and drain electrodes) then gives the following expression for the current

$$I_D = \mu (W/L) C ((V_G - V_T) V_D - V_D^2/2) \quad (2.7)$$

Two regions of interest can be seen in the output characteristics plot in Fig. 2.8a. Where $V_D < (V_G - V_T)$, referred to as the linear region, Eq. 2.7 can be approximated as

$$I_D = \mu (W/L) C (V_G - V_T) V_D \quad (2.8)$$

For larger values of V_D , referred to as the saturation region, the current saturates and Eq. 2.7 can be approximated as

$$I_D = \mu (W/2L) C (V_G - V_T)^2 \quad (2.9)$$

In practice, both Eqs. 2.8 and 2.9 are used to calculate the mobility of an OTFT and are referred to as the linear field-effect mobility and the saturation field effect mobility, respectively. Since the assumptions used in the derivation of Eqs. 2.8 and 2.9 are not strictly valid for organic materials, the linear and saturation field effect mobilities are not, in general, equal. However, they do represent an agreed upon figure-of-merit for which various OTFT devices can be compared and quantified.

2.5 Determination of Threshold Voltage, On/Off Ratio and Subthreshold Slope

It is standard practice to determine the threshold voltage from a plot of $I_D^{1/2}$ vs V_G . In the saturation region where $V_D < (V_G - V_T)$ a linear fit to the data can be extrapolated back to $I_D = 0$ V. The point where the extrapolation crosses the voltage axis is referred to as the threshold voltage.

The on/off ratio can be determined as the ratio of the largest measured current to the smallest measured current. This can be determined by inspection of a semi-log plot of I_D vs V_G as seen in Fig. 2.9b. The subthreshold slope can be determined from the same plot. It is defined as the change in gate voltage associated with a one-decade change in current in the region below the threshold voltage.

2.6 Determination of Contact Resistance

OTFTs often have a relatively large resistance at the interface between the electrode and semiconductor layer. If this contact resistance is on the order of or larger than the resistance of the semiconductor channel, the current-voltage measurements and thus the calculated mobility values can be adversely affected. It is possible to determine the contact (or parasitic) resistance $R_P = R_S + R_D$ where R_S (R_D) is the resistance at the source (drain) contact. For a set of OTFTs fabricated with different L and the same W , the total resistance, $R_T = R_{CH} + R_P$ (channel resistance plus parasitic resistance), of the OTFT device can be determined from the slope of the linear region of the output characteristics and plotted as a function of

channel length for various gate voltages.³⁹ R_P can then be determined as the intercept ($L = 0$) value of the resistance axis. The mobility can then be corrected for contact resistance³⁹ from this plot using the equation

$$\frac{\partial \left[(dR_{on} / dL)^{-1} \right]}{\partial V_G} = \mu(V_G, T) W C_{gate}, \quad (2.10)$$

where R_{on} is the slope determined from the R_T vs L plot. Equation 2.10 can be obtained from Eq. 2.8 by explicitly accounting for how the resistance (dV_D / dI_D) changes as a function of channel length.

2.7 Growth Properties of Organic Films

One goal of organic electronics has been to develop materials with mobilities approaching or surpassing that of amorphous Si.^{40,41} Since carrier mobility is related to molecular alignment, much effort has gone into studying and optimizing the morphology of organic semiconducting materials of which Pn and P3HT are important and commonly used examples. Thin films of these materials are typically formed onto a carefully prepared substrate by either thermal deposition, spin coating in solution or drop-casting from solution. The growth surface of such a substrate is usually the top surface of the device dielectric layer. This surface does not only influence the growth morphology of the film but also influences carrier transport in the film. Both surface roughness and surface energy are important properties of the substrate. For example, a surface roughness greater than 3 – 5 Å has been associated with decreased mobility in Pn films.⁴²⁻⁴⁴ Also changes in surface energy (by treatment with different self-assembled monolayers) of a SiO₂ dielectric layer or by

the use of different dielectric materials have been correlated with changes in mobility.^{30,45-63} In the majority of cases studied, the observation of changes in morphology have been limited to correlations. The fact that changes in surface energy change the growth mode as well as the electrostatic interactions at the dielectric/semiconductor interface, make it difficult to develop a systematic understanding of the effects on mobility. Overall, it is clear that transport properties of organic semiconducting materials are affected by a variety of issues such as materials purity, deposition conditions, ambient doping, etc. that have not been well controlled in much of the literature.

It is well established, regardless of the deposition conditions, bottom gate – top S/D (i.e. top contact) thin-film transistor (TFT) devices typically exhibit better performance than bottom gate – bottom S/D (i.e. bottom contact) TFT devices.⁶⁴ This has been attributed to better nucleation and growth of the organic film on the dielectric surface as compared to the electrode surface.⁶⁵ For bottom contact devices, the electrodes are patterned onto the dielectric surface prior to deposition of the organic film. Therefore the poor ordering of the organic film at the edge and surface of the electrode is believed to increase the carrier injection barrier.⁶⁶ Thus the presumably favorable geometry, in which the S/D bias is applied directly at the interface where the gate voltage induces the conduction channel, has not been available for use in OTFT devices.

In the alternate geometry with top contact devices, the electrodes are patterned onto both the dielectric surface and over a fully formed organic film. Because organic semiconducting materials are typically sensitive to chemical processing, top

contact electrodes cannot be patterned using photolithography. For this reason they are most commonly thermally deposited through a shadow mask. In the simplest interpretation, the organic film exhibits the same ordering at the edge of the electrodes as in the channel between the electrodes. However, it is known that for the most common electrode material, gold, there is substantial interdiffusion of the deposited gold into the semiconductor film, with unknown effects on the nature of the interface. Furthermore, for this application, shadow masks are limited in resolution to a feature size of about 100 μm .

From the discussion above, it is clear that developing a clean and controllable method for fabricating the interface of S/D electrodes with the organic semiconductor is highly desirable.

2.8 Toward Flexible Circuits

Important goals for the synthesis of organic semiconductor materials have been to improve the mobility of the films and to develop both p-type and n-type materials that can be deposited as thin-films onto flexible substrates. In 1977, Heeger, Shirakawa and MacDiarmid discovered that the conductivity of the conjugated polymer polyacetylene could be varied over 11 orders of magnitude by adding trace amounts of donor or acceptor materials.⁶⁷ For their work, they won the 2000 Nobel Prize in Chemistry. Later, in 1983, Ebisawa reported a field effect behavior using the same material.⁶⁸ One of the first reports of TFT behavior in the organic semiconductor materials P3HT and 6T came from Assadi⁶⁹ in 1988 and Horowitz⁷⁰ in 1989, respectively. The TFT behavior of the small molecule

semiconductor material Pn was reported in 1991.^{71,72} By 1993, Garnier had begun to synthesize a variety of hexyl substituted 6T molecules with α,ω -DH6T exhibiting ordered films with a mobility a factor of 25 larger than 6T. The n-type organic semiconductor material NTCDI was first investigated by Katz²⁸ in 1996. The mobility of this material was improved in 2000 by attaching partially fluorinated side chains to the molecule.

Beyond the synthesis and characterization of organic semiconductor materials for TFT applications is the build-up of integrated circuits. A demonstration of this came as early as 1995.⁷³ In this work, a five stage ring oscillator was fabricated on a Si substrate with both Pn and poly(thienylene vinylene) (PTV) as the active organic semiconductor material. Doped polysilicon was used as the gate electrode with gold S/D electrodes deposited onto a silicon nitride dielectric layer. Integrated circuits consisting of all polymer components on a flexible substrate were demonstrated in 1998.³⁴ A 15 bit mechanically programmable code generator was fabricated on a polyimide substrate with PTV as the organic semiconductor material.⁷⁴ PANI was used to fabricate electrodes that were separated by a poly(hydroxystyrene) (PHS) dielectric layer.³⁴

The fabrication of these electronic circuits based on organic materials has typically been done using traditional processing methods such as photolithography and thermal evaporation. These methods use hazardous chemicals and complex, costly equipment. Such techniques were designed for fabricating devices from inorganic materials and therefore, do not necessarily exploit the properties of organic materials. The real advantage of flexible electronics will come from the development

of simple, cost effective methods for fabricating large volumes of flexible, light-weight electronics that have been specifically designed and optimized to take advantage of the unique properties of both organic semiconductor materials and flexible substrates.

Chapter 3 Printing

3.1 Introduction

Printing is an ancient art dating back to the 8th and 9th centuries A.D. An example of such a printed work is the Diamond Sutra, shown in Fig. 3.1. This was fabricated using a technique referred to as block printing. Printing using movable type based on clay⁷⁵ was invented in 1041 and based on metal⁷⁶ in 1232. Ushering in a more modern style of printing, Gutenberg is credited with having invented the modern printing press in the 1450s. Lithography, which is a form of printing based on a planographic process that relies on patterning inks onto a flat surface using hydrophilic and hydrophobic interactions, was invented in 1798.

The semiconductor industry has developed a form of pattern transfer for the fabrication of solid-state electronics based on Si called photolithography. The technique relies on a change in solubility of a photo-sensitive film (photoresist) when exposed to ultraviolet (UV) light. The photoresist is applied to and patterned on Si wafer substrates in the manufacturing of computer chips and on glass substrates in the manufacturing of flat panel displays. Either way, the fabrication methods are limited to batch processing of finite size substrates. Serious efforts are underway to develop larger scale manufacturing processes that can fabricate electronic devices in a continuous fashion in a manner more similar to the fabrication of magazines or newspapers. In order to accomplish this, the added requirement of flexible substrates will be needed. As a testimony to the importance of such efforts, Xia¹⁰ lists no less than 18 different non-photolithographic patterning methods being developed to

fabricate devices at the micrometer and nanometer length scales. The table is reproduced here as Table 3.1. The earliest reference dates back to 1974, with a majority of the references coming from the 1990's. Even though printing is an old technique with a rich history in fabricating and/or reproducing images and writing, it is being revisited as a method for fabricating active electronic devices and circuits.



Figure 3.1: Diamond Sutra. One of the oldest known examples of a printed document. [By permission of the ©British Library Board. All Rights Reserved]

Method	Resolution ^[a]	Ref.
Injection molding	10 nm	77-82
Embossing (imprint)	25 nm	83-91
Cast molding	50 nm	92-94
Laser ablation	70 nm	95-100
Micromachining with a sharp stylus	100 nm	101
Laser-induced deposition	1 μm	102,103,104
Electrochemical micromachining	1 μm	105
Silver halide photography	5 μm	106,107,108
Pad printing	20 μm	109
Screen printing	20 μm	110
Ink-jet printing	50 μm	111-115
Electrophotography (xerography)	50 μm	116,117
Stereolithography	100 μm	118-121
Soft lithography		122-125
Microcontact printing (μCP)	35 nm	13,14
Replica molding (REM)	30 nm	126
Microtransfer molding (μTM)	1 μm	127
Micromolding in capillaries (MIMIC)	1 μm	128
Solvent-assisted micromolding (SAMIM)	60 nm	129

[a] The lateral dimension of the smallest feature that has been generated. These numbers do not represent ultimate limits.

Table 3.1. Non-photolithographic methods for micro- and nanofabrication.¹⁰

Various types of printing techniques will be reviewed in this chapter as they pertain to the patterning and/or assembly of components needed to fabricate active electronic devices.

The printing industry has been primarily interested in reproducing pictures and/or text on a page. Both are passive features composed of two components - an ink and a substrate (the page). The ink is designed for passive color and high visual contrast against the substrate. The substrate can be made from various materials such as paper, plastic, metals, glass, etc. For the printing of active devices the substrate materials may not change much but the 'inks' will have to be very different. Visual contrast and passive color will no longer be important properties. Admittedly, transparency over certain optical ranges may be important for some applications; however, active 'inks' will primarily be chosen for their conductivity, semiconducting properties or insulating properties. Such 'inks' will need to be prepared and processed in ways that optimize these properties. This will most likely require techniques very different from those used to prepare and process passive inks, therefore traditional printing techniques will be only briefly discussed. The bulk of this chapter will be dedicated to introducing and reviewing printing methods being developed that will meet the needs for printing active materials.

3.2 Traditional Printing

Traditional printing as defined here includes techniques such as gravure printing, pad printing, screen printing and flexography. With these techniques, an ink

is spread on a plate or drum that contains regions that hold or store the ink. An example of a gravure cylinder is shown in Fig. 3.2a. The engraved cells hold the ink, which is then transferred to the substrate upon printing. Pad printing is similar to gravure printing but incorporates an additional step with the ink first transferred to a pad and then transferred off the pad to the substrate upon printing as shown in Fig. 3.2b. Screen printing involves ink being squeegeed through a screen where the image to be printed is contained in the screen. The holes in the screen allow ink to be transferred to the substrate as illustrated in Fig. 3.2c. Flexography uses a flexible rubber (or photopolymer) plate that contains a raised image. The flexible plate is attached to a cylinder and the raised image is covered with ink. The ink is then transferred from the raised surface to the substrate as shown in Fig. 3.2d.

The uniformity in these traditional printing methods is governed by how evenly the ink can be distributed across the printing surface. This is typically achieved by carefully controlling the rheology of the ink and spreading the ink onto a series of rollers.¹³⁰ Inks are highly engineered substances that contain pigments (for color), resins (for wettability, tack and gloss), solvents (for resin solubility and ink fluidity) and additives (for rub resistance, drying characteristics, ink body, etc.). These inks must be able to uniformly coat the printing plate (or cylinder) without drying and must be able to be transferred to the substrate without spreading. They must dry quickly once printed and not rub off the substrate. They must also retain a high visual contrast and not fade over time. The mixing and spreading process that these inks are subjected to can be both mechanically and chemically harsh.

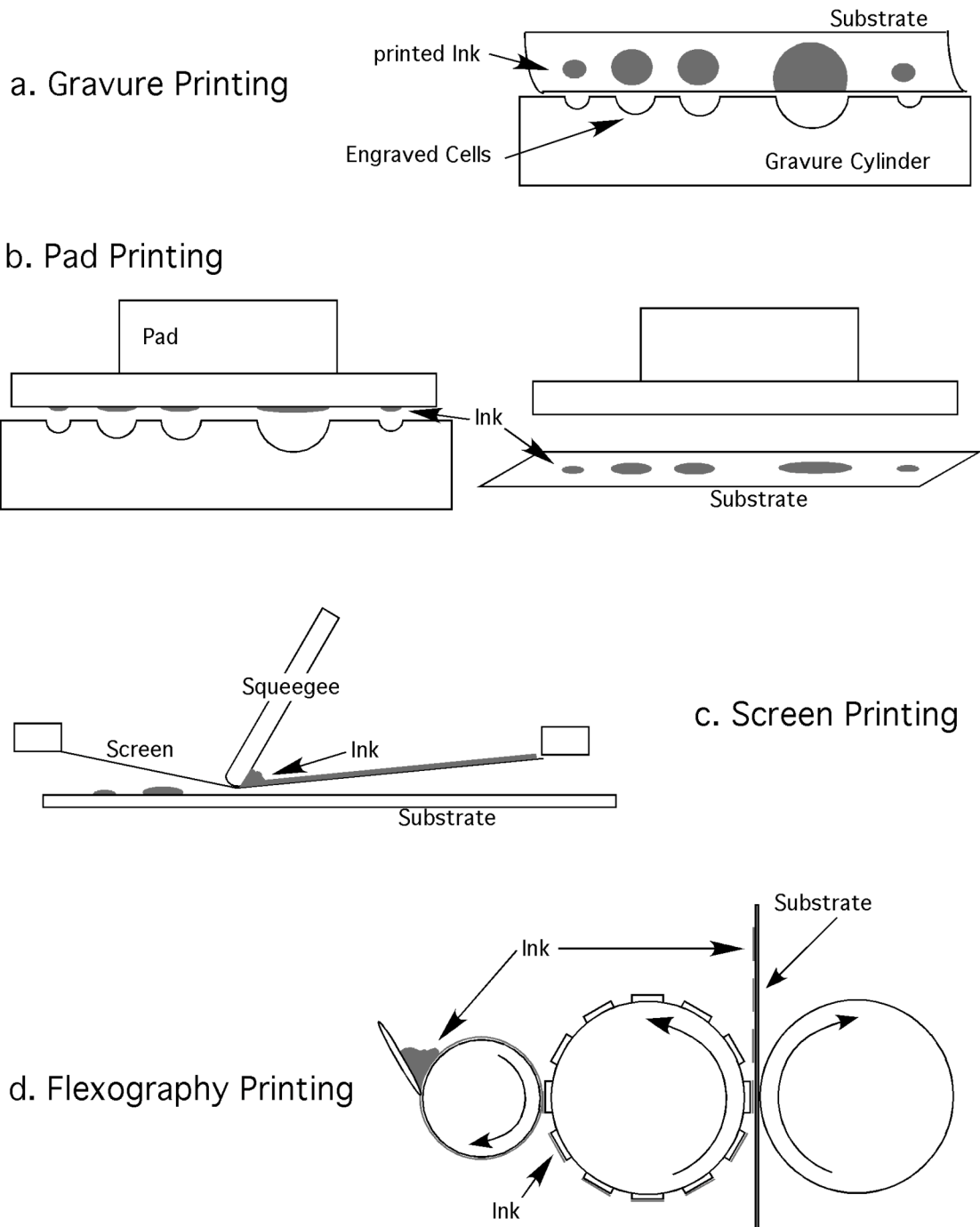


Figure 3.2: Examples of different types of traditional printing. a) gravure printing, b) pad printing, c) screen printing and d) flexography printing. [Adapted from Gamota¹ Figs 3.4.2, 3.5.1, 3.6.1 and 3.3.1]

This works well for passive inks that have been optimized for high visual contrast but, in general, may not be compatible with active inks that will need to be optimized for characteristics such as electrical properties. Therefore it will be necessary to look beyond traditional printing methods in order to develop printing techniques compatible with active materials.

3.3 Electrophotographic Printing

The most common form of electrophotographic printing is laser printing which was developed as a form of photocopying. With this technique, the ink is a very fine powder referred to as toner. The toner is fed using a roller. The image to be printed is created by exposing a photoconductive drum to laser light. The photoconductive drum becomes negatively charged where exposed to light. The toner adheres to the negatively charged areas on the drum and is then transferred to a substrate by a positive charge generated under the substrate. To date this type of printing has not found much success in the printing of active materials for flexible electronics.

3.4 Inkjet Printing

Inkjet printing¹⁵ is a digital form of printing that can be performed either in a continuous mode or a drop-on-demand mode. For the continuous mode, a stream of droplets passes through a set of signal drive electrodes. An electrical pulse to the electrodes causes a droplet to be deflected to the substrate. Undeflected droplets are collected and recirculated back to the ink reservoir. For the drop-on-demand modes,

a piezoelectric pulse is used to create a droplet by pushing ink through a nozzle. Nozzles are typically 20 – 30 μm in diameter and create ink droplets of about 10 – 20 pL. Droplet-on-demand mode results in better printing quality when compared to continuous mode inkjet printing with feature resolution on the order of 20 – 50 μm for standard inkjet printing.

Viscosity and surface tension are important parameters of the ink. Ink must fill the nozzle in approximately 100 μs and not drip out between demands. This typically requires a viscosity range of 2 – 100 cp and a minimum surface tension of about 35 mN/m. To prevent the ink from drying and clogging the nozzle, a liquid such as ethylene glycol can be added at a level of 10 – 20%. If an ink contains particulates, the particulates must remain uniformly suspended in the ink and not contribute to clogging in the nozzle. This usually requires a particulate size less than 1 μm .

High molecular weight polymers tend to be too viscous to easily print using inkjet printing. However inkjet printing of waxy and low molecular weight polymers is possible. Printed droplets can exhibit pinholes and can have a tendency to bead up when printed onto non-absorbent substrates (such as plastics). Also, edge roughness and printing resolution can be affected by droplet spreading characteristics and can be difficult to control. Some material's printing problems can be overcome by incorporating additives into the ink that can be post processed, such as the addition of UV curable polymers. Also precursor materials can be used directly as inks that are post processed such as precursor metal solutions.

A wide range of materials have been successfully inkjet printed. Calvert¹⁵ lists nanoparticle suspensions, sol-gels, conducting polymers, ceramic powders, solder, DNA and proteins as materials that have been inkjet printed. All of these materials must either be suspended or dissolved in order to be inkjet printed. Some organic semiconductor materials tend to be insoluble (pentacene for example) and, therefore, soluble forms of these materials have been investigated.¹³¹ Other organic semiconductor materials tend to be very sensitive to drying conditions such as P3HT.¹³² In either case inkjet printing of these materials has, to date, typically resulted in low quality films.

There have been attempts to improve the resolution associated with inkjet printing. One method used an undisclosed print head technology as part of a super-fine inkjet printing system.¹³³ This system is reported to have achieved a line width of 3 μm . Also, Sirringhaus¹³⁴ has developed a droplet-on-droplet technique in which the second droplet does not wet the first droplet. When printed, the second droplet slides off the first droplet, producing a sub 100 nm gap between the printed features, which are then used as source/drain electrodes for an OTFT device.

3.5 Soft Lithography

Photolithography is a well-known method for patterning flat surfaces. A layer of photoresist is spread uniformly on a surface and exposed with visible or UV light through a mask containing a pattern. The photoresist is then developed to expose the underlying surface only in the patterned area. The photoresist layer can then be used as an etch mask or as a window through which other materials can be deposited onto

the underlying surface. Photolithography has been used for decades in the fabrication of inorganic electronics; however, it has several disadvantages that limit its usage for non traditional materials: it allows for very little variation in the chemistry of either the resist layer or the substrate and it can only be performed on flat surfaces in a batch processing mode.

In an attempt to go beyond the limitations of photolithography, soft lithographic methods have been developed, as listed in Table 3.1. Soft lithography encompasses techniques such as microcontact printing^{13,14} (μ CP), replica molding¹²⁶ (REM), microtransfer molding¹²⁷ (μ TM), micromolding in capillaries¹²⁸ (MIMIC), and solvent-assisted micromolding¹²⁹ (SAMIM). These techniques all have in common a patterned elastomeric mold or stamp [typically made from polydimethylsiloxane (PDMS)]. Since the stamp (mold) is flexible, these techniques are compatible with non-flat surfaces.

Soft lithography techniques have also been used to print patterned layers from PDMS stamps onto substrates. For example, Au evaporated onto the patterned surface of a PDMS stamp and then treated with a thiol terminated SAM has been printed onto a GaAs substrate.¹³⁵ Also PDMS features have been printed onto Si substrates by treating the patterned surface of a PDMS stamp with a fluorinated SAM and then adding an extra layer of PDMS.¹³⁶ When contacted to the Si substrate, the top layer of PDMS can be transferred to the Si surface.

Unlike photolithography, which transfers a pattern using optical techniques, soft lithography is a direct printing method. Also, the stamp (mold) can be replicated from a reusable master template. Therefore, soft lithography has the potential to be a

less complex and less expensive method of patterning compared to photolithography. Additionally soft lithographic techniques can be used to directly pattern a wider range of surfaces comprised of polymers, sol-gels, biological materials, organic thin films and colloidal materials, in addition to inorganic surfaces.

3.6 Nanoimprint Lithography

In addition to the limitations discussed above, pattern sizes produced by photolithography are limited by the resolution of the optical system used to transmit light through the mask. Through decades of hard (and smart) work this resolution limit has been steadily reduced at, however, the expense of increased complexity and cost of the fabrication equipment. Nanoimprint lithography⁹⁰ (NIL) has been developed as a patterning technique that can simultaneously improve pattern resolution and reduce both equipment complexity and cost. It is based on a rigid template containing a patterned surface. The template is pressed into a resist layer that has been coated onto a substrate. Two types of NIL have been developed and are referred to as hot and cold embossing. Hot embossing uses a thermoplastic resist layer and cold embossing uses a UV curable liquid layer. The general process is illustrated in Fig. 3.3a.

In hot embossing, the patterned template surface is placed in contact with the thermoplastic resist layer. The resist layer is heated up above its glass transition temperature and the template is pressed into the resist layer. After a specified time the resist layer is cooled down below its glass transition temperature and the pressure

is released. The template is then removed to reveal a replica of the template surface contained in the surface of the resist layer.

In cold embossing [sometimes referred to as step-and-flash imprint lithography¹³⁷ (SFIL)] the patterned template surface is placed in contact with a UV curable liquid layer. The resist layer is then cured by exposure to UV light. The template is then removed to reveal a replica of the template surface contained in the surface of the resist layer. In this case, the template (or possibly the substrate) must be transparent to UV light. This is similar to replica molding¹²⁶ which typically uses a flexible template; however, SFIL has been developed using a rigid, transparent template.

Several variations of hot embossing have been reported^{138,139} as a means of reducing the operating pressure and/or temperature. One technique eliminates the resist layer entirely.¹⁴⁰ NIL is also being expanded to include imprinting into a variety of active materials as opposed to sacrificial resists.¹⁴¹ The resolution of NIL has been demonstrated at the 10 nm level.¹⁴² Most of the developmental work associated with NIL is directed toward inorganic substrates and is targeted as a disruptive technology competing against photolithography and e-beam lithography.

As is illustrated in Fig. 3.3b, the same processing method used for NIL can be used to transfer a patterned layer (printable layer) from one substrate (the transfer substrate) to a second substrate (the device substrate). The only requirement is that the printable layer adhere more strongly to the device substrate than to the transfer substrate. This process was developed during this thesis research and will be referred to as transfer printing. In general, the transfer printing process does not rely on

temperature, but only on contact of the printable layer to the surface of the device substrate where an appropriate differential adhesion exists between the two interfaces containing the surfaces of the printable layer. Think of decals for detailing model cars and airplanes or temporary tattoos.

It is with such a process that we wish to develop the ability to fabricate flexible electronics. Plastic substrates present an obvious choice of materials for this application, not only because they are flexible, but also because of their low density, optical clarity, low cost, compatibility with roll-to-roll processing, etc. There are two main classes of plastics – thermoplastics and thermosets. Once fully cured, thermoset plastics are highly cross-linked polymers that are not easily reprocessed. They are used extensively as adhesives, of which epoxy is an example. In contrast, thermoplastic polymers can be reprocessed by heating to a temperature above their glass transition temperature. This is the temperature at which the viscosity of the thermoplastic material is low enough for the materials to flow. In general, both types of plastic should be compatible with the transfer printing process. However, the contents of this thesis will primarily be limited to the incorporation of thermoplastic polymers into the fabrication of flexible electronics as both substrate and dielectric materials.

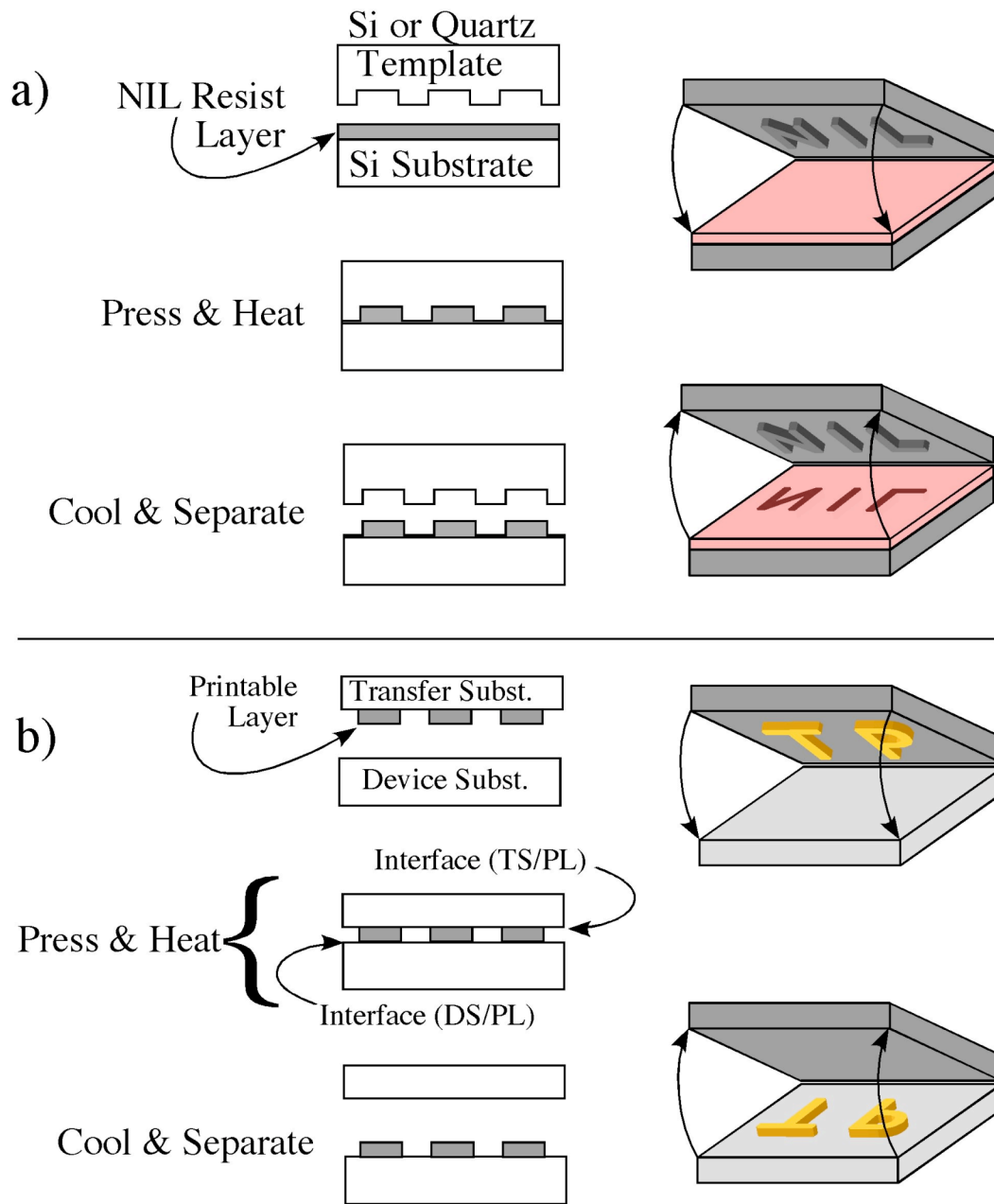


Figure 3.3: Illustration of a) Nanoimprint Lithography (NIL) and b) the transfer printing method.²²

In Chapter 4, the transfer printing method will be presented as a general process for transferring a variety of printable materials onto thermoplastic substrates. The process will be extended to allow the sequential assembly of all the components needed to fabricate organic thin-film transistors (OTFTs) onto a single, flexible, plastic substrate. Each component, be it a metallic electrode, a polymer dielectric film or an organic semiconductor film, will be printed in the same manner (elevated pressure and temperature for some period of time) thus avoiding both the complexity of mixed processing methods and the use of harsh or incompatible chemicals. Unlike other printing processes such as inkjet¹⁴³ and micro-contact printing^{144,145}, the transfer printing process is inherently compatible with nano-scale features¹⁶ and the resulting devices will be shown in Chapters 6 and 7 to be as good as or better than similar reference devices fabricated on inorganic, rigid substrates using traditional processing methods.

Chapter 4 Transfer Printing Methods

4.1 Introduction

In the previous chapter, transfer printing was introduced. The process is relatively simple and is expected to be compatible with many different materials (both organic and inorganic). The technique relies on differential adhesion, which can be understood in terms of the work of adhesion at the interfaces between the printable layer and the transfer substrate and between the printable layer and the device substrate. These interfaces are labeled as (TS/PL) and (DS/PL) respectively as previously noted in Fig. 3.3b.

The work of adhesion (cohesion) can be defined as the reversible work done to separate unit areas of two different (identical) materials from contact to infinity, in vacuum.¹⁸ The works of cohesion and adhesion can be related to the surface energies of a materials in the following ways

$$W_C(i) = 2\gamma_i \quad (4.1)$$

$$W_A(i/j) = \gamma_i + \gamma_j - \gamma_{ij} \quad (4.2)$$

where γ_i is the surface energy of materials i and γ_{ij} is the interfacial energy. Equation 4.2 is referred to as the Dupré equation.¹⁸

When printing an unpatterned layer (a uniform material that covers the surface of the transfer substrate) to a uniform device substrate, the work of adhesion of the printable layer is required to be larger at the interface with the device substrate (interface DS/PL) than at the interface with the transfer substrate (interface TS/PL).

The requirement for the differential adhesion is straightforward:

$$W_A(DS/PL) > W_A(TS/PL) \quad (4.3)$$

When Eq. 4.3 is satisfied, the printable layer will remain on the device substrate once the transfer substrate is removed. However, if the print material's work of cohesion is less than the works of adhesion for the printable layer with both substrates ($W_A(DS/PL)$ and $W_A(TS/PL) > W_C(PL)$), then the printable layer will be only partially transferred. Such a partial printing is referred to as inking.

If, during the transfer printing process, the transfer substrate makes contact with the device substrate (as would be the case for a patterned printable layer) then, in addition to Eq. 4.3, the work of adhesion between the substrates must be less than the work of cohesion of both of the substrates so that the substrates do not stick together and can be cleanly separated, that is

$$W_C(DS) \text{ and } W_C(TS) > W_A(DS/TS) \quad (4.4)$$

must be satisfied.

A printable layer can contain multiple layers and can also be sequentially assembled onto a device substrate, as illustrated in Fig 4.1. For this, the work of adhesion at the interface between the transfer substrate and the printable layer must be less than the work of adhesion associated with all other interfaces between surface i and surface j and also less than the work of cohesion of all other layers. These adhesion and cohesion requirements for sequential and multiple layer printing are expressed as

$$W_A(TS/PL) < W_A(i/j) \text{ and } W_C(i) \quad (4.5)$$

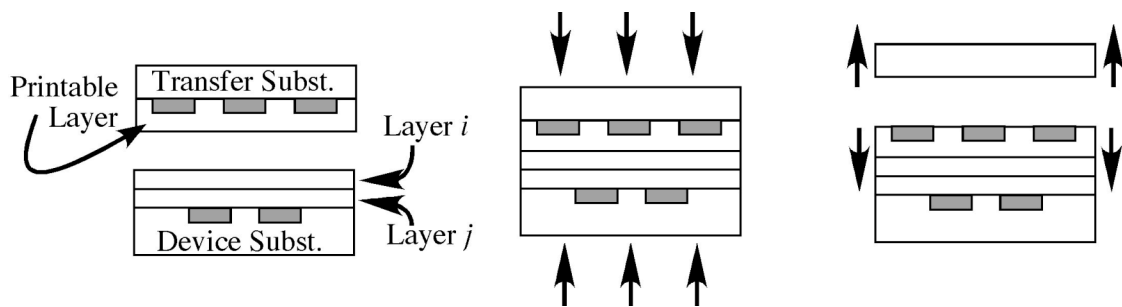


Figure 4.1: Illustration of the transfer printing method for simultaneous printing of multiple layers and for sequential printing of layers.²²

4.2 Transfer Printing Procedure

Transfer printing was accomplished using a Nanonex 2500 imprint machine, which uses a sample configuration as shown schematically in Fig. 4.2. This machine utilizes gas as the pressure medium, allowing imprint pressures up to 600 PSI and three 500 Watt tungsten-halogen lamps as the heat source, allowing a maximum temperature of 300 °C. In general, a transfer substrate containing a printable layer is placed onto a device substrate with the printable layer sandwiched between the two substrates. The substrates are placed in the imprint machine between two silicone rubber sheets. The imprint chamber is closed and evacuated to a pressure of -14 PSI for 3 min. and the rubber sheets are mechanically sealed together by a solenoid actuated metal ring, resulting in a vacuum seal around the substrates. The desired chamber pressure and sample temperature is achieved by back-filling the imprint chamber with dry nitrogen gas and then turning on the lamps. The lamps are PID (proportional, integral, derivative) controlled and the temperature is monitored by a thermocouple in contact with a Si wafer positioned in contact with the bottom rubber sheet as illustrated in Fig. 4.2. Alignment of features in sequential printing steps was

performed prior to insertion into the printing chamber using a Nanonex 2500 manual contact aligner that was modified to hold 1 cm square substrates.

To characterize the success of a transfer print, both the transfer substrate and the device substrate were observed visually under an optical microscope. In addition, a height profilometer and an atomic force microscope were used to measure surface profiles and changes in surface properties resulting from a transfer print.

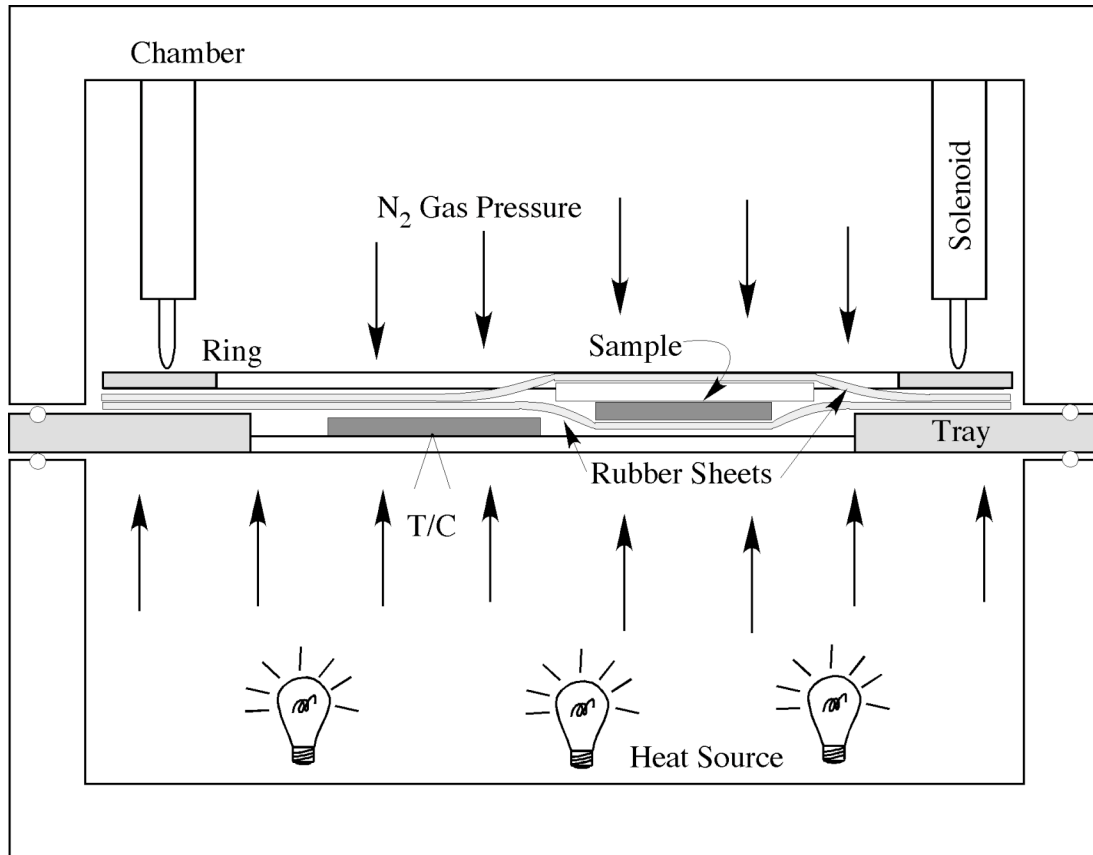


Figure 4.2: Schematic illustration of the transfer print configuration. The top and bottom sections of the chamber seal against the sample tray. The solenoids engage the ring against the sample tray to vacuum seal the sample (transfer substrate/printable layer/device substrate stack) between two silicone rubber sheets. The chamber is pressurized using N₂ gas and heated using three, 500 Watt lamps. The temperature is measured with a thermocouple (T/C) in contact with a Si wafer piece.²²

As an illustration of what is possible with transfer printing a number of examples are presented below.

4.3 Gold Printed onto Plastic

Figure 4.3 shows an example of 200 nm wide Au lines transfer printed onto a PET device substrate. The Au lines were fabricated onto a Si transfer substrate using e-beam lithography. A typical printing condition for Au onto PET is 500 PSI and 170 °C for 3 min. Figure 4.4 shows a similar example of a 200 μ m wide Au line printed onto PET. The Au line was fabricated onto a Si transfer substrate using photolithography. Prior to printing, the Au line was used as an etch mask for the Si transfer substrate that was subsequently plasma etched in a PlasmaTherm 790 to a depth of 700 nm. After printing, the Au feature was found to be embedded below the plastic surface by the depth of the substrate etch, as shown in the accompanying graph from a line profile scan. As a third example, Fig. 4.5 shows a serpentine Au line printed onto a kapton substrate. The Au line was fabricated onto a Si transfer substrate using photolithography. Before printing, polyimide (HD-2562 from Miro-Systems) was spin coated (for example at 4000 rpm for 60 sec. and baked at 110 °C for 3 min.) onto the transfer substrate containing the patterned metal line. The double layer was then transfer printed at 250 PSI and 150 °C for 3 min.

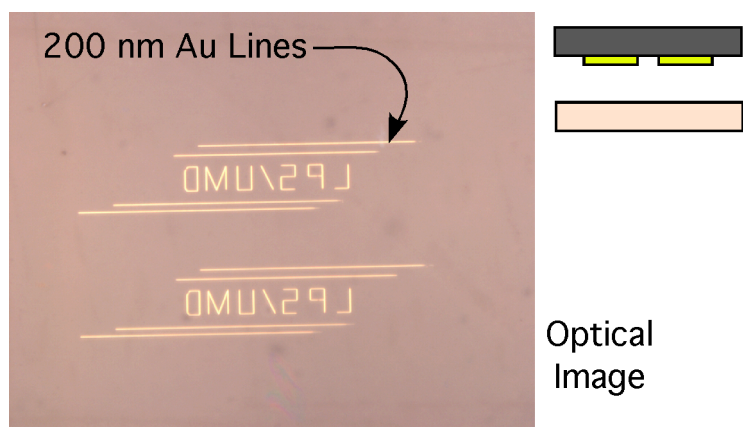


Figure 4.3: Optical image of 200 nm Au lines transfer printed onto a PET substrate.²¹

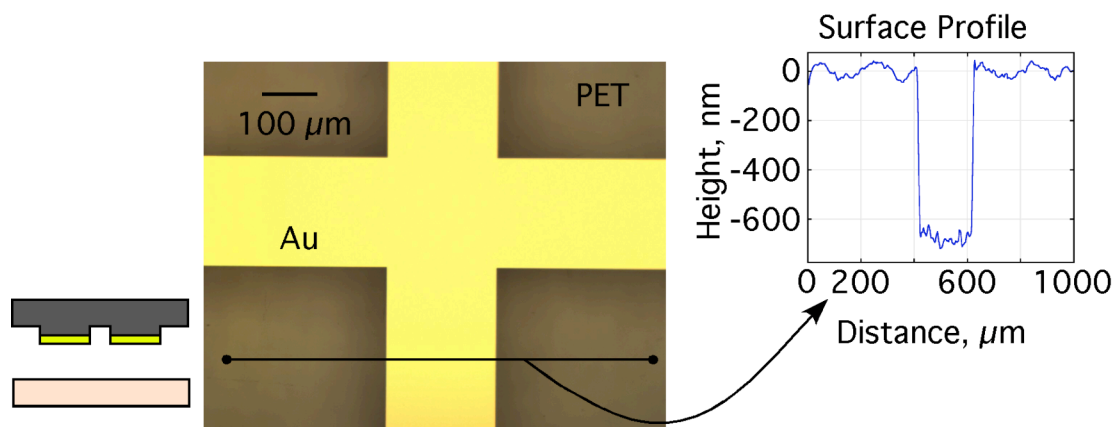


Figure 4.4: Optical image of a 200 μm Au line transfer printed onto a PET substrate. Prior to printing, the Au was used as an etch mask and the Si substrate was etched to a depth of 700 nm. The profilometer scan shows that the Au line is embedded below the surface of the PET substrate by the depth of the transfer substrate etch.¹⁴⁶

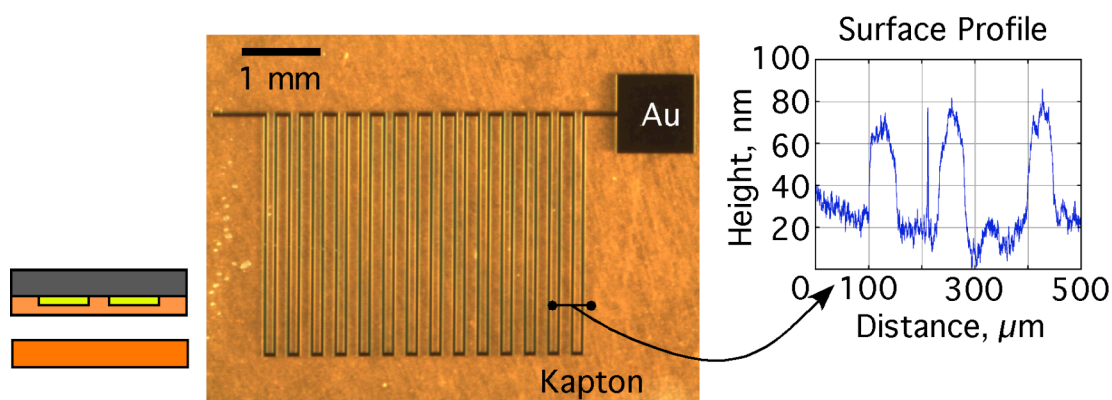


Figure 4.5: Optical image of a Au serpentine line transfer printed onto a Kapton substrate. The profilometer scan shows that the Au lines protrude above the surface of the kapton.¹⁴⁶

4.4 Pentacene Printed onto Plastic

Figure 4.6 shows three examples of pentacene transfer printed onto a) PVC, b) PET and c) latex device substrates. As will be discussed in detail later, the optimum printing conditions for Pn are 600 PSI and 120 °C for 3 min. Figure 4.7 shows the result of a Pn film printed onto a patterned layer of photoresist. The Pn film was thermally deposited onto a SiO_2/Si transfer substrate in a high vacuum deposition chamber. A layer of photoresist was spin coated and patterned onto a Si device substrate using standard photolithography. The photoresist pattern contained features in the resist layer that were at least 2 mm long and separated by approximately 4 μm . This example illustrates that transfer printing can be employed to both print and pattern a Pn film. Figure 4.8 shows an example of transfer printing a bilayer containing both Au and Pn films. Here a Pn film was thermally deposited onto a SiO_2/Si transfer substrate in a high vacuum deposition chamber. Then, a Au film was thermally deposited through a shadow mask. The SiO_2/Si transfer substrate

contained regions of just Au, regions of just Pn and regions of Au over Pn. All three regions were successfully transfer printed as can be seen in the figure.

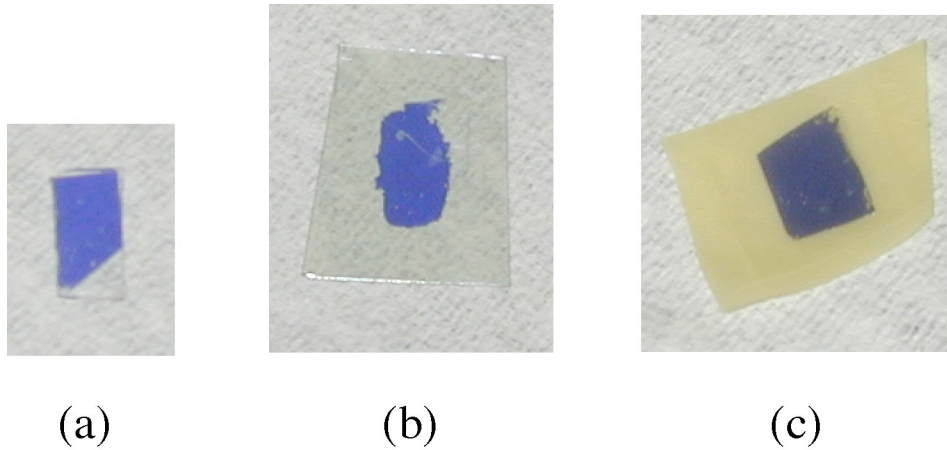


Figure 4.6: Optical images of Pn films transfer printed onto (a) PVC, (b) PET and (c) latex substrates.¹⁴⁶

4.5 Inorganic Features Printed onto Plastic

Figure 4.9 shows an example of InP bars printed onto a PET device substrate that contained an electrode subassembly from previous printing steps. The InP bars were fabricated as part of a MEMS device.¹⁴⁷ They were suspended above an air gap and connected to the transfer substrate only at the ends of each bar. For this example the requirements for transfer of a bar was that the adhesion of the bar to the surface of the device substrate be larger than the mechanical strength of the connection at the ends of the bar. Based on this example and other work,^{148,149} it is expected that many other inorganic materials and geometries can also be transfer printed.

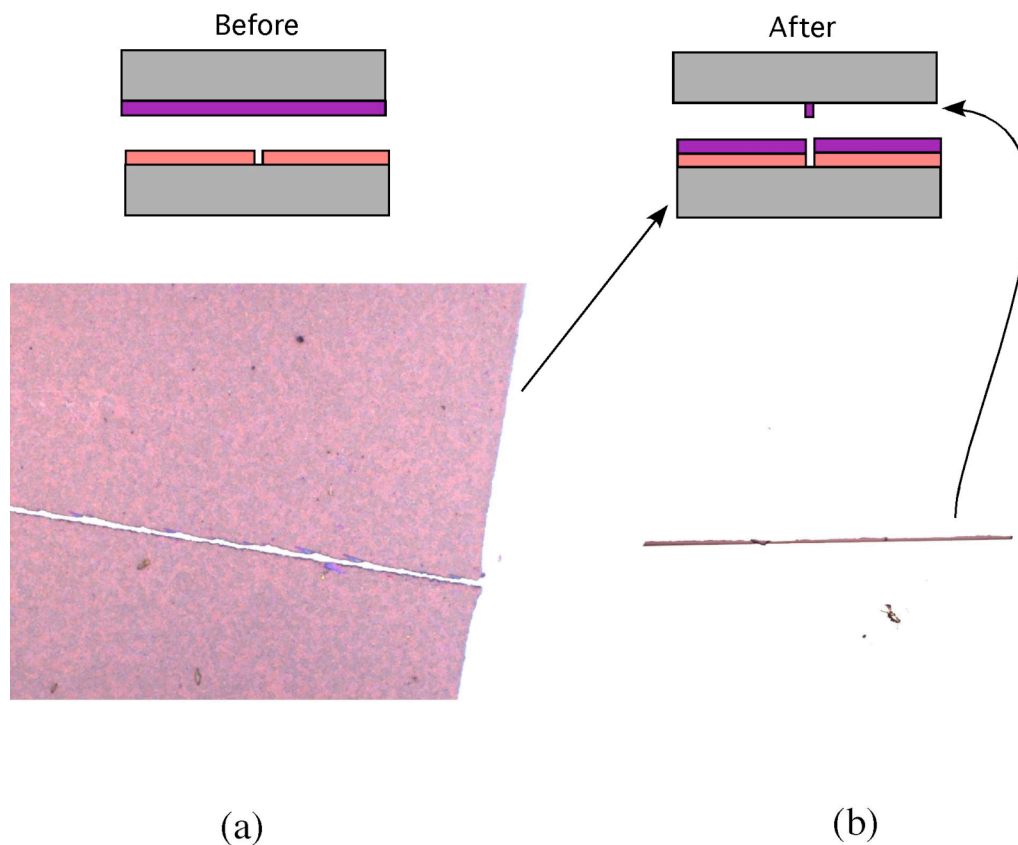


Figure 4.7: Optical image of a $4\mu\text{m}$ line patterned into a Pn film. As shown in the before and after illustrations, the Pn was patterned by transfer printing against a patterned layer of photoresist.¹⁴⁶

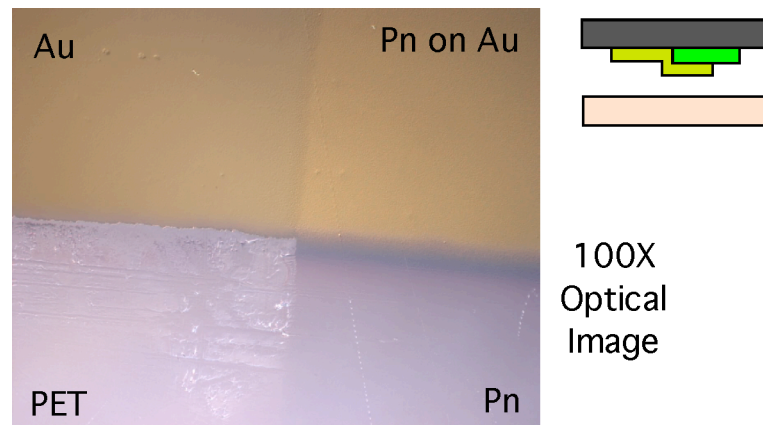


Figure 4.8: Optical image of a Pn/Au bilayer transfer printed onto a PET substrate.²¹

Although the focus of this thesis is organic electronics on flexible substrates, the ability to print inorganic objects patterned at the micron or submicron scale onto plastic substrates presents compelling opportunities for the fabrication of versatile, high-speed flexible electronics.¹⁵⁰ This should be seriously considered as an important direction for future work.

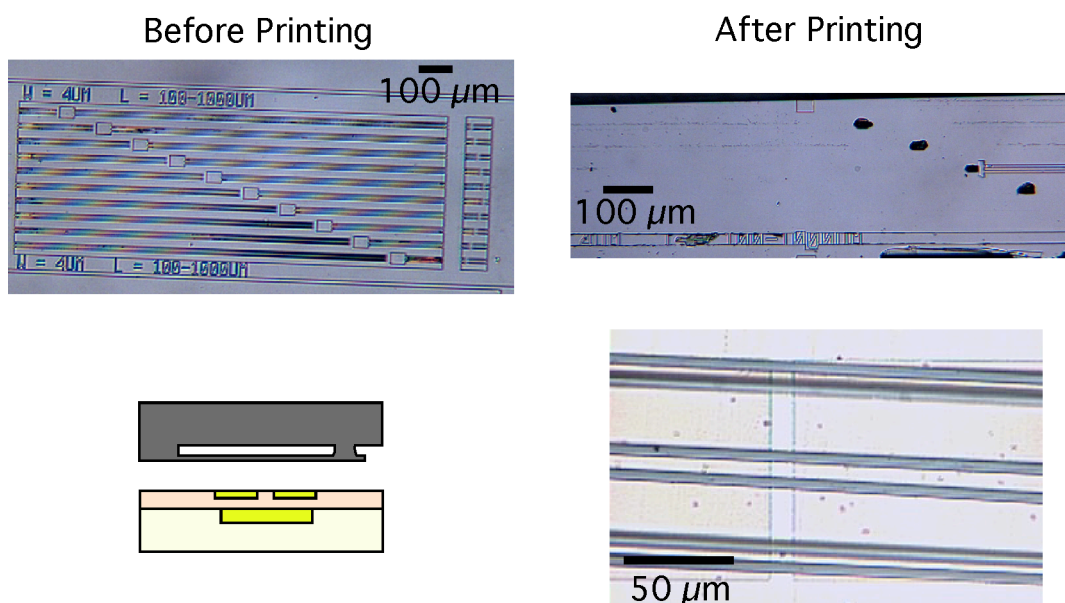


Figure 4.9: Optical image of InP bars transfer printed onto a PET substrate containing previously printed electrodes. The top left image shows the InP substrate containing the bars prior to printing. The top right image shows the InP substrate after printing. The bottom right image shows the InP bars after having been printed onto the PET substrate.¹⁴⁶

4.6 Carbon Nanotubes Printed onto Plastic

Figure 4.10 shows an example of a network of carbon nanotubes (CNT) printed onto a PET substrate. A set of electrodes were first printed onto the PET substrate and then a patterned CNT network was aligned with and printed onto the

device substrate surface (which included areas of both Au and PET). The CNT network was grown via CVD using Fe catalyst particles on a SiO₂/Si substrate with methane and ethylene feed gasses. The network was patterned using standard photolithography to define areas where the CNTs were protected by photoresist. The CNTs not protected by the patterned photoresist were removed using an oxygen plasma treatment. After patterning the CNT network, the protective layer of photoresist was removed with acetone.

Spray coated CNT films have also been transfer printed onto both Kapton and polycarbonate (PC) substrates, as shown in Fig. 4.11(a) and (b) respectively. CNTs purchased from Carbon Solutions were dispersed in deionized water containing sodium dodecyl sulfate surfactant molecules to minimize clumping. A 0.1% solution was spray coated onto a SiO₂/Si transfer substrate through a metal stencil mask. For the example in Fig. 4.11a, the transfer substrate containing the CNT film was spin coated with polyimide (HD-2562 from Miro-Systems) at 4000 rpm for 60 sec. and baked at 130 °C for 3 min. The CNT/PI bilayer was then transfer printed onto a Kapton device substrate at 250 PSI and 150 °C for 3 min. For the example in Fig. 4.11b, the transfer substrate containing the CNT film was spin coated with a 7 wt% solution of PC in cyclohexanone at 2500 rpm for 60 sec. and baked at 90 °C for 3 min. Prior to use, the PC solution was heated to 90 °C and filtered through a series of filters with the last step using a 0.2 µm filter. The CNT/PC bilayer was then transfer printed onto a PC device substrate at 500 PSI and 150 °C for 3 min.

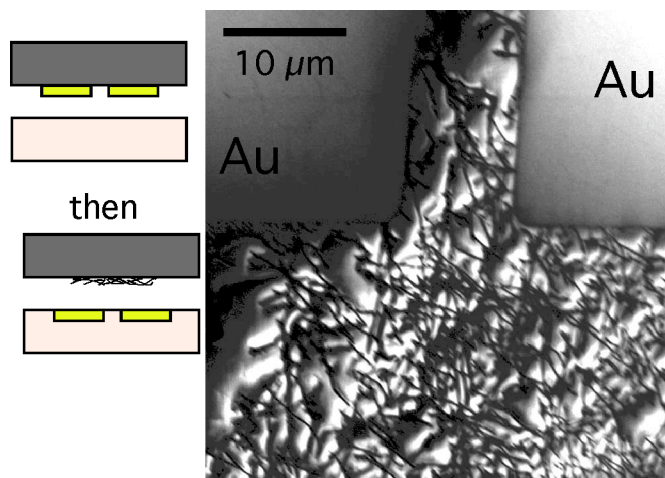


Figure 4.10: SEM image of CNT network transfer printed onto a PET substrate containing previously printed Au electrodes.¹⁴⁶

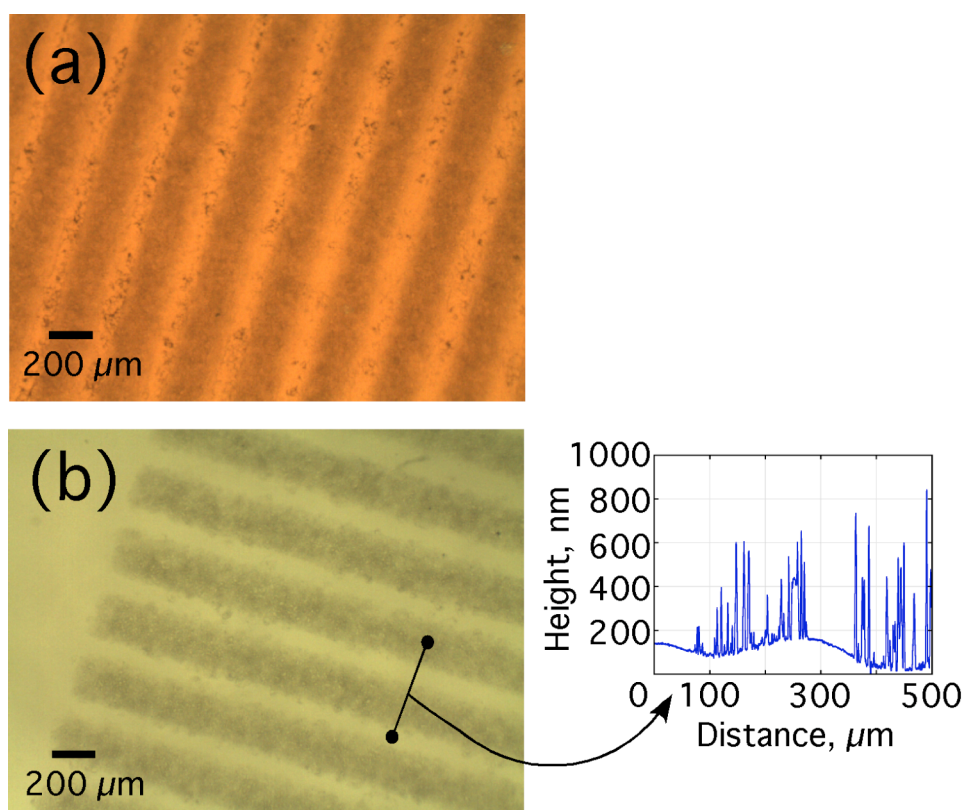


Figure 4.11: Optical images of spray coated CNT films after having been transfer printed onto (a) Kapton and (b) polycarbonate substrates. The profilometer scan shows the roughness of the polymer/CNT surface after printing. Courtesy of A. Southard, UMD.¹⁴⁶

4.7 Metallic Nanowires Printed onto Plastic

Figure 4.12 shows an example of network of Ag nanowires that were printed onto a PET device substrate.¹⁵¹ 200 nm diameter Ag nanowires were electrochemically grown in the pores of a commercially available alumina membrane. The nanowires were harvested, dispersed in water and drop-cast onto a SiO₂/Si transfer substrate. The nanowire network was printed onto a PET device substrate at 500 PSI and 175 °C for 3 min. In general the diameter of the nanowires and the density of the network can be changed, thus providing a control of both the transparency and resistance of the printed network.¹⁵¹

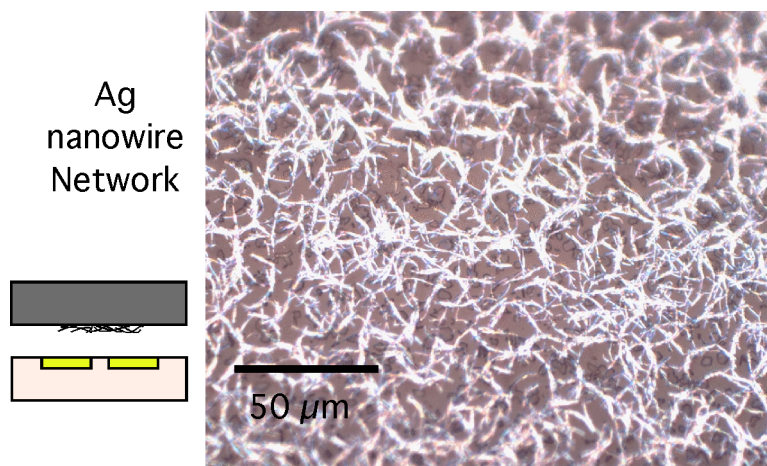


Figure 4.12: Optical image of Ag nanowires printed onto a PET substrate.¹⁴⁶

4.8 Single Atomic Layers Printed onto Plastic

Figure 4.13 shows an example of a graphene sheet (single atomic layer of graphite) printed onto a PET device substrate containing a previously printed set of electrodes).¹⁵² The graphene sheet was obtained by rubbing graphite onto the surface

of a SiO_2/Si transfer substrate. A set of electrodes were first printed onto the PET substrate and then the graphene sheet was aligned with and printed onto the device substrate surface (which included areas of both Au and PET). This image shows part of a flexible graphene TFT device (before the addition of the gate electrode and dielectric layer).¹⁵²

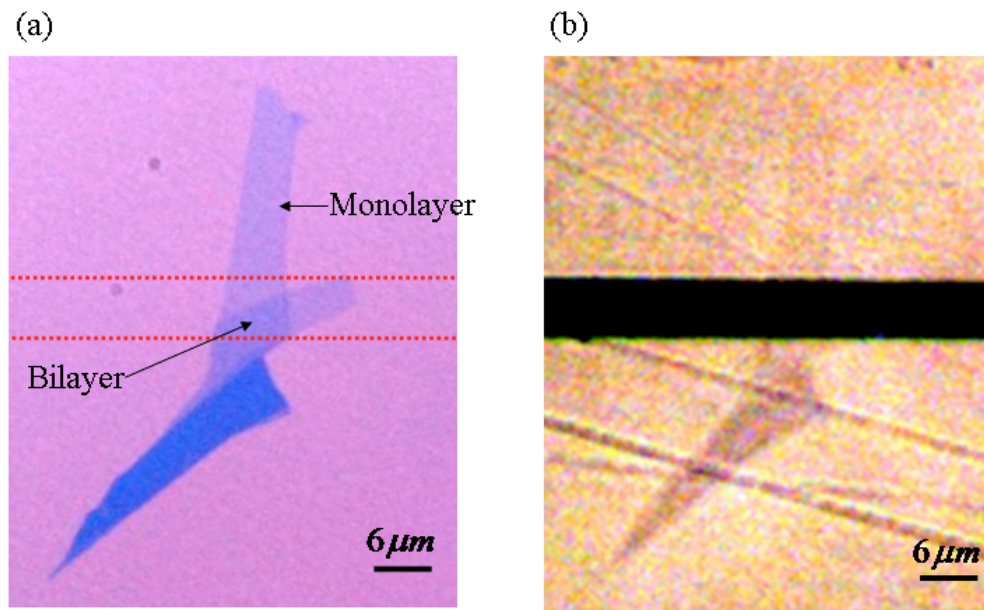


Figure 4.13: Optical image of a graphene sheet (a) before printing and (b) after transfer printing onto a PET substrate containing previously printed S/D electrodes.¹⁵²

The preliminary results obtained for graphene raise exciting possibilities for developing transfer printing as an improved materials preparation method for this important new electronic material. More generally, the transfer printing process will enable other layered materials such as dichalcogenides and clay minerals to be printed as isolated, single atomic layers, onto a variety of substrates.

The transfer printing process introduced above and the accompanying examples of materials printed onto plastic substrates represent compelling evidence of

the utility of this method as a technique for the fabrication of electronic devices on plastic substrates. As an example, the fabrication of OTFTs on plastic substrates will necessitate the sequential assembly of dissimilar materials onto a common substrate. The methodology developed for the sequential printing of materials incorporated into the fabrication of OTFTs will be presented and discussed in detail in the next chapter.

Chapter 5 Flexible OTFT Devices Transfer Printed onto Plastic Substrates

5.1 Introduction

The examples discussed in Chapter 4 illustrate the simplicity and versatility of the transfer printing method and the variety of materials that are compatible with the process. Some of the examples allude to the ability to use the transfer printing method to sequentially assemble dissimilar components onto a single substrate. This ability can be exploited to develop the means for fabrication of thin-film electronics onto flexible substrates. Thin-film transistors typically consist of a gate electrode, a set of source/drain (S/D) electrodes separated from the gate by a dielectric layer and a semiconductor film in contact with both the S/D electrodes and the dielectric layer (see Fig. 2.8 in Chapter 2). As an example of what can be accomplished, transfer printing methods have been developed for the fabrication of TFTs based on both organic and carbon based semiconductor materials. Even though OTFTs will be highlighted in this thesis, it is important to realize that the transfer printing method is also compatible with a wide range of inorganic semiconductor materials.

A flexible OTFT device system that is based on using thermoplastic materials for both the device substrate and the dielectric layer has been designed. Since gold (Au) has been shown to have a work function compatible with organic semiconductors¹⁷ and because Au electrodes can be fabricated relatively easily on silicon (Si) transfer substrates by photolithographic methods, Au was chosen as the material for both the gate and S/D electrodes. The initial work of fabricating OTFTs

onto flexible substrates focused on successfully demonstrating the printing of active OTFT devices based on using pentacene (Pn) (a small molecule semiconductor), poly(3-hexylthiophene) (P3HT) (a polymeric semiconductor) and carbon nanotube mats (CNTM) (a macromolecule) as the active component.²¹

In the following sections, the general preparation of printable layers on transfer substrates will be discussed. Several important requirements associated with the sequential assembly of these printable layers on a thermoplastic substrate will then be presented and discussed.

5.2 Fabrication of Au Electrodes onto Si Transfer Substrates

Both 100 nm thick Au gate and 30 nm thick Au S/D electrodes were fabricated directly onto Si transfer substrates using standard photolithography. To facilitate the transfer printing of the Au electrodes, subsequent treatments to the Au surface were developed in order to adjust adhesion strength. It was found that, after metals deposition, the adhesion of the Au electrode could be improved by exposure to a 200 Watt, 19 SCCM, 250 mTorr O₂ plasma for typically 5 min. Where needed, chemical modification of the electrodes and transfer substrate surfaces was performed after fabrication of the electrodes. Such surface treatments typically included a vapor phase exposure to benzyl mercaptan for 2 hrs in a custom made vapor deposition chamber and then exposure to (tridecafluoro-1,1,2,2-tetrahydrooctyl) trichlorosilane (as a release layer) for 2 min. in a second vapor deposition chamber. After each SAM treatment the electrode assemblies were rinsed in 2-propanol (IPA) and at the end stored in a dry nitrogen purge box.

5.3 Dielectric Polymers Spin Coated onto Si Transfer Substrates

Several different polymers were used as dielectric layers. The details for each material are presented below.

PMMA was used as purchased from MicroChem with a molecular weight of 950,000. Concentrations of both 4% in anisole (A4) and 7% in anisole (A7) were used depending on the desired film thickness. The PMMA was spin coated at either 2500 rpm or 4000 rpm depending on the desired film thickness and baked on a hotplate at 90 °C for 3 min. The resulting dielectric film thickness ranged from 200 - 600 nm depending on the polymer concentration and spin coating speed.

Polyhydroxystyrene (PHS) (also called polyvinylphenol) was used as purchased from Sigma Aldrich with a molecular weight of 8,000 and was typically dissolved to a concentration of ~5 wt% in IPA. Typically the PHS was spin coated at 4000 rpm or 2500 rpm for 60 sec. and baked on a hotplate at 150 °C for 3 min. Prior to spin coating, the solution was filtered through a 0.2 µm filter. The resulting dielectric film thickness ranged from 200 - 600 nm depending on the solution concentration and spin speed.

Polystyrene (PS) was used as purchased from Sigma Aldrich with a molecular weight of 280,000 and was typically dissolved to a concentration of ~7 wt% in toluene. Typically the PS solution was spin coated at 2500 rpm for 60 sec. and baked on a hotplate at 90 °C for 3 min. Prior to spin coating, the solution was filtered through a 0.2 µm filter. The resulting dielectric film thickness was approximately 720 nm.

Polycarbonate (PC) (GE Lexan 1300) with a molecular weight of approximately 39,000 was typically dissolved to a concentration of 10 wt% in cyclohexanone. Typically the PC solution was spin coated at 2500 rpm for 60 sec. and baked on a hotplate at 90 °C for 3 min. Prior to spin coating, the solution was heated to ~85 °C and filtered through a set of filters of decreasing pore size with the last step using a 0.2 μm filter. The resulting film thickness was approximately 460 nm.

Polyimide (PI) PI2562 was purchased from HD Microsystems. For some applications, such as an adhesion layer for printing to Kapton substrates, the PI was used as purchased. For other applications T9039 thinner was added to the PI in order to obtain thinner films. Typically the PI was spin coated at 4000 rpm for 60 sec. and baked on a hot plate at 110 °C for 3 min. The resulting film thickness was approximately 1.8 μm for undiluted PI and 720 nm for a dilution of approximately 2:1 (PI2562:T9039).

5.4 Organic Film Deposition onto SiO₂/Si Transfer Substrate

The Pn organic semiconductor material with a purity of 95% was used as purchased from Sigma Aldrich. It was loaded into a high vacuum thermal deposition chamber and evaporated at a rate of 0.1 Å/sec with the Pn crucible at 180 °C and the sample holder at approximately 30 °C. A 50 nm thick film of Pn was evaporated through a stainless steel shadow mask onto a silicon wafer with a 500 nm thick layer of thermal oxide (SiO₂/Si). When removed from the deposition chamber, the Pn film was immediately stored in a dry nitrogen purge box.

The P3HT organic semiconductor material was used as purchased from Merk. The 94.5% regioregular P3HT, with $M_n = 13,000$ and $M_w = 26,200$ g/mole, was dissolved in chloroform (>98%, Aldrich) to a concentration of 0.5 mg/mL. The P3HT solution was dispensed manually onto the SiO₂/Si substrate after passing through a 0.2 micron PTFE filter. Spin casting was performed under ambient conditions with an acceleration of 1000 RPM/s up to a speed of 1250 RPM for 60 seconds followed by a 2 min. bake at 80 °C. The resulting P3HT film thickness was approximately 20 nm.

The CNT films were grown on a SiO₂/Si transfer substrate by chemical vapor deposition (CVD)³⁵. Prior to growth, the substrate was dipped first into a 30 µg/mL solution of Fe(NO₃)₃ in 2-propanol and then into hexane. Using the iron particles as a catalyst, the nanotubes were then grown in a tube furnace at 900 °C using a mixture of H₂, CH₄, and C₂H₄ feed gases.¹⁵³

5.5 Issues and Requirements for both Single and Multi- Layer Transfer Printing

As outlined above, transfer printing requires (1) that the necessary differential adhesion be established for a printable layer between the surface of the transfer substrate and the top surface of the device substrate in each sequential step of fabrication and (2) that, for a patterned printable layer, the work of adhesion between the surface of the transfer substrate and the surface of the device substrate be low enough to allow the transfer substrate to be cleanly removed after printing. Furthermore, the structure and properties of the printed components must be

maintained without degradation during the printing process. The fabrication of OTFTs on plastic using the transfer printing method was first developed with PET as the transfer substrate, a Pn semiconductor film patterned onto a SiO₂/Si transfer substrate, Au electrodes patterned onto a Si transfer substrate and PMMA a dielectric layer. These are not necessarily the optimum materials and definitely are not the only materials that can be incorporated into flexible electronics via transfer printing. They are, however, the materials that were first used to develop the transfer printing method. Therefore, in the following sections, the issues and specific methods associated with developing the transfer printing process for the fabrication of the flexible device system will be based on these materials.

5.5.1 Differential Adhesion

The first print process to be addressed is the transfer of the Au gate electrode to the PET device substrate. Gold is known to adhere poorly to the surface of a Si wafer (characterized by a thin native oxide layer and therefore referred to as a SiO₂ surface)¹⁵⁴. Consistent adhesion between the SiO₂ transfer substrate surface and the Au electrode is established by first cleaning the Si wafer. The cleaning process consisted of sequential 5 min. soaks in trichloroethylene (TCE), acetone, methanol and IPA followed by a rinse in IPA and a 20 min bake in a 120 °C drying oven. Standard photolithography was performed followed by the deposition of Au directly onto the Si surface (i.e. omitting the Ti or Cr adhesion layer used in standard lithography). This allows the work of adhesion between the Au electrode and the SiO₂ surface to be large enough for the electrodes to survive lift-off and yet small

enough to transfer print to PET. However, Au electrodes did not always cleanly transfer print to an untreated PET surface, but routinely transfer printed to a corona (high voltage electrical discharge) treated PET surface (i.e. the treated surface of as-purchased Dupont Mulinex 453/700). These observations lead to conclusions concerning the comparative works of adhesion and cohesion:

$$W_A(\text{Au/PET+corona}) > W_A(\text{Au/PET}) \sim W_A(\text{Au/SiO}_2)$$

$$W_c(\text{Au}) > W_A(\text{Au/SiO}_2)$$

A full list of all cohesion and adhesion conditions determined from every step of the transistor fabrication process is presented in Table 5.1.

In printing patterned electrodes, both the electrode surface and the transfer substrate surface come into contact with the device substrate. Under the print conditions for the Au electrodes, it was found that the bare SiO₂ transfer surface could not be removed from the PET device surface without destroying the device. This suggests that there is too high a work of adhesion between the PET and SiO₂:

$$W_c(\text{PET}) < W_A(\text{PET+corona/SiO}_2).$$

A similar problem occurs in nanoimprint lithography (NIL) where higher pressure and temperature have been associated not only with improved filling around template structures and decreased stress flow patterns,²⁰ but also with increased adhesion of the imprint resist layer to the template.¹⁵⁵ To counteract the increased adhesion, NIL imprint templates are typically treated with a fluorinated silane self-assembled monolayer (SAM).¹⁵⁶ This SAM treatment acts as a release layer to decrease the surface tension of the template surface, and thus the work of adhesion to most other materials.

Sequential Print Step	Adhesion Requirement		
Gate electrode	$W_A(\text{SiO}_2/\text{Au})$ <	$W_A(\text{SiO}_2 \text{ with RL/ PET})$ <	
	$W_C(\text{Si})$ $W_C(\text{PET})$ $W_C(\text{Au})$ $W_A(\text{Au+Thiol/PET})$	$W_C(\text{PET})$ $W_C(\text{Si})$	
Dielectric and Source-Drain Electrodes	$W_A(\text{PMMA/SiO}_2 \text{ with RL})$ <	$W_A(\text{Au/SiO}_2)$ <	
	$W_C(\text{Si})$ $W_C(\text{PMMA})$ $W_C(\text{Au})$ $W_C(\text{PET})$ $W_A(\text{PET/PMMA})$ $W_A(\text{PMMA/Au})$ $W_A(\text{PET/Au+Thiol})$	$W_C(\text{Si})$ $W_C(\text{Au})$ $W_C(\text{PMMA})$ $W_C(\text{PET})$ $W_A(\text{PMMA/Au+Thiol})$ $W_A(\text{PMMA/Au})$ $W_A(\text{PET/Au+Thiol})$	
Patterned Pn layer	$W_A(\text{Pn/SiO}_2)$ <	$W_A(\text{SiO}_2/\text{PMMA})$ <	$W_A(\text{SiO}_2/\text{Au})$ <
	$W_C(\text{Pn})$ $W_C(\text{PMMA})$ $W_C(\text{PET})$ $W_C(\text{Au})$ $W_C(\text{SiO}_2)$ $W_A(\text{Pn/Au})$ $W_A(\text{Pn/PMMA})$ $W_A(\text{PMMA/Au+Thiol})$ $W_A(\text{PMMA/Au})$ $W_A(\text{PMMA/PET})$ $W_A(\text{PET/Au+Thiol})$	$W_C(\text{PMMA})$ $W_C(\text{PET})$ $W_C(\text{Au})$ $W_C(\text{SiO}_2)$ $W_A(\text{PMMA/Au+Thiol})$ $W_A(\text{PMMA/Au})$ $W_A(\text{PMMA/PET})$ $W_A(\text{PET/Au+Thiol})$	$W_C(\text{PMMA})$ $W_C(\text{PET})$ $W_C(\text{Au})$ $W_C(\text{SiO}_2)$ $W_A(\text{PMMA/Au+Thiol})$ $W_A(\text{PMMA/Au})$ $W_A(\text{PMMA/PET})$ $W_A(\text{PET/Au+Thiol})$

Table 5.1: For each sequential printing step, the adhesion rule is that for all interfaces between the surface of the transfer substrate and the (possibly mixed) surface of the device substrate, the work of adhesion must be less than both the works of cohesion for all materials above and below that interface and the works of adhesion for all interfaces above and below that interface. This is illustrated here for the model OTFT discussed in Section 5.2.2. Note that the (before printing) top surface of the Au electrodes is treated with a thiol compound causing the two Au surfaces to have different works of adhesion. In addition, the SiO_2 transfer substrate surfaces with Au electrodes were treated with a release layer (RL) *after* fabrication of the electrodes, as noted in the text.²²

The same procedure can be used in transfer printing to reduce the work of adhesion between the SiO₂ transfer surface and the PET device surface. However, the release layer must be applied so as not to affect the transfer printing of the Au gate electrode. If applied before fabrication of the Au electrode, it was found that the release layer reduced the adhesion of Au to the Si transfer substrate surface so severely that the electrodes did not survive lift-off. Therefore, application of the release layer after fabrication of the metal electrodes was investigated.

The release layer molecule, (tridecafluoro-1,1,2,2-tetrahydrooctyl) trichlorosilane, is specifically designed with a silane end group that will attach to a SiO₂ surface and is not expected to attach to a metallic surface. However, it was found that following direct exposure of the transfer substrate containing Au electrodes to the release layer, the Au electrodes did not transfer print to PET. Since the silane end group is known to react with water, the lack of transfer was attributed to the release layer molecules reacting with adsorbed water molecules on the surface of the Au electrodes (e.g. $W_A(\text{Au/SiO}_2) > W_A(\text{Au+silane/PET+corona})$).

The problem was overcome by protecting the metallic surface during the application of the release layer. This was accomplished by first treating the Au electrode surface with a thiol terminated SAM, benzyl mercaptan, to saturate the Au surface so that there was no place on the electrode surface where a release layer molecule could attach. This procedure led to successful transfer printing of the Au electrodes as determined visually upon removal of the transfer substrate after printing.

Modifications of the work of adhesion can be expressed as:

$$W_A(\text{SiO}_2 + \text{silane}/\text{PET} + \text{corona}) < W_C(\text{PET})$$

$$W_A(\text{Au}/\text{SiO}_2) < W_A(\text{Au} + \text{thiol}/\text{PET} + \text{corona}).$$

The same two-step SAM treatment was found to facilitate successful transfer printing of the Au S/D electrodes from a Si transfer substrate when the top surface of the device substrate was the PMMA surface of the dielectric layer. This yields a similar conclusion about the relative work of adhesion for Au transfer to PET and PMMA:

$$W_A(\text{Au}/\text{SiO}_2) < W_A(\text{Au} + \text{thiol}/\text{PMMA}).$$

It was found, experimentally, that treatment with octadecanethiol improved the adhesion of Au to PMMA and PET in comparison to treatment with benzyl mercaptan. The reason is assumed to be related to increased entanglement of the longer chain molecule at the Au/polymer interface. The octadecanethiol treatment was used only in special cases such as larger area electrodes. Additionally, an O₂ plasma etch applied to the surface of the Au electrode was found to increase adhesion at the Au/polymer interface. The mechanism for this increase may be related to the removal of organic contaminants but this has not been verified and is an area of possible further investigation.

The polymer dielectric layer can be assembled onto the device substrate using any one of three methods: (1) spin coated directly onto the device substrate, (2) spin coated onto a blank (possibly surface treated) Si transfer substrate and transfer printed onto the device substrate or (3) spin coated onto the transfer substrate containing the

S/D electrodes and transfer printed as a double layer onto the device substrate. The third method was used because it eliminated one transfer printing step. Transfer printing of the polymer dielectric and Au source-drain electrodes requires the adhesion characteristics (for more detail see Table 5.1):

$$W_A(\text{PET/PMMA}) > W_A(\text{PMMA/SiO}_2 + \text{silane}).$$

The final transfer printing step involves the patterned organic semiconductor layer. For the device geometry in Fig. 5.1, the organic layer must transfer to a mixed surface containing both metallic and polymeric species. Transfer printing Pn onto such a device substrate prepared with 100 nm thick Au S/D electrodes embedded into PMMA yielded the results shown in Fig. 5.2a. As can be seen in the profilometer line scan, the S/D electrodes protrude about 30 nm above the PMMA surface. The protrusion of the electrodes is surprising since the PMMA layer was spin coated onto the transfer substrate containing the S/D electrodes prior to transfer printing. It seems likely that elastic stresses are generated around the electrodes during the printing process, and then are relaxed by a displacement of the electrodes when the transfer substrate is removed. The transfer substrate containing the Pn film shows clear evidence of remaining Pn after transfer printing of the organic semiconductor layer. The pattern of the residual Pn on the transfer substrate after printing indicates a low adhesion of the thin Pn film to the PMMA surface of the device substrate. The incomplete transfer of the Pn layer is consistent with a protrusion of the electrodes, preventing conformal contact between the Pn layer and the full device substrate surface (comprised of both Au electrode surface and PMMA dielectric surface). Repeating the process for the Pn layer with thinner electrodes (20 - 30 nm Au)

yielded the result shown in Fig. 5.2b. The thinner transfer-printed electrodes protrude by only ~ 5 nm and the transfer substrate, after printing, shows no observable residual Pn. Devices fabricated with the thinner electrodes yielded far more consistent device properties than those fabricated with thicker electrodes. The important differential adhesion characteristics for printing the patterned Pn onto the source-drain assembly are:

$$W_A(\text{Pn/PMMA}) > W_A(\text{Pn/SiO}_2)$$

$$W_A(\text{Pn/Au}) > W_A(\text{Pn/SiO}_2)$$

$$W_C(\text{PMMA}) > W_A(\text{PMMA/SiO}_2).$$

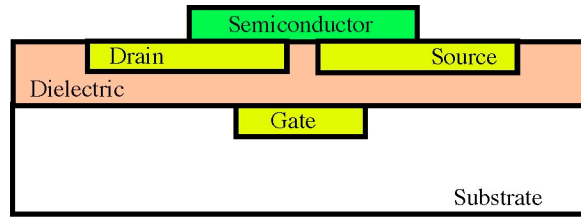


Figure 5.1: Illustration of the cross-sectional structure of a bottom-contact transfer printed OTFT device.²²

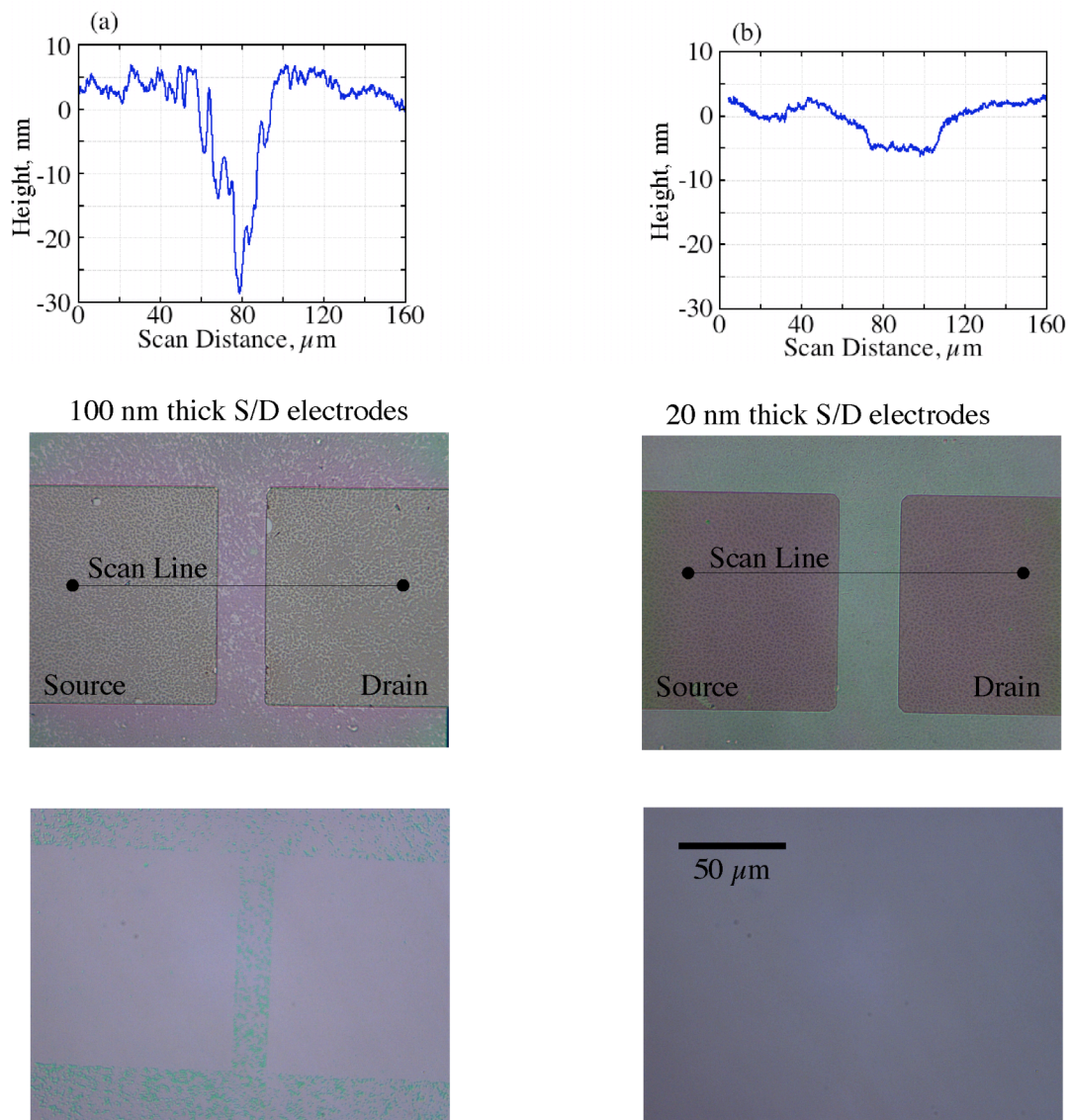


Figure 5.2: Profilometer scan of (a) 100 nm and (b) 20 nm thick S/D electrodes (100 μm wide) printed onto a PMMA coated PET substrate with corresponding optical image of electrodes after printing the Pn. Also shown are optical images of the Pn transfer substrate after printing showing the residual Pn. Note: the magnification is the same for all the optical images.²²

5.5.2 Assembly of Model System using Transfer Printing

The first transfer printing step (illustrated in Fig. 5.3a) was to print the gate electrode onto the PET device substrate. The sample (printable layer between transfer and device substrate) was placed in the imprint machine with the transfer substrate on the bottom and a Si blank on top of the device substrate. The printing was performed at 500 PSI and 170 °C for 3 min.

The second step (illustrated in Fig. 5.3b) was to align the PMMA coated S/D electrodes with the previously printed gate electrode. The transfer substrate (containing both S/D electrodes and polymer dielectric layer) and the device substrate (containing the gate electrode) were aligned, brought into contact and held together by static forces. The aligned substrates were placed in the imprint machine with the transfer substrate on the bottom and a Si blank on top of the device substrate. The PMMA dielectric layer and S/D electrode double layer were transfer printed at 500 PSI and 170 °C for 3 min. At this point the device substrate contained a bottom gate – bottom S/D electrode sub-assembly and was ready for printing of the organic semiconductor layer (illustrated in Fig. 5.3c). As will be discussed in detail in Chapter 6, the conditions for transfer printing the Pn layer were found to have important effects on the transport properties of the resulting device. The optimized pressure/temperature conditions for Pn transfer printing were found to be 600 PSI and 120 °C. Figure 5.3 pictorially illustrates the transfer printing recipe presented above used for the fabrication of OTFTs on a plastic substrate. An optical image of a fabricated device is shown in Fig. 5.4.

In addition to OTFT devices, capacitors were also fabricated using the transfer printing method. For this application, two identical electrodes were printed onto a PET device substrate. The first electrode was printed in the same way as the gate electrode and the second electrode was printed in the same way as the S/D electrodes. A typical capacitor geometry consisted of two, 3 mm x 200 μm Au electrodes separated by a polymer dielectric layer. Such a capacitor was used to measure the capacitance used in Eq. 2.10.

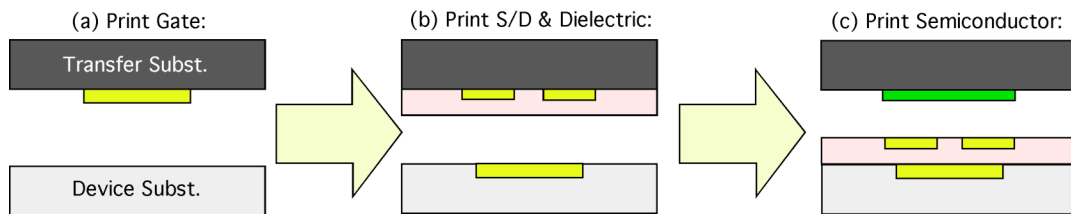


Figure 5.3: Illustration of the transfer printing recipe for the fabrication of bottom gate/ bottom S/D OTFT devices onto flexible substrates. (a) illustrates the printing of the gate electrode, (b) illustrates the printing of the dielectric and S/D electrodes and (c) illustrates the printing of the semiconductor.

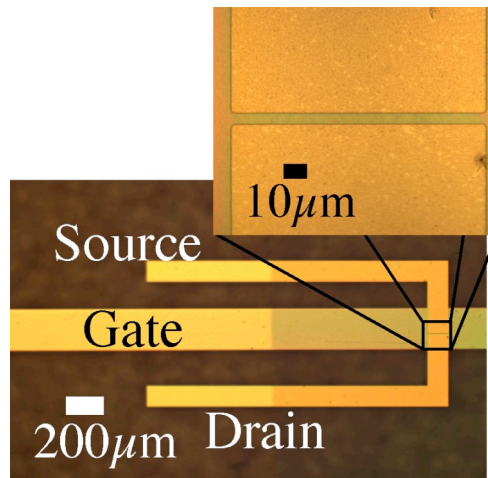


Figure 5.4: An optical image of a typical transfer printed device. Note that the Pn layer is visible on the right half of the image. The faint vertical line over the electrodes in the center of the image is the edge of the patterned Pn layer. This device has a 200 μm wide gate electrode, a channel length $L = 9 \mu\text{m}$ and a channel width $W = 100 \mu\text{m}$.²²

5.6 Conclusion

Materials combinations and transfer printing methods that allow complete device fabrication using only the properties of differential adhesion have been developed for the fabrication of an organic TFT on a flexible substrate. The incompatibility of the adhesion properties of some interface pairs was addressed by using SAMs to modify the surface tension. The process has been demonstrated for a model system consisting of a Pn thin film transistor on a PET substrate with Au gate and S/D electrodes separated by a PMMA (PHS) dielectric layer. The relative adhesion strengths and the order of the materials layers needed for successful fabrication were established, with results listed systematically in Table 5.1. The result allows the device components to be sequentially assembled onto the plastic substrate via transfer printing, avoiding the need for any mixed processing of the device substrate. Continuing work on characterizing and understanding the adhesion properties for different materials combinations is important for achieving the full potential of transfer printing.

Chapter 6 Electronic Characteristics of Transfer Printed Pn TFTs

6.1 Introduction

Being able to transfer materials sequentially is a necessary, but not sufficient, condition for creating electronic devices with transfer printing. The other necessary conditions are that the transferred materials retain their electronic properties as semiconductors, conductors and dielectrics, and that high quality interfaces between the materials can be established in printing. In this chapter, it will be demonstrated that successful results have been achieved using the non-traditional electronic material pentacene, which has been incorporated into transfer printed thin-film transistors.

6.2 Proof-of-Concept of Printed Pn TFTs

More detailed studies have been performed on Pn devices fabricated using the transfer printing techniques. The preliminary transfer printing recipes for these devices were not optimized but were similar to those described in Chapter 5. The current-voltage (I_D - V_D) curves for such a device, with channel length $L = 21 \mu\text{m}$ and channel width $W = 100 \mu\text{m}$, are shown in Fig. 6.1. These data exhibit a classic TFT response as a function of gate voltage. This device has a saturation field-effect mobility of $0.09 \text{ cm}^2(\text{Vs})^{-1}$ and an on/off ratio of approximately 10^4 .

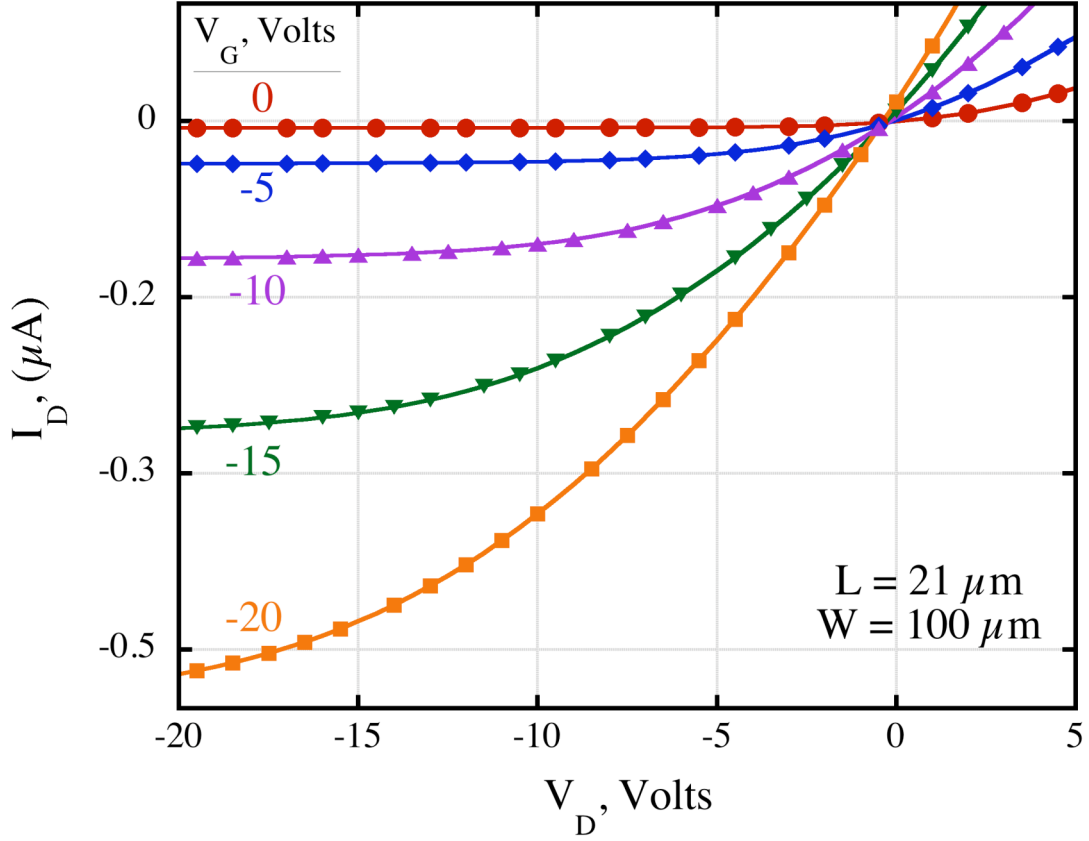


Figure 6.1: Output characteristics (I_D vs. V_D) for a proof-of-concept Pn TFT device fabricated on a PET substrate via transfer printing.²¹

For comparison, reference devices were fabricated using the as-grown, non-printed Pn film as deposited onto the SiO_2/Si substrate. These devices have a channel length of $L = 100 \mu\text{m}$ and a width $W = 3 \text{ mm}$. An optical image of a Pn reference device is shown in Fig. 6.2. Output and transfer characteristics for a typical reference device were shown previously in Figs. 2.9a and b, respectively. Reference devices fabricated using Pn films from several depositions were measured and the mobility was found to be variable within the range $0.08 - 0.13 \text{ cm}^2/\text{Vs}$. Even without optimization, the proof-of-concept Pn devices fabricated using transfer printing perform on par with Pn reference devices.

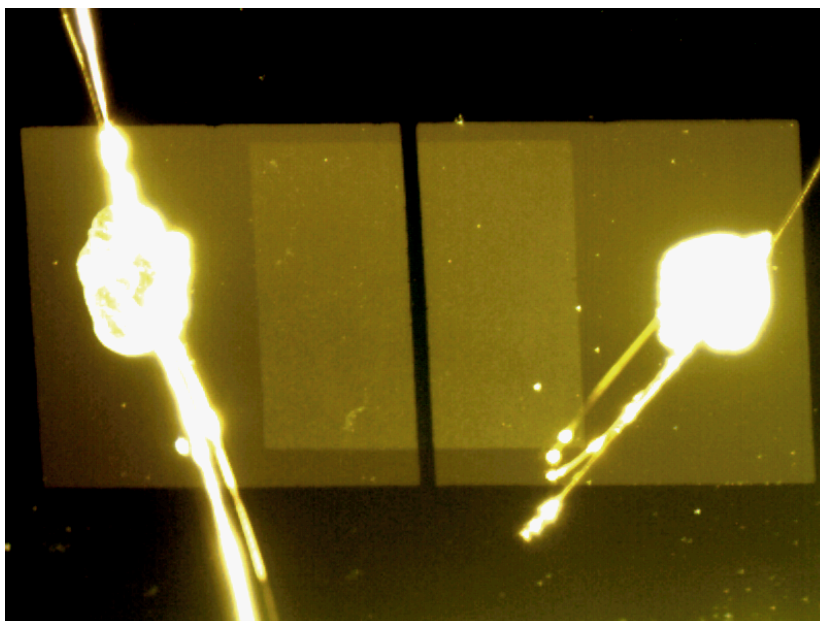


Figure 6.2: Optical image of a Pn reference device with $L = 100 \mu\text{m}$ and $W = 3 \text{ mm}$. The two large squares are the Au S/D electrodes. The continuous Pn film in the center of the image is visible only where covered by the Au electrodes. The bright spots are dots of Ag paint used to connect Au wires to the electrodes. The dark background is the SiO_2 surface of the substrate.

6.3 Optimization of Printed Pn TFTs

Further work has been conducted to optimize the fabrication of transfer printed Pn TFTs. During the optimization work, devices with both PMMA (referred to as Pn/PMMA/PET) and PHS (referred to as Pn/PHS/PET) dielectric layers were fabricated. Performance of these devices was examined as a function of both printing pressure and temperature. The calculated mobility of a selection of such devices is shown in Fig. 6.3. Included in the figure for comparison is the range of mobility values for the reference devices. Clearly, the transfer printed devices show an optimum mobility for printing conditions of 600 PSI and 120 °C. It is seen that, for properly chosen transfer printing parameters, the transfer printed devices have a

larger mobility than the reference devices. This is interesting because the active part of the Pn film for a transfer printed device is the (as-grown) top surface, which (prior to printing) exhibits a terraced structure shown previously in Fig. 2.3 as opposed to the (as-grown) bottom surface in contact with the SiO₂/Si substrate that is presumably much smoother and has been optimized for good transport characteristics. The good quality of a transfer printed device suggests that the (as-grown) top surface has gone through a structural change during the transfer printing process. This will be discussed in detail in Chapter 8.

In order to evaluate the transport properties of optimized Pn transfer printed devices, sets of devices with different channel lengths ($L = 3 - 45 \text{ } \mu\text{m}$) were fabricated where the Pn layer was printed at 600 PSI and 120 °C for 3 min. The output (I_D vs. V_D) and transfer (I_D vs. V_G) characteristics for a Pn/PMMA/PET device with channel length $L = 15 \text{ } \mu\text{m}$ are shown in Fig. 6.4 and those for a Pn/PHS/PET device with channel length $L = 12 \text{ } \mu\text{m}$ are shown in Fig. 6.5. From these and the associated data for all the devices as a function of channel length and gate voltage, the total resistance, R_T , (ie. slope in the linear region) of each I_D vs V_D curve was determined in the voltage range $V_D = -5$ to -15 V . The plot of total resistance vs channel length for the Pn/PMMA/PET and Pn/PHS/PET device sets is shown in Figs. 6.6a and b, respectively. As discussed in Chapter 2 the contact resistance was determined from the intercept of the plot of R_T vs L and the mobility corrected for contact resistance was determined using Eq. 2.10. These values along with threshold voltage, on/off ratio and subthreshold slope are listed in Table 6.1.

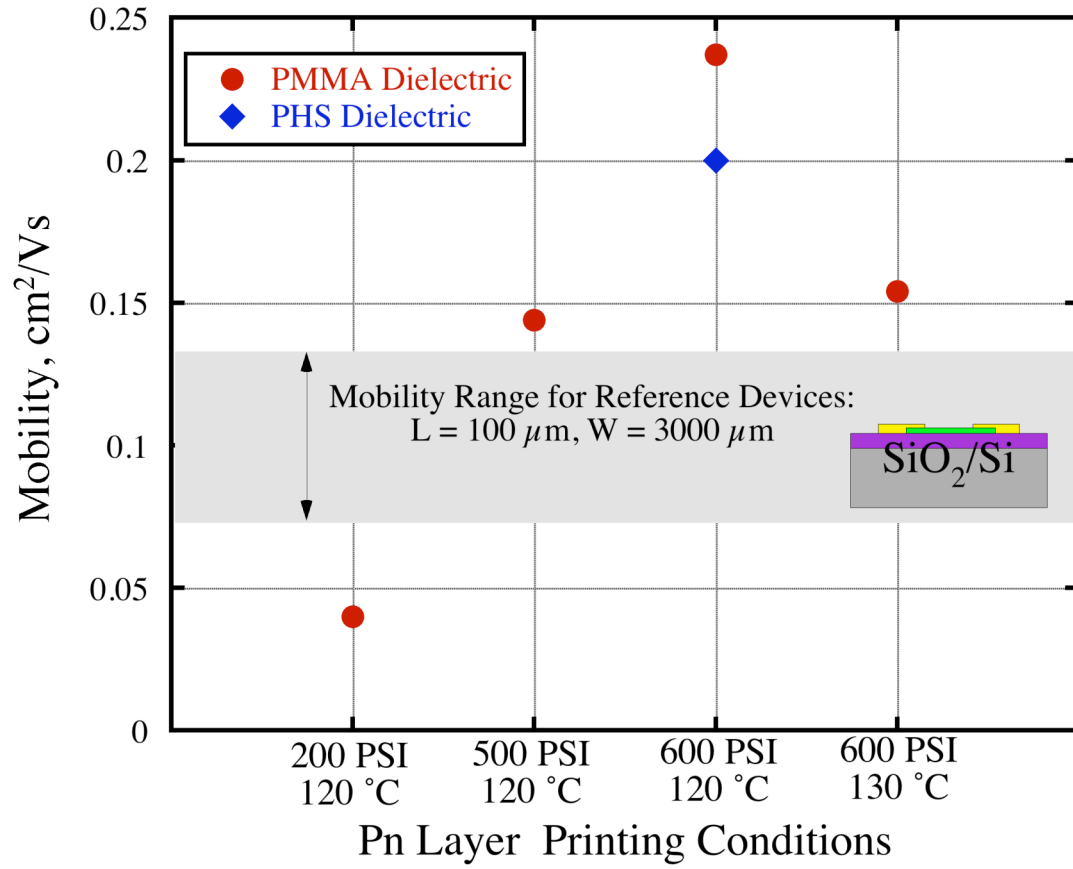


Figure 6.3: Mobility of transfer printed Pn devices with PMMA (circles) and PHS (diamond) dielectric layers as a function of printing conditions compared with mobility range of Pn reference devices, shaded area.²²

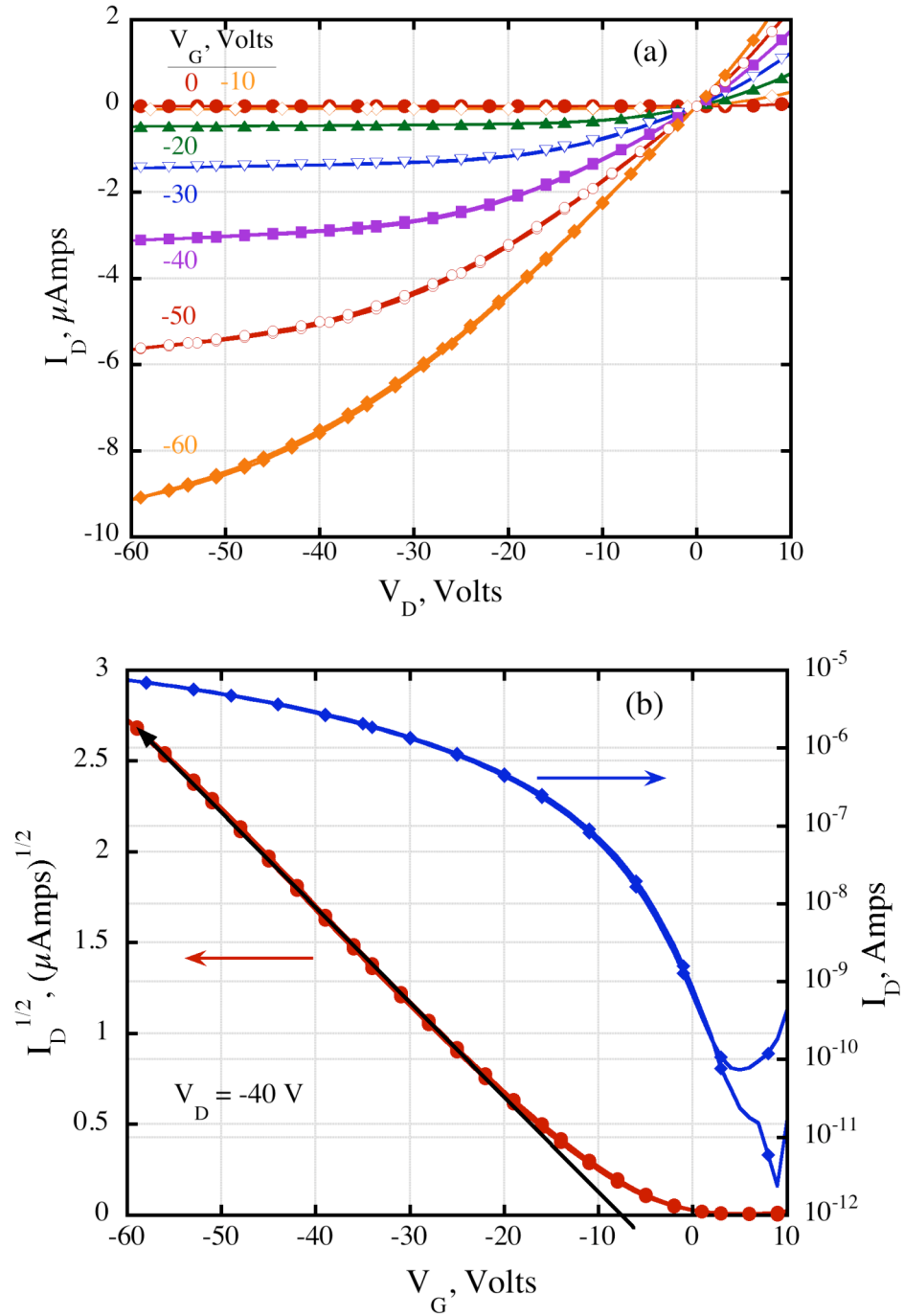


Figure 6.4: (a) Output (I_D vs. V_D) and (b) transfer (I_D vs. V_G) characteristics of a transfer printed Pn TFT with a PMMA dielectric layer, a channel length $L = 15 \mu\text{m}$ and a channel width $W = 100 \mu\text{m}$.²²

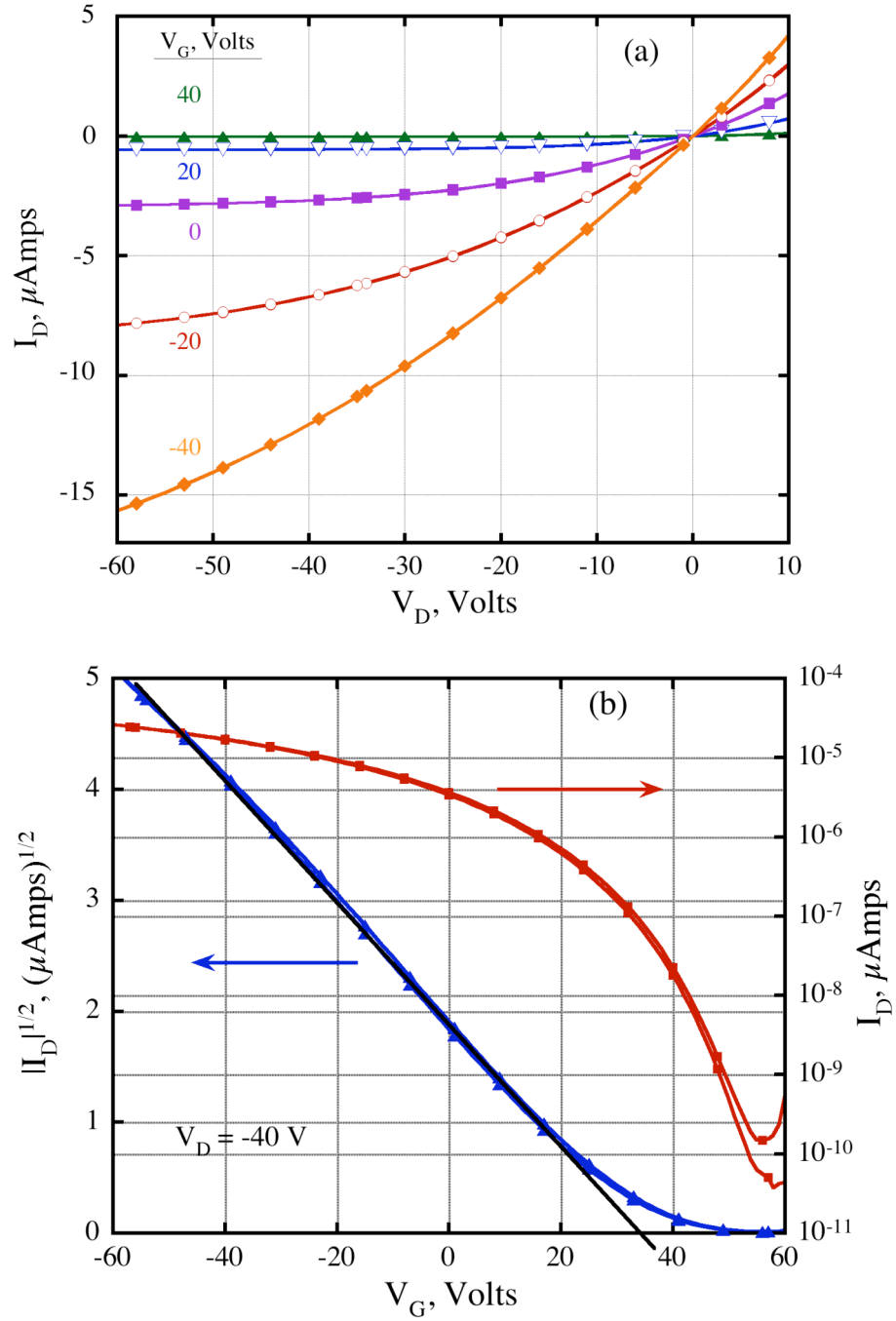


Figure 6.5: (a) Output (I_D vs. V_D) and (b) transfer (I_D vs. V_G) characteristics of a transfer printed Pn TFT with a PHS dielectric layer, a channel length $L = 12 \mu\text{m}$ and a channel width $W = 100 \mu\text{m}$.²²

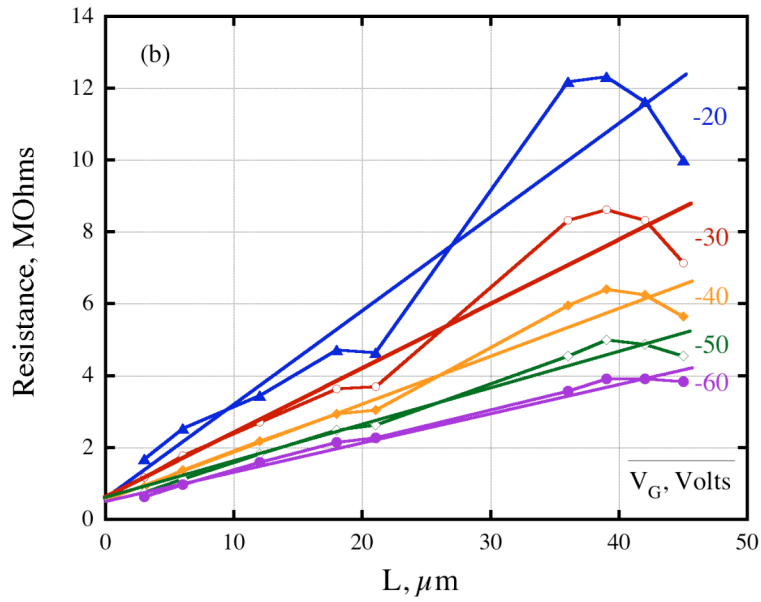
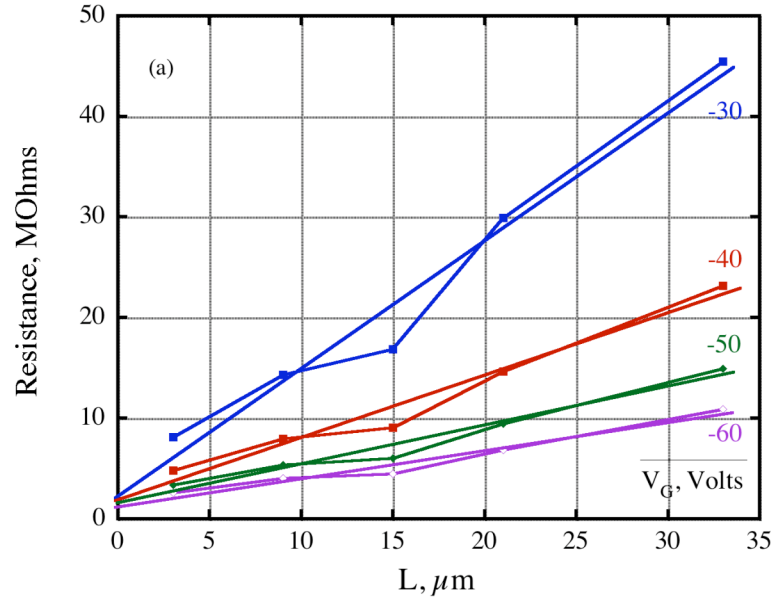


Figure 6.6: Resistance vs Channel length for Pn OTFTs with a (a) PMMA and (b) PHS dielectric layer. Straight lines represent linear fits for each gate voltage that is extrapolated to $L = 0 \mu\text{m}$.²²

Dielectric Layer	μ , cm ² /Vs	V _T , Volts	S, V/Decade	On/Off Ratio	R _P , M Ω
PMMA	0.237	-7	3.5	$\sim 10^5$	2
PHS	0.2	34	6	$>10^5$	0.5

Table 6.1: Pn OTFT device parameters for Pn layer printed at 600 PSI and 120 °C. Note: μ is mobility¹, V_T is threshold voltage¹, S is sub-threshold slope¹ and R_P is the parasitic (contact) resistance.^{39,22}

The mobilities listed in Table 6.1 for the Pn devices with different polymer dielectrics are similar. However, the threshold voltage associated with the PHS dielectric layer is much larger than that associated with the PMMA dielectric layer. This is expected to be related to the polar nature of these polymers and will be discussed in more detail in terms of the polymer surface energies in context with the P3HT devices presented in Chapter 7.

6.4 X-ray Measurements of Transfer Printed Pn Films

To characterize the effect of transfer printing on the film structure of an organic semiconductor film, x-ray diffraction (XRD) experiments were performed under ambient conditions on a 1” square Pn film transfer printed onto a PMMA (PHS) coated PET substrate. (00 l) x-ray diffraction patterns of the Pn films were measured in a coupled Θ -2 Θ reflection geometry. Details of the experimental procedure and of the basal spacing correlation length calculations are presented

elsewhere.²³ Briefly, the basal spacing correlation length refers to the number of molecules well correlated (i.e. arranged crystallographically) with each other in the direction normal to the substrate surface.

Although Pn has been shown to exhibit four polymorphs (with basal spacings of 14.1 Å, 14.4 Å, 15.1 Å and 15.4 Å), 50 nm thick films thermally deposited onto a SiO₂/Si substrate exhibited the 15.4 Å phase as shown in the lower panel of Fig. 6.7. After transfer printing (see Fig. 6.7, upper panel) the 15.4 Å phase persisted indicating that the printing process did not affect the rotation of Pn molecules along the (00/) direction.

The basal spacing correlation length (a measure of the crystalline grain size of the Pn film perpendicular to the substrate surface) was investigated as a function of printing conditions, with the results plotted in Fig. 6.8 as a percent increase compared to an unprinted Pn film as deposited onto an SiO₂/Si transfer substrate. The basal spacing correlation length for the printed films is equal to or greater than that of an unprinted Pn film for all the printing conditions that were studied. Furthermore, the correlation length and the mobility are both largest for the same printing conditions of 600 PSI and 120 °C (compare Fig. 6.8 with Fig. 6.3). Even though the x-ray measurements are a bulk measurement, and the transport properties are associated with the semiconductor/dielectric interface,¹⁵⁷ it is clear that the out-of-plane structure of the Pn film changes irreversibly under the same conditions of pressure and temperature that yield an increase in mobility.

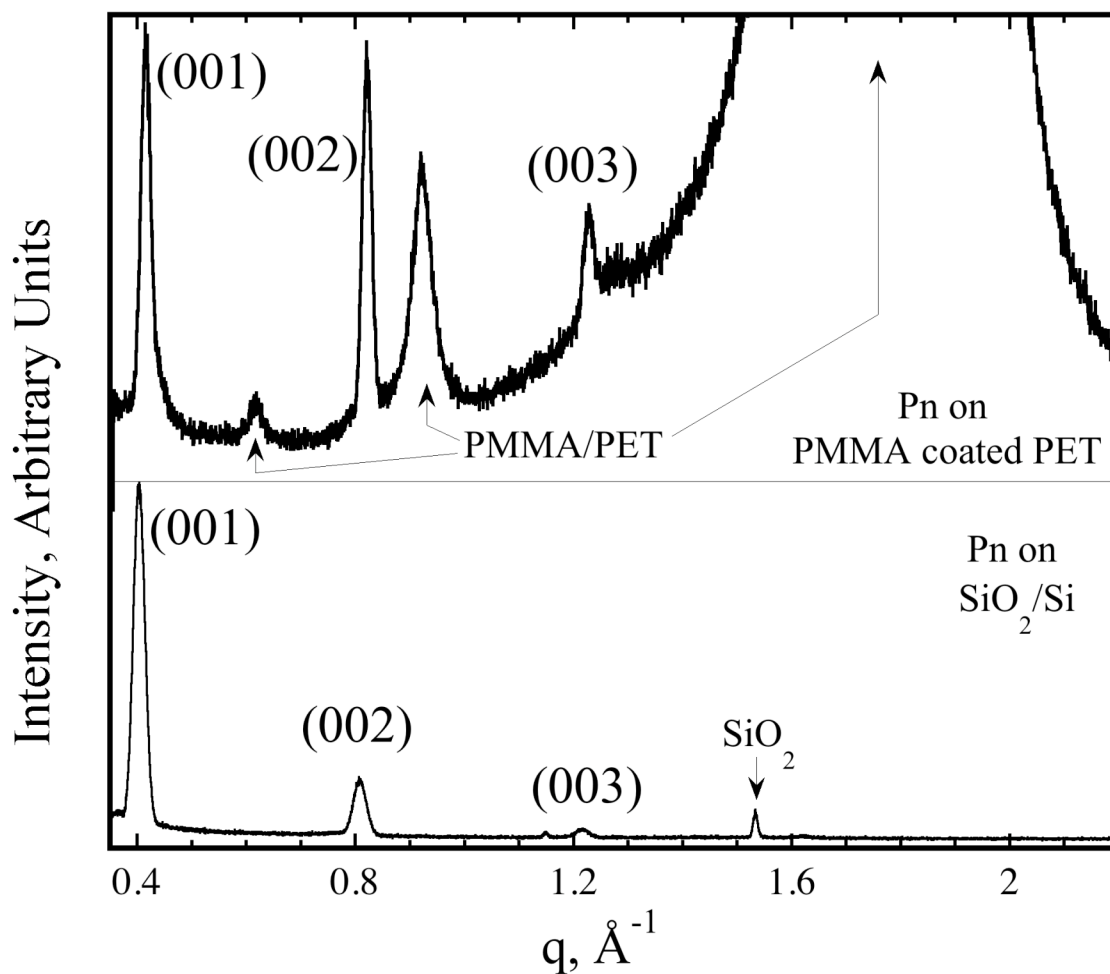


Figure 6.7: (00*l*) x-ray diffraction patterns of 50 nm Pn films (upper panel) after having been transfer printed onto a PMMA coated PET substrate and (lower panel) as deposited (i.e. unprinted) on a Si wafer with a 500 nm thick thermally oxidized surface. The first three (00*l*) reflections are visible along with, as labeled, reflections from the associated substrate.²²

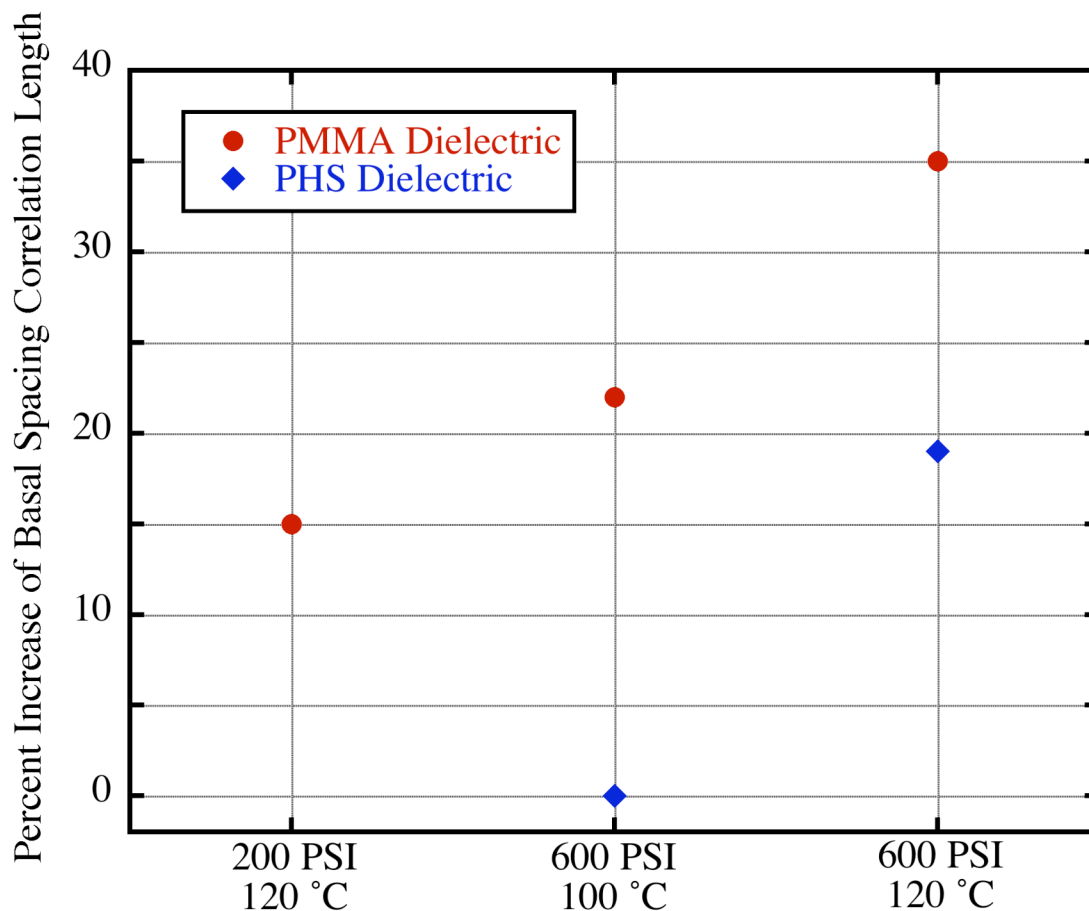


Figure 6.8: Percent increase (compared to Pn on SiO₂ before printing) of basal spacing correlation length as a function of Pn printing conditions.²²

6.5 Conclusion

Based on the above results for Pn (a small molecule semiconducting material), the transfer printing method appears to be quite promising for the fabrication of high-quality flexible organic electronics. In an attempt to prove the robustness of these results, it is desirable to extend this printing process to other materials such as polymeric semiconductor materials. This has been done for P3HT as will be discussed in the next chapter.

Chapter 7 Electronic Characteristics of Transfer Printed P3HT TFTs

7.1 Proof-of-Concept of Printed P3HT TFT

P3HT devices were fabricated using the transfer printing technique as a further test of the impact of transferprinting on the electronic characteristics of printed materials. The transfer printing recipe for this device was initially not optimized but was similar to that described in Chapter 5 for Pn. The current-voltage (I_D - V_D) curves for such a device are shown in Fig. 7.1. Though of low quality, these data exhibit a TFT response as a function of gate voltage. The device was measured in ambient conditions, which is known to dramatically affect the mobility and on/off ratio of P3HT devices³⁹ and is likely responsible for the poor on/off ratio and transistor action.

7.2 Optimization of Printed P3HT TFTs

Further work was done to optimize the fabrication of transfer printed P3HT TFTs. During the optimization work, devices with a PMMA dielectric layer on a PET substrate (P3HT/PMMA/PET), devices with a PS dielectric layer on a PET substrate (P3HT/PS/PET) and devices with a PC dielectric layer on a PC substrate (P3HT/PC/PC) were all fabricated. The specific printing conditions of the gate electrode were the same as for the previously fabricated Pn devices with the exception that a printing temperature of 130 °C was used with the PC substrate. For the printing of the combined polymer dielectric layer and S/D electrodes, the surface treatments, printing conditions and dielectric properties are listed in Table 7.1.

Prior to printing of the P3HT film, the transfer substrate was cleaved into ~ 1 cm square pieces and the P3HT films were patterned manually into 3mm squares using a fine tipped cleanroom swab. It was determined empirically that the optimum printing condition for the P3HT layer was 600 PSI and 100 °C for 3 min.

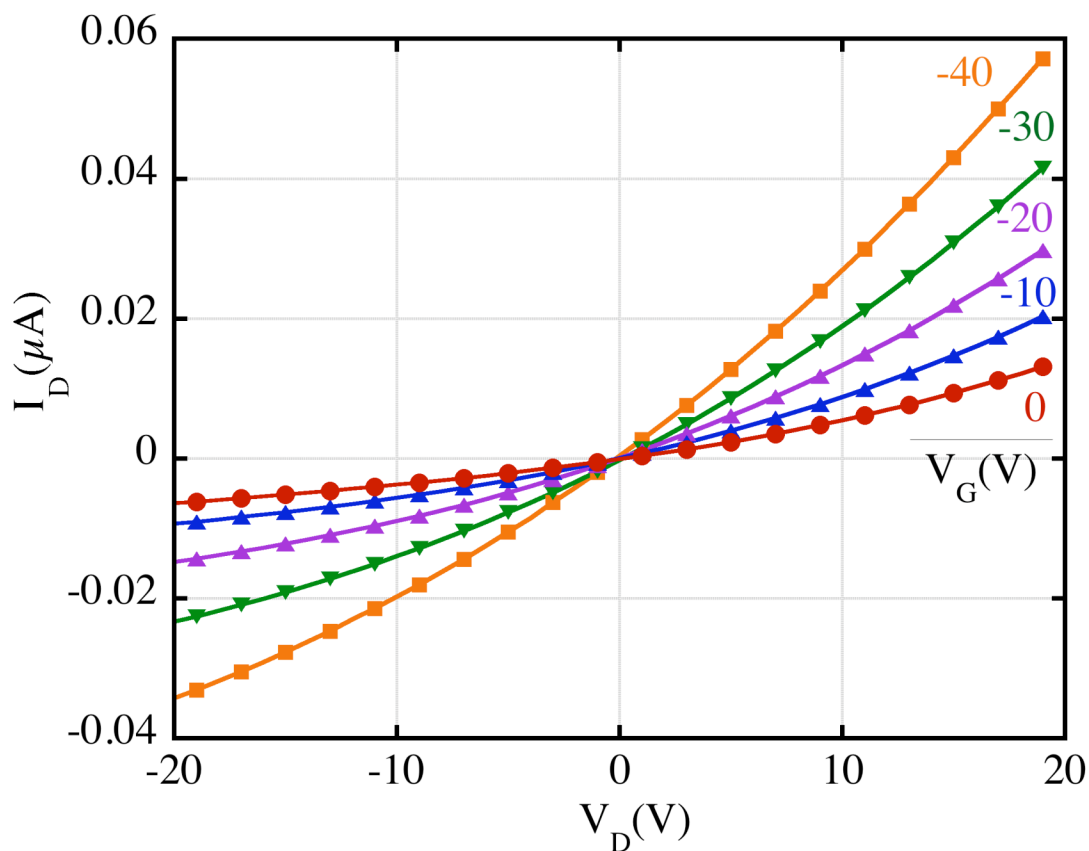


Figure 7.1: Output characteristics (I_D vs. V_D) for a Proof-of-concept P3HT TFT device fabricated onto a PET substrate with a PMMA dielectric layer using the transfer printing method.²¹

7.3 Fabrication of P3HT Reference Devices [by A. Southard]

In order to better study the contact resistance and mobility of P3HT, a set of reference devices with varying channel length (L) were fabricated. These reference devices were made and tested by A. Southard of UMD and are included here for completeness. They are important as a performance metric for the transfer printed

P3HT devices. These devices were fabricated by patterning Au S/D contacts using standard photolithography onto an SiO₂/Si substrate (a 10 Å thick chromium wetting layer and a 100 nm thick Au layer were deposited via thermal evaporation and lift-off was performed). A set of S/D electrodes was fabricated with channel lengths $L = 3 - 1300 \mu\text{m}$ and width $W = 200 \mu\text{m}$. The substrate and electrodes were rinsed with semiconductor grade acetone, methanol, and isopropanol (IPA) and dried with nitrogen prior to spin casting the P3HT film. A gate contact was made by removing P3HT from around the periphery of the device with a cleanroom swab, scratching through the oxide layer with a diamond scribe and filling in the scratch with silver paint. Devices were kept inside a nitrogen glove box until electrical characterization was performed under a separate N₂ atmosphere on a Cascade probe station.

7.4 Optimized Printed P3HT Device Characteristics

Sets of transfer printed devices were fabricated for each different dielectric material with $L = 3$ to $45 \mu\text{m}$. The output and transfer characteristics of a P3HT/PMMA/PET device with channel length $L = 15 \mu\text{m}$ and channel width $W = 100 \mu\text{m}$ are shown in Figs. 7.2a & b respectively. The linear region of the output characteristics was fitted to a straight line in the region from the source/drain voltage $V_d = -5$ to -15 V for gate voltages $V_g = -20$ to -60 V . The slopes of these linear fits represent the total resistance (contact resistance + P3HT channel resistance) and are plotted in Fig. 7.3 as a function of channel length (L) for each gate voltage. From this graph, the contact resistance was determined by extrapolating the resistance curves to $L = 0$ and the mobility (corrected for contact resistance) was determined using

Eq. 2.10. For each polymer dielectric layer a 3 mm x 200 μm capacitor was fabricated by replacing the S/D electrodes by an electrode with a 3mm x 200 μm feature that overlapped an identical area of a gate electrode. For each capacitor, the capacitance was measured using a BK Precision 820 capacitance meter. The obtained values are listed in Table 7.1.

The contact resistance, mobility, threshold voltage and on/off ratio for the P3HT/SiO₂/Si reference devices and the P3HT/PMMA/PET, P3HT/PS/PET and P3HT/PC/PC flexible devices are listed in Table 7.2.

As is evident in Table 7.2, the contact resistance determined for the three flexible device sets is noticeably lower than for the reference device set. This implies a better metal/semiconductor interface associated with laminated electrodes as compared to spin coating the semiconductor film over the top of the electrodes. Furthermore, as previously seen for Pn devices, the mobility of the printed P3HT devices is larger than that of the reference devices. In Chapter 6, Section 3, the origin of these results for Pn was attributed to annealing under pressure. It is expected that the same mechanism is valid for P3HT and will be discussed in detail for Pn films in Chapter 8.

S/D Electrodes & polymer dielectric	P3HT/PMMA/PET	P3HT/PS/PET	P3HT/PC/PC
Electrode Thickness	45 nm	45 nm	45 nm
Electrode Surface Treatment	O ₂ plasma & Benzyl mercaptan SAM	O ₂ plasma	O ₂ plasma
Transfer Substrate Surface Treatment	Release Layer SAM	None	None
Polymer/Solvent	7% 950K PMMA in Anisole	7% 40K PS in Toluene	10% PC in Cyclohezanone
Polymer spin coating	2500 rpm for 60 sec Bake 90 °C for 3 min.	2500 rpm for 60 sec Bake 110 °C for 3 min.	2500 rpm for 60 sec Bake 90 °C for 3 min.
Polymer thickness (prior to printing)	600 nm	720 nm	460 nm
Printing Conditions	500 PSI 170 °C 3 min.	500 PSI 170 °C 3 min.	500 PSI 150 °C 3 min.
Dielectric layer capacitance	4 nF/cm ²	3.2 nF/cm ²	6.3 nF/cm ²

Table 7.1: Parameter associated with the fabrication and printed of the S/D eletrodes and polymer dielectric layers onto plastic substrates.²⁵

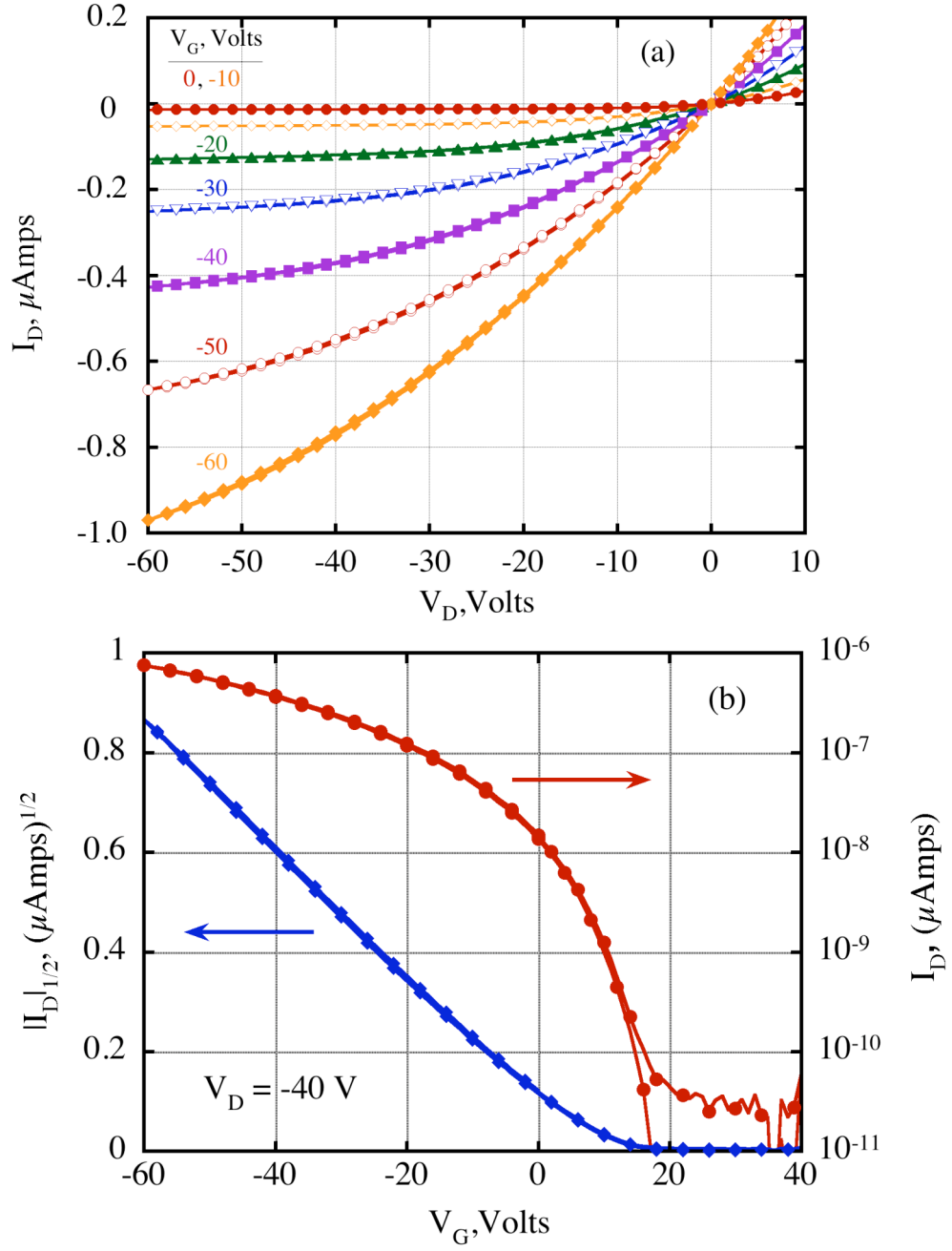


Figure 7.2: (a) Output (I_D vs. V_D) and (b) transfer (I_D vs. V_G) characteristics of a transfer printed P3HT TFT with a PMMA dielectric layer, a channel length $L = 15$ μm and a channel width $W = 100$ μm .²⁵

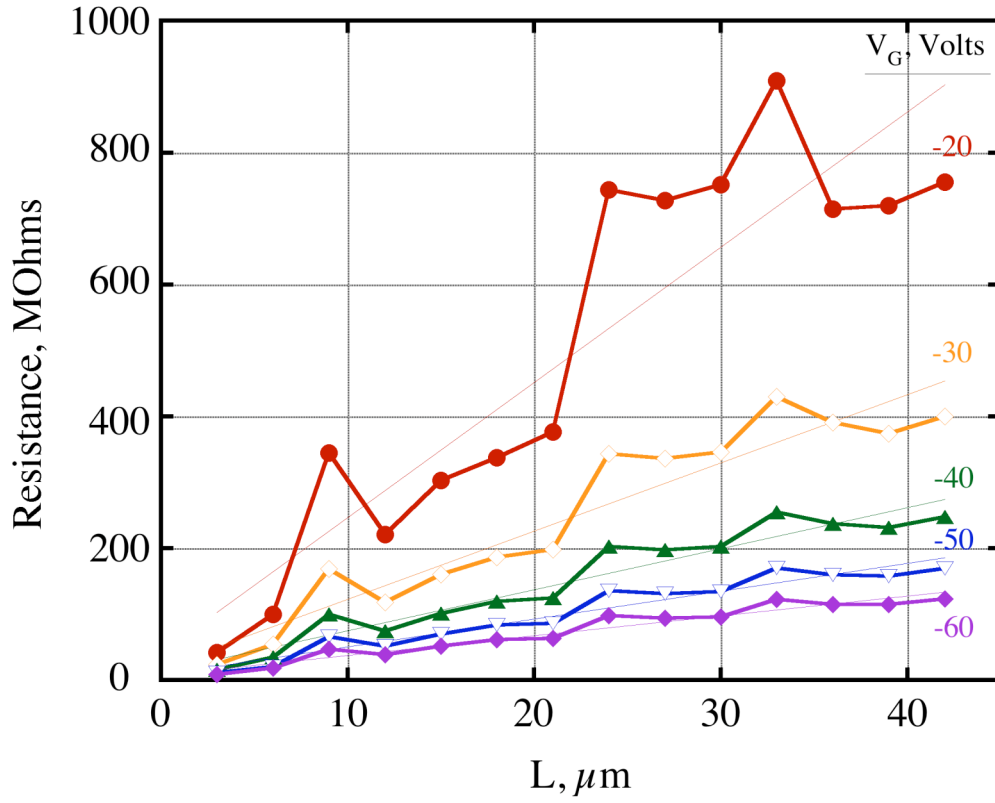


Figure 7.3: Resistance vs Channel length for P3HT TFTs with a PMMA dielectric layer. Straight lines represent linear fits for each gate voltage.²⁵

Device (# of devices)	μ , cm^2/Vs	$R_p * W$, $\text{M}\Omega * \text{cm}$	V_T , Volts	On/Off Ratio
P3HT/SiO ₂ /Si (9) <i>Reference samples</i>	0.007	0.56	13	$\sim 5 \times 10^4$
P3HT/PMMA/PET (15)	0.0186	0.18	18.5	$\sim 10^5$
P3HT/PS/PET (13)	0.0196	0.13	-9.5	$\sim 5 \times 10^4$
P3HT/PC/PC (14)	0.0408	0.23	-5	$\sim 10^4$

Table 7.2: Device properties of reference and flexible P3HT OTFTs.²⁵

7.5 Dielectric Effects

In addition to the devices listed in Table 7.2, transfer printed P3HT OTFTs were also fabricated with PHS dielectric layers. These devices, however, appeared to behave as though they had a threshold voltage so large that they could not be turned off with an applied gate voltage up to 60 V. For this reason, these devices have not been included in the results listed above. However these devices are of interest in that the Pn devices with a PHS dielectric layer also exhibited a large threshold voltage in comparison to those with a PMMA dielectric layer as shown in Table 6.1. Clearly the semiconductor/dielectric interaction is important in terms of device performance. Others^{59,58} have studied the role of dielectrics in the performance of OTFTs and have shown that surface roughness, charge trapping and surface energies are important parameters. For most of these reports, the organic semiconductor was deposited directly onto the dielectric surface. The morphology of the resulting thin film is therefore extremely sensitive to the growth process.

Transfer printing provides the advantage that the formation of the dielectric/semiconductor interface is not a growth process, but rather a mechanical contact between two pre-existing surfaces. Thus, changes in resulting morphology due to annealing during the transfer printing process will presumably be dependent only on differences in polymer chemistry at the semiconductor/dielectric interface. This should be the case for the results shown in Table 7.2 for the P3HT OTFTs using three different dielectric materials. For these devices, the threshold voltage appears to track the polar component for surface energy (as determined from contact angle methods¹⁵⁸) as is shown in Fig. 7.4. Work in is progress to expand these results to

include other polymer dielectric materials such as PVN, P α MS, PVPyr, PVC, PVA, PVAc and PI dielectric layers.

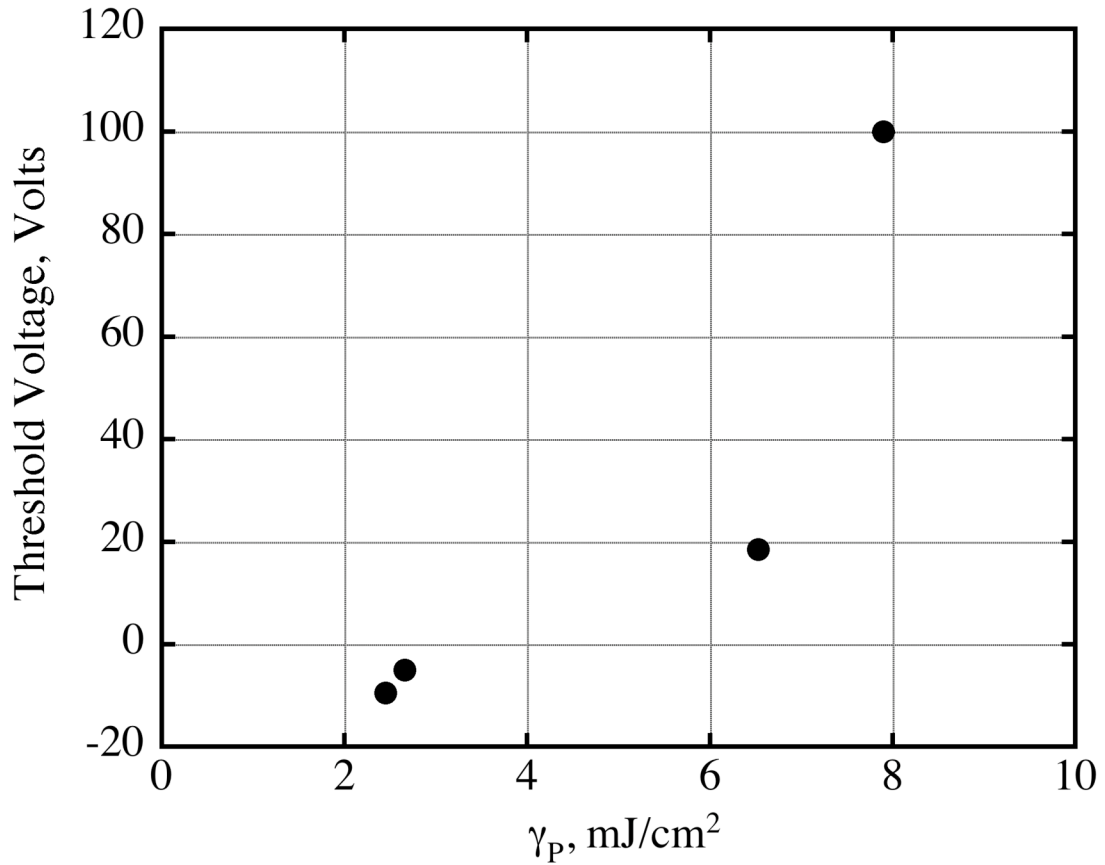


Figure 7.4: Plot of Threshold voltage vs polar component of the surface energy for P3HT devices fabricated with PMMA, PS, PC and PHS dielectric layers. Note: the threshold voltage is estimated for the devices fabricated with PHS.²⁵

7.6 Conclusion

Three different polymer gate dielectrics have been used in fabricating high quality P3HT TFT devices on flexible substrates via the transfer printing process. The devices are easily assembled onto a PET substrate with either a PMMA

or PS dielectric layer or onto a PC substrate with a PC dielectric layer, with minor processing changes (e.g. use of release layers) to adjust for differences in adhesion. The contact resistance of all the flexible OTFT devices presented here is notably better than that of the unprinted reference devices. Also, the mobility of all the flexible OTFT devices presented is better than that of the unprinted reference devices. Flexible devices based on Pn that were presented in the previous chapter showed similar improvements. It was shown that the choice of dielectric materials can strongly affect the properties of the resulting OTFT device. The different substrate and dielectric materials along with the incorporation of both small molecule and polymeric organic semiconductor materials into OTFT devices constitutes an important step toward illustrating the simplicity and flexibility of the transfer printing process.

Chapter 8 *In-situ* Transport Measurements of Transfer Printed Pn Thin-Films

8.1 Introduction

The transfer printing process can be thought of as an annealing under pressure. Therefore, the process may create conditions that modify certain materials properties, thus affecting the characteristics of fabricated devices.¹⁵⁹ For the organic semiconductor Pn, we have previously shown that transfer printing can produce devices with mobilities approximately a factor of two better than devices constructed from (unprinted) vapor-deposited Pn with thermally deposited top contacts.²² Understanding the mechanism for such changes in properties may allow further improvement in the design and fabrication approaches. Here we address the question by directly measuring device characteristics during the transfer printing process. The key results show that annealing under pressure has the potential to dramatically improve the transport properties of electronic devices that use organic films as the active component.

In an active OTFT, an accumulation layer is generated at the semiconductor/dielectric interface by the application of a gate voltage, thus allowing a source-drain (S/D) current to flow in the channel. Since the active region of the OTFT device is localized to within a few nanometers of the interface between the organic semiconductor and the dielectric material,^{38,157,160,161} much effort has gone into improving the structure of the organic layer at this interface.^{26,42,72,162-164} In developmental research, OTFTs have been fabricated by thermally depositing a Pn

thin-film onto a doped silicon wafer with a thermal oxide surface (SiO_2/Si). With the addition of evaporated top-contact S/D electrodes, the resulting device (here referred to as the reference device) uses the oxide layer as the dielectric and the wafer itself as the gate electrode.^{40,49,165-168} In this geometry, (see Fig. 8.1a), the as-grown bottom surface of the Pn film is in contact with the dielectric layer and the terraced top surface (see AFM image, Fig. 2.3) plays little or no role in device performance. When using transfer printing techniques, the organic semiconductor layer, after having been thermally deposited onto a sacrificial SiO_2/Si wafer (referred to as a transfer substrate), is transfer printed onto a plastic substrate containing an electrode subassembly as is illustrated in Fig 8.1b. This device (here referred to as the flexible device) is configured as a bottom-contact Pn OTFT with the as-grown top surface of the Pn film in contact with the dielectric layer.

During transfer printing it is possible to think of having both a reference and a flexible device in parallel as is illustrated in Fig. 8.2a (i.e. stack Fig 8.1a on top of Fig. 8.1b while retaining only one set of S/D electrodes). The reference device then consists of a doped Si global gate, a SiO_2 dielectric layer and laminated top-contact S/D electrodes. For this device, the as-grown bottom surface of the Pn film is in contact with the dielectric layer. The flexible device then consists of a patterned Au gate electrode, a polymer (in this case PMMA) dielectric layer and bottom-contact S/D electrodes. For this device, the as-grown top surface of the Pn film is in contact with the dielectric layer.

In order to avoid cross-talk between the reference and flexible devices during *in-situ* transport measurements, it was necessary to 1) eliminate the printed Au gate

electrode from the reference device and 2) replace the SiO₂/Si substrate with a quartz substrate for the flexible device. The two modified devices are shown schematically in Fig. 8.2b and c. So as not to be confused with the original configurations of the reference and flexible devices shown in Fig. 8.1, the *in-situ* devices will be referred to as control and plastic devices, respectively. Unfortunately, the quality of the as-grown Pn film is not as good on the quartz substrate as on the SiO₂/Si substrate. This means that the mobility values measured for the plastic device will be lower than what has been previously reported for flexible devices that have shown a factor of two improvement as compared to control devices ²². In spite of this limitation, however, the *in-situ* measurements can still be used as an important probe with which to study transport properties of transfer printed Pn films.

For the control device, a 50 nm thick Pn film was thermally deposited onto a thermally oxidized Si transfer substrate. The doped Si wafer was used as the gate electrode and the 500 nm thick SiO₂ layer as the dielectric. Gold S/D electrodes were transfer printed onto a PET substrate and used as laminated top contact electrodes. For the plastic device, a 50 nm thick Pn film was thermally deposited onto a quartz transfer substrate and then placed on top of an electrode subassembly that was previously transfer printed onto a polyethylene terephthalate (PET) substrate with Au gate and S/D electrodes separated by a 600 nm thick poly(methyl methacrylate) (PMMA) dielectric layer. The channel width was 100 μm and the channel length was 6 μm for both the control and plastic devices.

Given these two device geometries, it is possible to investigate properties of the semiconductor layer by studying the effects of transfer printing. Since both the

control and plastic devices experience the same transfer printing environment, any changes will be due to the transfer printing process itself. In order to implement these comparisons, we have developed the capability to perform *in-situ* transport measurements on OTFTs during the transfer printing process. The setup for these *in-situ* experiments will be presented and the results discussed below

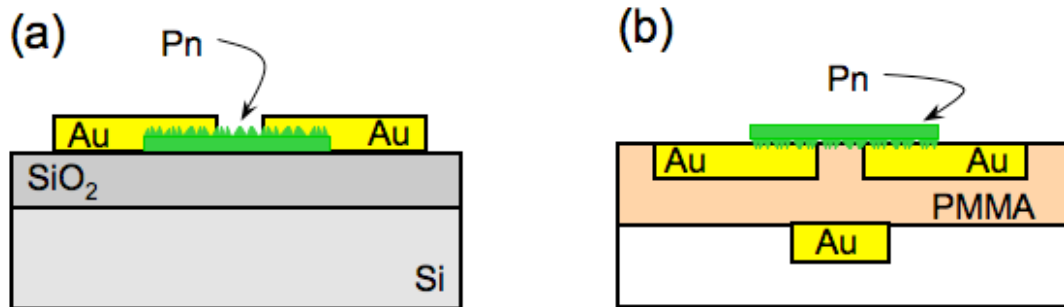


Figure 8.1: (a) Cross-section illustration of the OTFT reference device geometry with thermally evaporated electrodes highlighting the as-grown pentacene bottom surface as the active device interface. (b) Cross-section illustration of the OTFT flexible device geometry highlighting the as-grown pentacene top surface as the active device interface.²⁴

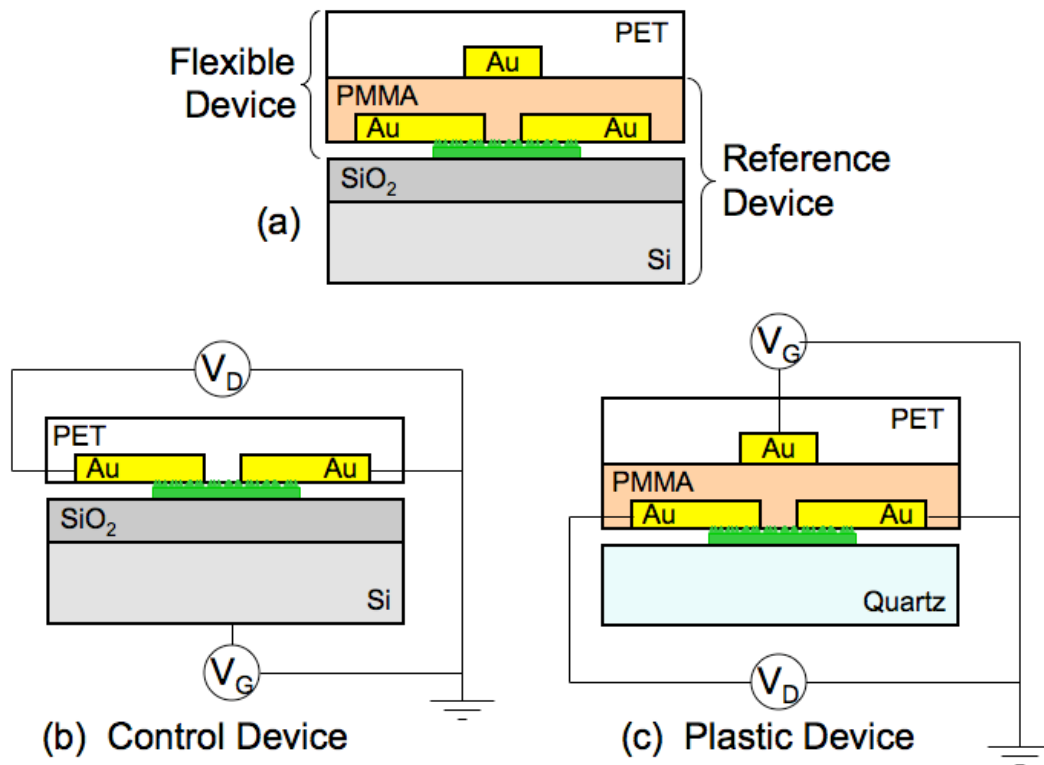


Figure 8.2: (a) Cross-section illustration of the typical geometry for transfer printing pentacene to a flexible electrode subassembly, which can be thought of as a reference device and flexible device sharing the same semiconducting layer. (b) Cross-section illustration of the OTFT control device geometry using the as-grown pentacene bottom surface as the active device interface. (c) Cross-section illustration of the OTFT plastic device geometry using the as-grown pentacene top surface as the active device interface.

8.2 Experimental Setup

To perform *in-situ* transport measurements in the imprint machine, a modification of an existing thermocouple feedthrough was made to include an electrical feedthrough for the drain and gate connections and grounding the source to the imprint chamber and to the source measure unit (Keithly 2400 SourceMeter). Connections to the device were made by passing the wires through a small hole in the bottom silicone sheet, which was subsequently sealed with silicone caulk. The wires were connected to the device electrodes with silver paint. To ensure a reproducible

temperature profile in the imprint chamber, a blank piece of Si wafer was placed below the silicone rubber sheets as a heat sink in contact with the thermocouple. The temperatures reported here are the thermocouple temperatures unless otherwise noted.

8.3 *In-situ* Transport Data and Discussion

For *in-situ* measurements, the printing sequence was to first increase pressure up to 600 PSI, second to increase temperature in steps up to a maximum value, third to decrease temperature back down to room temperature in similar steps and finally to release the pressure. At each step of temperature or pressure, output and transfer characteristics were measured. For the plastic and control devices, sets of *in-situ* transport measurements are shown in Figs. 8.3a - c and Figs. 8.3d - f respectively. These were acquired at 600 PSI & 30 °C (before heating), 600 PSI & 170°C (during heating) and 600 PSI & 30 °C (after heating). As can be easily seen by a comparison of Figs. 8.3a and c, the room-temperature transistor response of the plastic device has drastically improved after heating. The transport characteristics then remained essentially constant as the pressure was released. In contrast, the control device (Figs. 8.3d and f) shows a strong OTFT response before heating and a notable decreased response after heating.

From the data in Fig. 8.3, mobility as a function of printing condition is plotted in Fig. 8.4, where the mobility was calculated using the Eq. 2.8. Fig. 8.4a corresponds to the plastic device and Fig. 8.4b corresponds to the control device. Several important features are evident. First, consistent with a previous report,¹⁶⁹ laminated electrodes, as compared to thermally deposited electrodes result in a

substantial improvement in mobility for the control device (compare dark column to light gray column at 30 °C before heating in Fig. 8.4b).

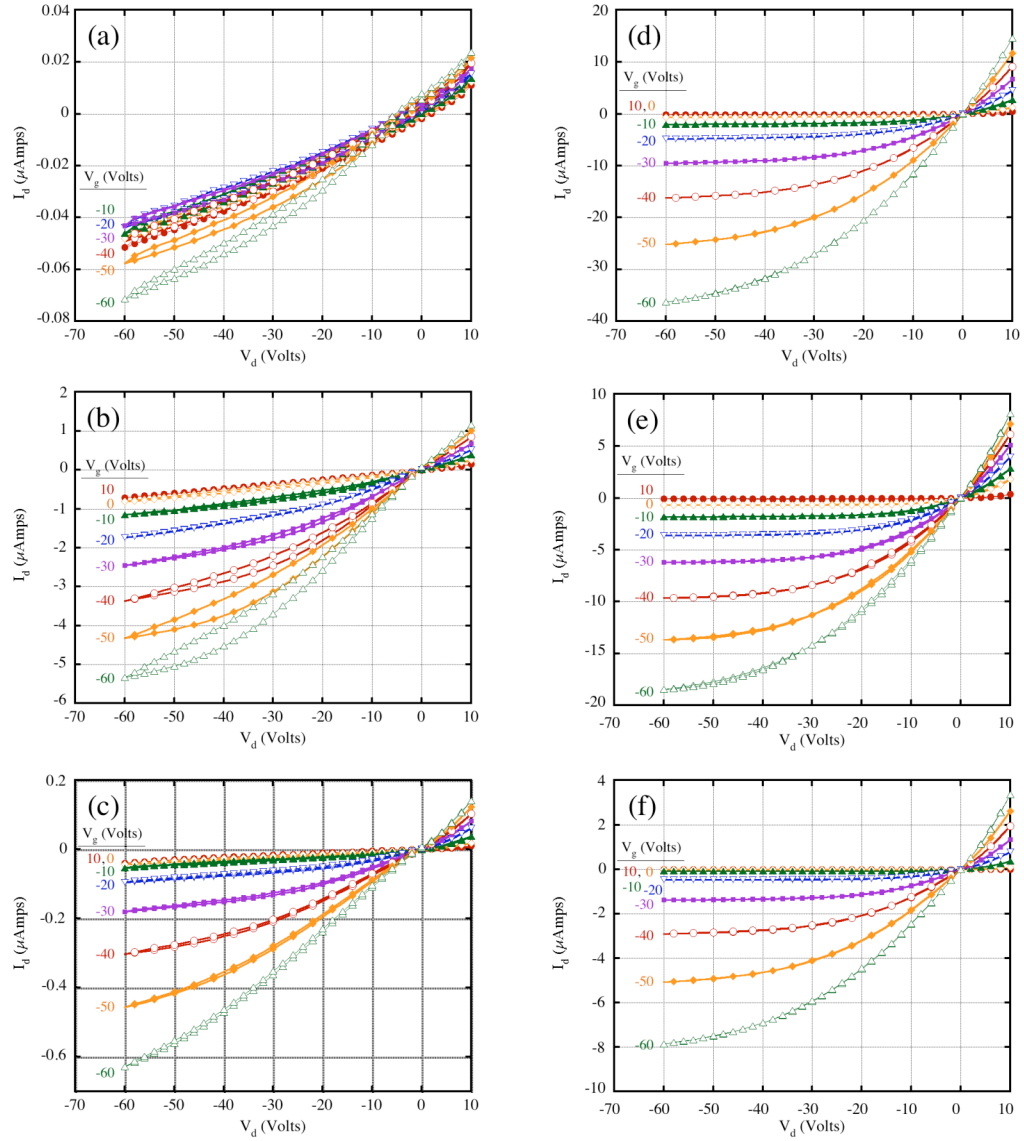


Figure 8.3: *In-situ* I_D vs. V_D transport measurements of the flexible device for thermocouple temperatures of (a) 30 °C before heating, (b) 170 °C during heating and (c) 30 °C after heating, and of the reference device for thermocouple temperatures of (d) 30 °C before heating, (e) 170 °C during heating and (f) 30 °C after heating. All data correspond to a pressure of 600 PSI.²⁴

Second, for the control device, the increase in mobility from 30 °C to 90 °C can be described using the Arrhenius equation for mobility

$$\mu = \mu_0 \exp(-E_a/k_B T) \quad (8.1)$$

where μ_0 is the free carrier mobility, E_a is the activation energy and k_B is Boltzmann's constant. Fitting the data below 90 °C, on heating, results in an activation energy of 19 meV which is consistent with recently reported activation energies for Pn.^{167,170} For temperatures above 90 °C, the mobility of the control device decreases with increasing printing temperature and remains dramatically below what would be expected from Eq. 8.1 (filled circles in Fig. 8.4b) after cooling. In contrast, the mobility of the plastic device dramatically increases with printing temperature above 120 °C and a net improvement remains after the sample is cooled. These two mobility vs. temperature profiles demonstrate irreversible changes taking place at the semiconductor/dielectric interface at the imprint temperatures and pressures.

The transfer printing process is seen to improve the transistor behavior of the plastic device, which incorporates the as-grown top surface, and negatively affect the behavior of the control device, which incorporates the as-grown bottom surface. This may not be surprising when considering the nature of the two Pn surfaces. The as-grown bottom surface forms on the SiO₂/Si substrate surface and is therefore flat; in contrast, the as-grown top surface exhibits a terrace structure¹⁷¹ (Fig. 2.3).

Incorporating this terraced surface into an OTFT device would result in isolated islands of Pn in contact with the dielectric layer. At such an interface, any electrical transport from island to island would require out-of-plane transport which would reduce the performance of the OTFT device and is consistent with the low mobility of the plastic device prior to an increase in printing temperature.

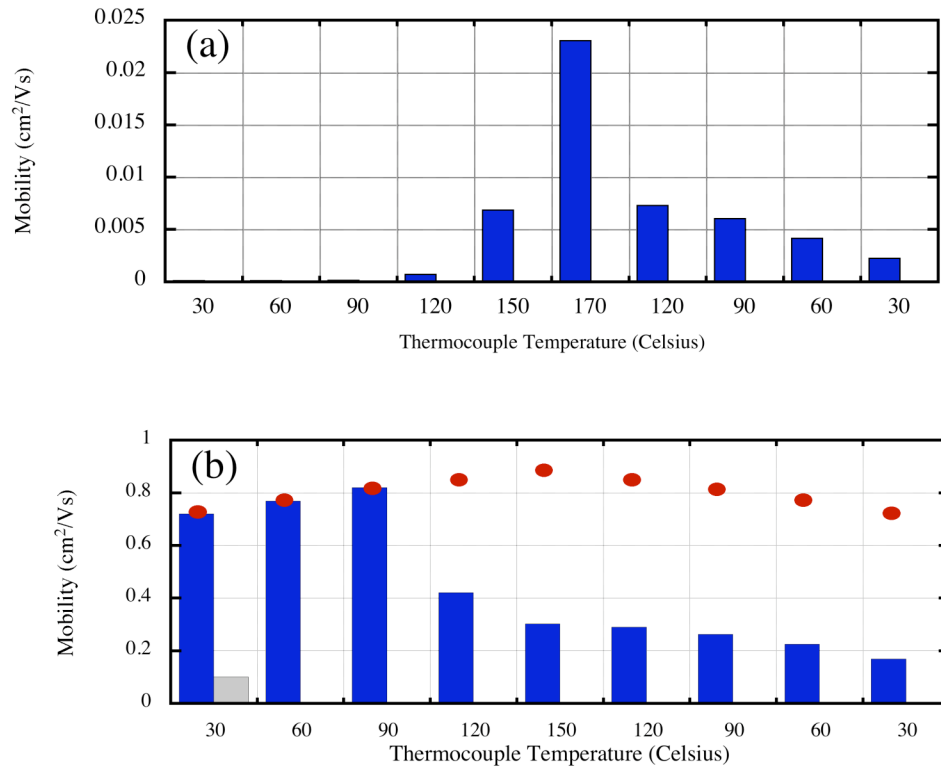


Figure 8.4: Mobility of the (a) flexible device and (b) reference device during the heating and cooling phases of the transfer printing process with pressure held at 600 PSI. The red dots in (b) correspond to the calculated mobility due only to thermal excitation. The second (light gray) bar in (b) for 30 °C corresponds to the mobility of a reference device with thermally deposited top electrodes.²⁴

As discussed in Chapter 6, x-ray diffraction measurements indicate that the basal spacing correlation length of a 50 nm thick Pn film increases as much as 35% during transfer printing.^{22,23} This is a bulk measurement and therefore, does not give a direct measure of the morphology at the dielectric interface; however, it does prove that the arrangement of Pn molecules in the film is irreversibly modified during transfer printing. We can assume therefore that the Pn molecules at the as-grown top and as-grown bottom surfaces are also rearranged during printing. Since the initial growth parameters for the deposition of the Pn film on the SiO₂ dielectric surface were optimized for mobility at the Pn/SiO₂ interface, it is not surprising that any rearrangement of the Pn molecules at the as-grown bottom surface would result in a less optimum interface with respect to mobility (i.e. lower mobility for a transfer printed reference device). In addition, heating may introduce unfavorable changes in the interaction of the laminated electrodes with the Pn. In contrast, the original top surface of the Pn film has poor transport characteristics. In this case, given sufficient molecular mobility to change the crystal habit, it is unlikely that the as-grown top surface of the Pn film retains its original terraced structure under the transfer printing conditions of 600 PSI and 120 °C (sample temperature). Smoothing of the Pn film to conform to the dielectric layer would allow the electronic transport to become more two-dimensional and is a reasonable explanation for the observed improvement of the electronic mobility of the transfer printed plastic device.

8.4 Conclusion

In-situ transport measurements of a Pn OTFT during the transfer printing process have been performed. The printing of the organic film onto a flexible substrate and the lamination of S/D electrodes onto a reference device both resulted in higher mobility devices than a reference device with thermally deposited, top S/D electrodes. By comparison of these *in-situ* results for the Pn/PMMA/PET devices, it is concluded that the morphology of the P3HT thin-film also changes due to thermal annealing under pressure in such a way as to improve the mobility of the printed OTFT devices. Since Pn is a small molecule material and P3HT is a polymeric material, it appears that annealing of organic thin-films is a general process that, for the appropriate printing conditions, has the potential to dramatically improve the transistor properties of an organic thin-film.

The ability to perform these *in-situ* measurements provides opportunities for new data analysis. Taken together, x-ray measurements and *in-situ* measurements show that improvements for the flexible device can be attributed to a rearrangement of the Pn molecules at the Pn/dielectric surface. It is reasonable to conclude that the improvement in mobility of the flexible device is related to an evolution toward a more two-dimensional surface during the transfer printing process. However, the resulting interface cannot be as good as the as-grown bottom surface, since the previously observed mobility improvement^{21,22} (~2x) is less than the improvement due to laminated S/D electrodes for the reference device. This might suggest that the

annealing-induced rearrangement of the Pn molecules at the dielectric/Pn interface does not produce a complete relaxation of the initial terraced interface. This shows that there is room for further improvement of organic electronics printed onto flexible substrates. Additionally, such improvements should not be limited to transfer printed organic semiconductor films. A similar thermal annealing under pressure may have benefits for other printed organic films such as those deposited using inkjet techniques.

Chapter 9 Concluding Remarks and Suggestions for Future Work

9.1 Introduction

Material combinations and transfer printing methods that allow complete device fabrication using only the properties of differential adhesion have been developed for the fabrication of organic TFTs on a flexible substrate. The relative adhesion strengths and the order of the materials layers needed for successful fabrication were established empirically. The incompatibility of the adhesion properties of some interface pairs was addressed by using SAMs to modify the surface tension of the appropriate interface. The process has been demonstrated most extensively for a model system consisting of a Pn thin film transistor on a PET substrate with Au gate and S/D electrodes separated by a PMMA dielectric layer. The results allow the device components to be sequentially assembled onto the plastic substrate via transfer printing, avoiding the use of any chemicals and the need for any mixed processing on the device substrate. All the components are assembled onto the devices substrate in exactly the same way using only pressure and temperature.

In addition, a number of OTFTs were fabricated using both Pn and P3HT organic semiconductor materials, several different dielectric materials (PMMA, PHS, PS and PC) and two different substrate materials (PET and PC). All the devices showed high-quality TFT behavior and low contact resistance in comparison to the unprinted reference devices using an SiO₂ dielectric layer of a Si substrate.

Extending this research will involve addressing both a broader materials base and fabrication methods for flexible electronic applications. A selection of issues that will need to be addressed are illustrated in the following sections.

9.2 CNT CTFTs on Flexible Substrates

A bottom-gate, bottom-contact CNT TFT device fabricated via transfer printing from a film deposited on a SiO₂/Si transfer substrate by chemical vapor deposition (CVD)³⁵ is shown in the SEM and AFM inset images of Fig. 9.1. In the SEM image, the CNTs show up as dark due to charging of the insulating PMMA.¹⁷² In the AFM image, the CNTs are clearly seen crossing the boundary onto the Au electrode. The gate-voltage dependence of the current at two drain voltages is shown for a top-gate, top-contact CNT device. The current increases for both positive and negative gate voltages, which is consistent with ambipolar behavior. Previous reports of CNT films on SiO₂ and polyimide (with no gate electrode and transferred by etching the original SiO₂ support) found only p-type behavior.^{173,174} The large hysteresis in gate voltage observed in CNT devices on SiO₂^{175,176} is not observed in this device. The current in this transistor does not go to zero due to the presence of metallic CNTs in the film; high on-off ratios would require processing capable of selecting only the semiconducting tubes. This work is being expanded in collaboration with Vinod Sangwan of UMD and currently includes sets of both bottom and top gate CNT CFTs on PET substrates for channel lengths ranging from 3 μm to 105 μm .¹⁷⁷

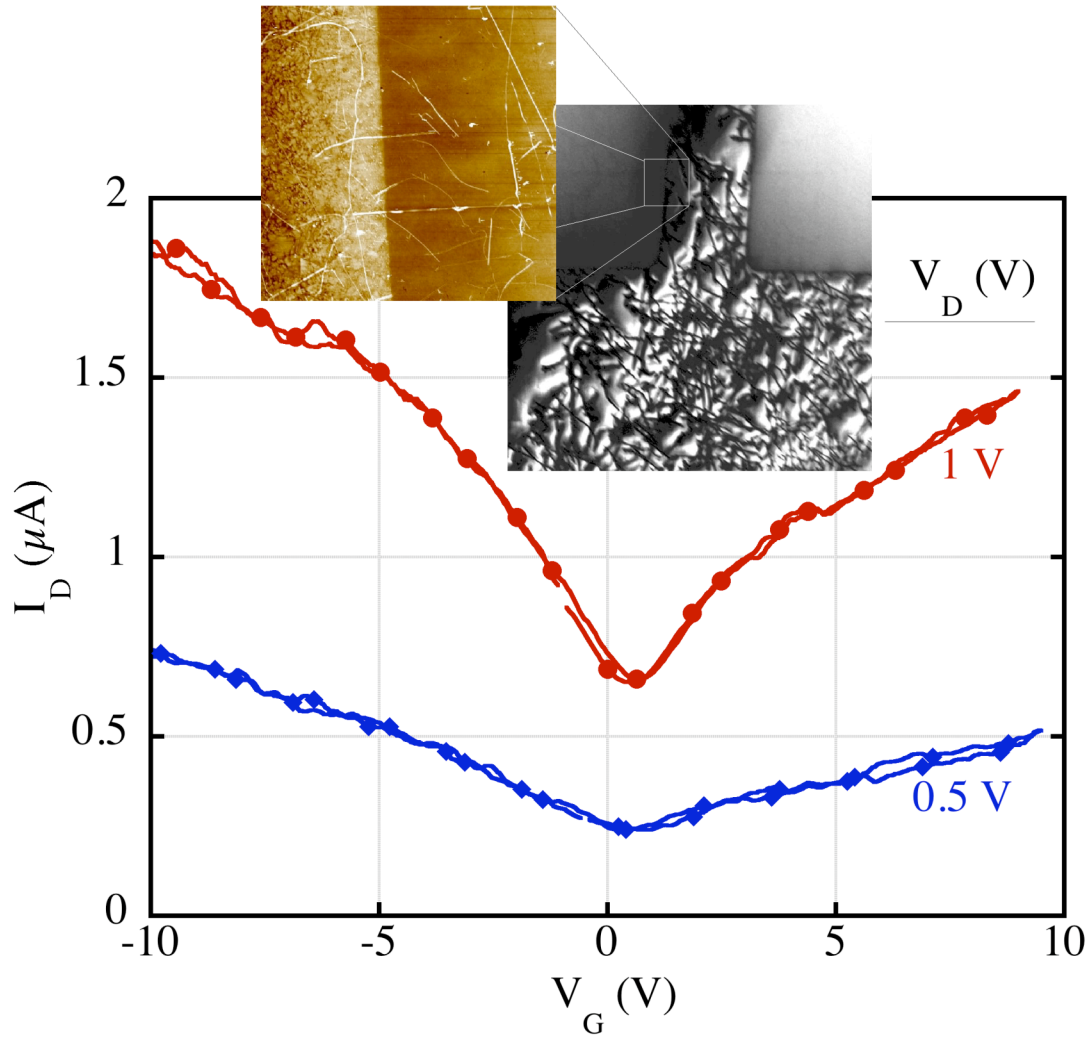


Figure 9.1: Transfer characteristics (I_D vs. V_G) at fixed drain voltages of 1.0 V (top curve) and 0.5V (bottom curve) for CNT TFT. Inset shows SEM and AFM images of the CNT film in the source-drain region after transfer printing onto a PMMA-coated PET substrate containing previously printed Au electrodes.²¹

9.3 Graphene CTFTs on Flexible Substrates

An optical image of a graphene sheet transfer printed onto a PET substrate containing previously printed Au S/D electrodes was shown in Fig. 4.13. This work was done in collaboration with Jian Hao Chen of UMD. Figure 9.2 shows the transfer characteristics of a top gate device that exhibits field effect mobility of

$1.0 \times 10^4 \text{ cm}^2/\text{Vs}$ for holes and $4 \times 10^3 \text{ cm}^2/\text{Vs}$ for electrons.¹⁵² Because of its atomic thickness, graphene constitutes a novel active device material that has recently commanded much interest.^{178,179,180} Prior to this example of graphene on plastic, this material was confined to the substrates SiO_2 or SiC for which fabrication processes have been developed.

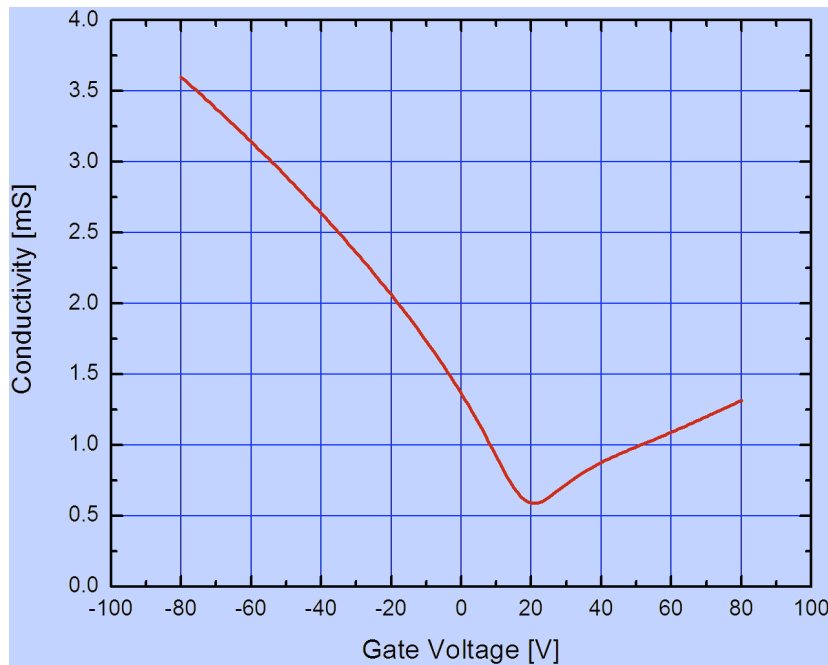


Figure 9.2: Transfer Characteristics of a top gate graphene CTFT printed onto a PET substrate with a PMMA dielectric layer.¹⁵²

9.4 Surface Modifications to Control Adhesion

A list of materials that have either been incorporated into high-quality devices or at least successfully printed onto a flexible substrate in the course of this research is provided in Table 9.1. Several entries are also included for materials that have been tested, but have not yet been successfully printed. Of course, there is a large list

of additional materials that one could envision as interesting materials to incorporate into flexible electronics. In a systematic attempt to expand our understanding of printable materials, six polymer dielectric layers and a Au feature have been separately printed against thirteen plastic substrates. The results of this printing test are shown in Fig. 9.3. Several observations can be noted by examining the information in Fig 9.3. 1) Kapton (except for the printing of Au features) is one of the best substrates for transfer printing. Kapton also has the highest glass transition temperature of all the plastic/polymer materials as can be seen in the plot in Fig. 9.4. 2) Printing is better on plastic substrates with larger surface energies and worse on plastic substrates with lower surface energies as can be seen in the plot in Fig. 9.5. Therefore chemical adhesion, and not just physical adhesion, must be important in the transfer printing process. 3) It is evident that materials containing oxygen double bonds print better (see Appendix A for the chemical structure of each of the plastic/polymer materials).

Understanding such printing trends is necessary to develop a predictive understanding of the issues of adhesion. One approach, now underway, is to correlate the ability to transfer print material A onto substrate B with the surface energies of these materials.

In evaluating $W_A(A/B)$ and $W_A(A/C)$, the surface energies in the Dupré equation (Eq. 4.2) can be separated into dispersive and polar components. Broadly interpreted, two materials which both have either strong dispersive (oleophilic) or strong polar (hydrophilic) components are likely to adhere well.¹⁸¹ For instance, a SiO_2 surface can be characterized as polar ($\gamma_{\text{Tot}} = 287 \text{ mJ/m}^2$, $\gamma_{\text{D}} = 78 \text{ mJ/m}^2$,

$\gamma_P = 209 \text{ mJ/m}^2$), whereas an organic surface can be characterized as dispersive (e.g. for PET, $\gamma_{\text{Tot}} = 47 \text{ mJ/m}^2$, $\gamma_D = 33 \text{ mJ/m}^2$, $\gamma_P = 10 \text{ mJ/m}^2$).^{182,183} Noble metals like Au, which do not form a polar oxide, adhere weakly to SiO_2 ; however, their electrons are highly polarizable, promoting stronger adhesion to materials with dispersive surfaces such as PET. In continuing work, the contact angle method¹⁹ is being used to determine the surface energy components of the materials listed in Fig. 9.3.

In addition Professor Teng Li of UMD is working to create a software program that can simulate the transfer printing process. His efforts could dramatically improve our attempts to incorporate new and/or surface treated materials into the fabrication of flexible electronics via the transfer printing method. In addition to the insights discussed above, Fig. 9.3 is expected to be an important metric against which Professor Li can test his simulations.

A final observation from the results in Fig. 9.3 comes from noting that, for both corona treated and untreated PET and FEP substrates, the treated substrate is better for printing. Figure 9.6 shows that these treated substrates, as compared to the untreated substrates, have a larger polar surface energy component; therefore, it can be concluded that a properly performed surface treatment that results in more polar surface can substantially increase the adhesion of a plastic/polymer material and thus substantially improve transfer printing processes.

In order to study the effects specifically of plasma surface treatments of plastic/polymer materials and to control the transfer printing of such materials, a collaboration with Dr. Deuk Yeon Lee (a postdoc at UMD with Professor Gottlieb Oehrlein) and others at NIST has been established to develop an indirect plasma

treatment process that can be used to modify the surface of a polymer in order to increase adhesion. So far indirect O₂ plasmas have been used to modify the adhesion of a PMMA surface and N₂ plasmas to modify the adhesion of a PET surface. A treated PMMA film was successfully transfer printed onto a PET substrate using the printing conditions; 500 PSI and 80 °C for 3 min. Printed at the same conditions, an untreated film did not successfully print. Work is underway to quantify and optimize this demonstration of improved adhesion and expand the treatment method to other materials of interest.

In addition to plasma treatments as a surface modifier, it should be possible to graft functional groups or dissimilar long chain polymers to many surfaces as a means of establishing a specific chemical interaction or physical entanglement.¹⁸⁴ Both types of surfaces modifications should be able to increase adhesion.

Substrate	Dielectric	Electrode	Semiconductor
Polyethylene Terephthalate Polycarbonate <u>Polyvinyl Chloride</u> <u>Polydimethylsiloxane</u> <u>Polyethylene Naphthalene</u> <u>Kapton</u> <i>FEP</i>	Polymethylmethacrylate Poly(hydroxystyrene) Polycarbonate Polystyrene <u>Poly(α-methylstyrene)</u> <u>Polyimide</u> <i>Glass Resin</i>	Au Films <u>200 nm Dia.</u> <u>Ag nanowires</u> <u>CNT mats</u> <u>PEDOT:PSS</u>	Pentacene CNT mats P3HT Graphene <u>DFH4T</u> <u>PDI</u> <u>Chitosan</u>

Bold (GREEN) - Incorporated into Printed Device

Underline(BLUE)- Successfully Test Printed

Italics (RED) - Unsuccessfully Test Printed

Table 9.1: Materials that have been successfully transfer printed and incorporated into high-quality OTFTs are shown in bold (green). Materials that have been successfully transfer printed but not incorporated into high-quality devices are shown in underline (blue). Materials that have not been successfully transfer printed are shown in italics (red).

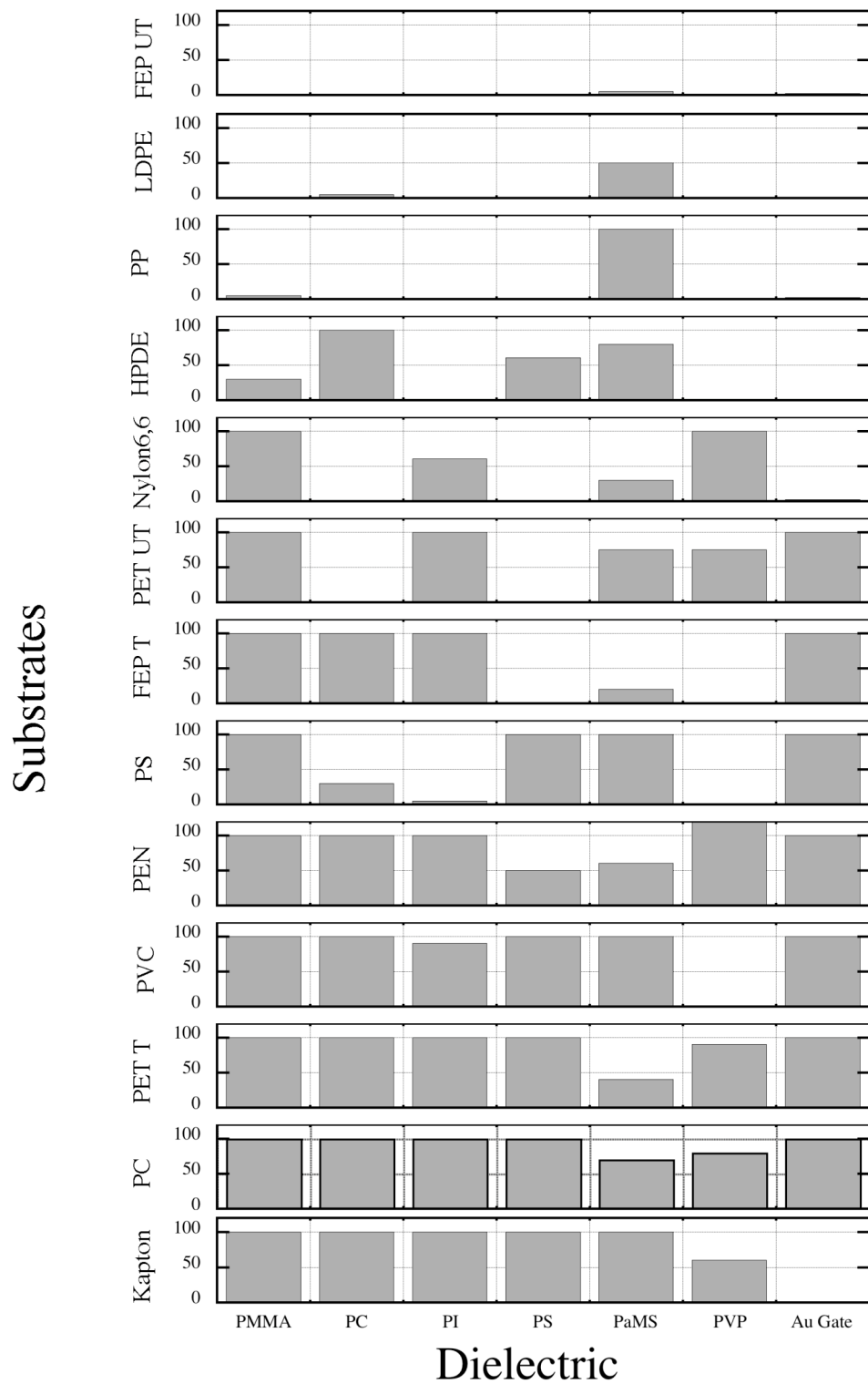


Figure 9.3: Transfer printing results, in percent printed, for six polymer dielectric materials and a Au feature printed against thirteen plastic substrates.

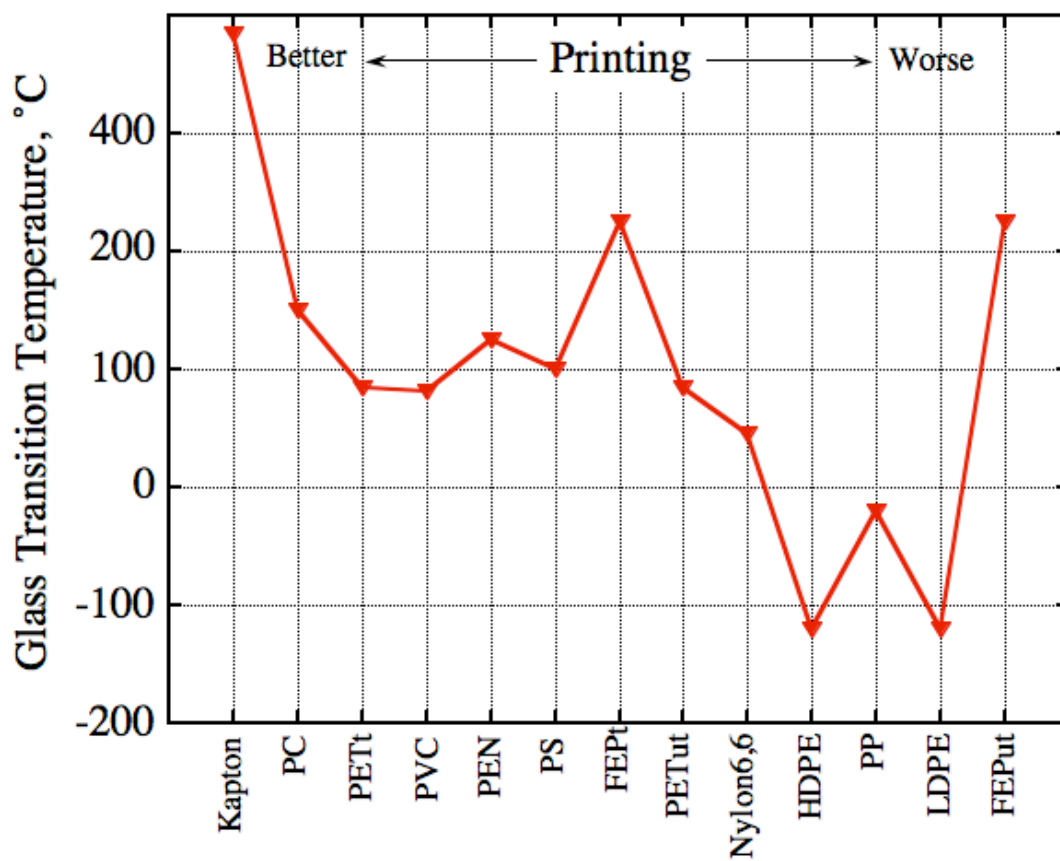


Figure 9.4: Glass transition temperature for plastic substrates that appear in Fig. 9.3.

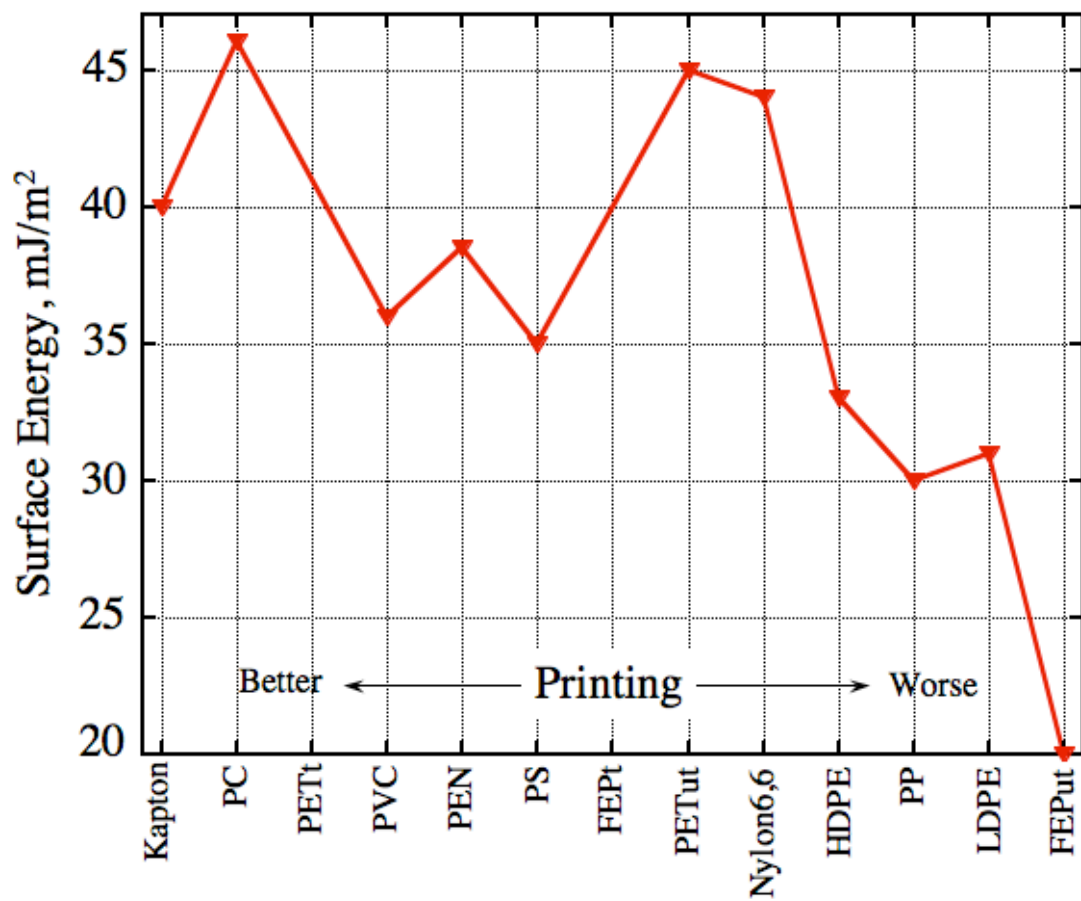


Figure 9.5: Surface energy for plastic substrates that appear in Fig. 9.3.

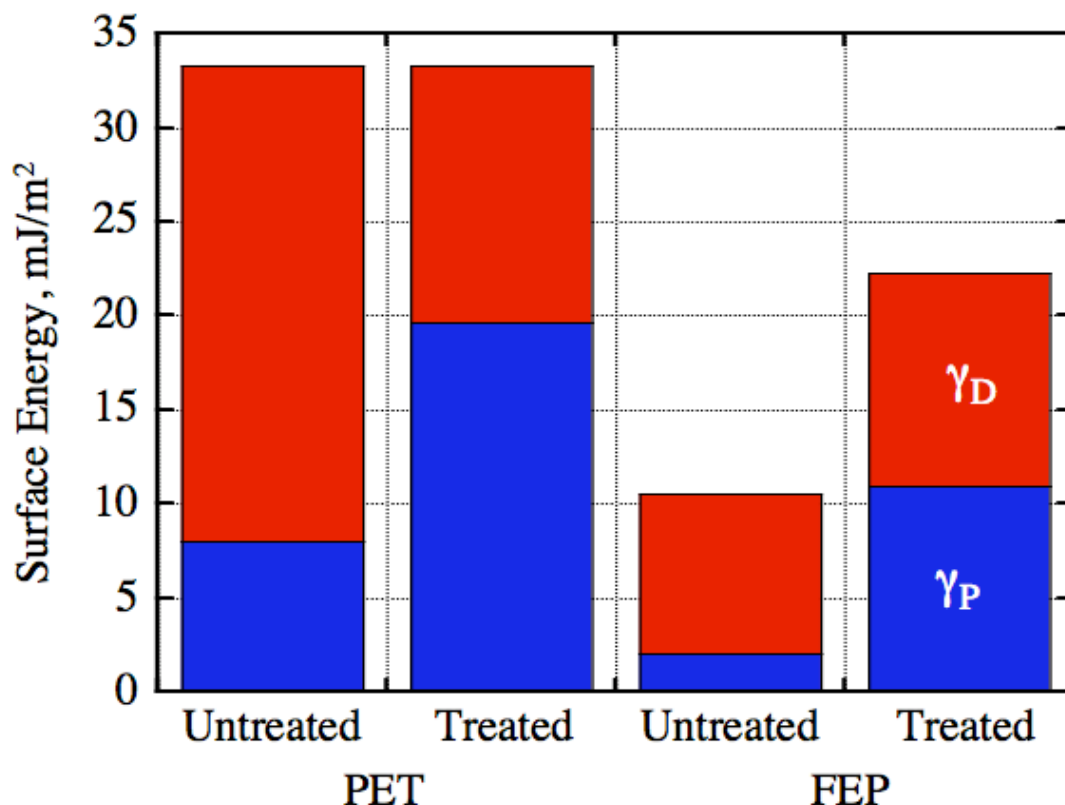


Figure 9.6: Dispersive (red) and polar (blue) componentd of the surface energy for the treated and untreated PET and FEP substrates that appear in Fig. 9.3.

9.5 Submicron Scale Devices

Device sizes at the nanometer scale should be achievable with the transfer printing method, limited only by the ability to pattern the printable layer, and the edge fidelity in the transfer printing. Since transfer printing is very similar to NIL, the same resolution limitation might be expected to be possible with both methods. A resolution of 10 nm has been shown with NIL.¹⁴² An example of transfer printing 200 nm Au lines was shown in Fig. 4.3. Also the printing of individual CNT and inorganic nanowires is a logical extension of the ability to print low density versions of the examples shown in Figs. 4.10 and 4.12, respectively.

9.6 Circuit Fabrication

In order to expand the transfer printing method to useful applications (and ultimately to a roll-to-roll fabrication process), the method will have to be demonstrated for large area substrates. In this direction we have printed 36 transistors onto a single, 1 inch piece of plastic. These devices are shown in Fig 9.7.

Another goal is to fabricate electronic circuits, containing complex combinations of individual devices, on plastic substrates. Figure 9.8 illustrates a first attempt at transfer printing two devices that can be hooked up to create an inverter circuit. The next step is to incorporate vias into the printing process so that different printed layers can be electrically connected as part of the printing process. An illustration of the succesful printing of vias is shown in both Figs. 9.9 and 9.10 showing a working solenoid with 24 vias and a transformer made from stacking two planar spiral solenoids, respectively. This work is being pursued in collaboration with Andrew Tunnell and Vince Ballarotto at the Laboratory for Physical Sciences.

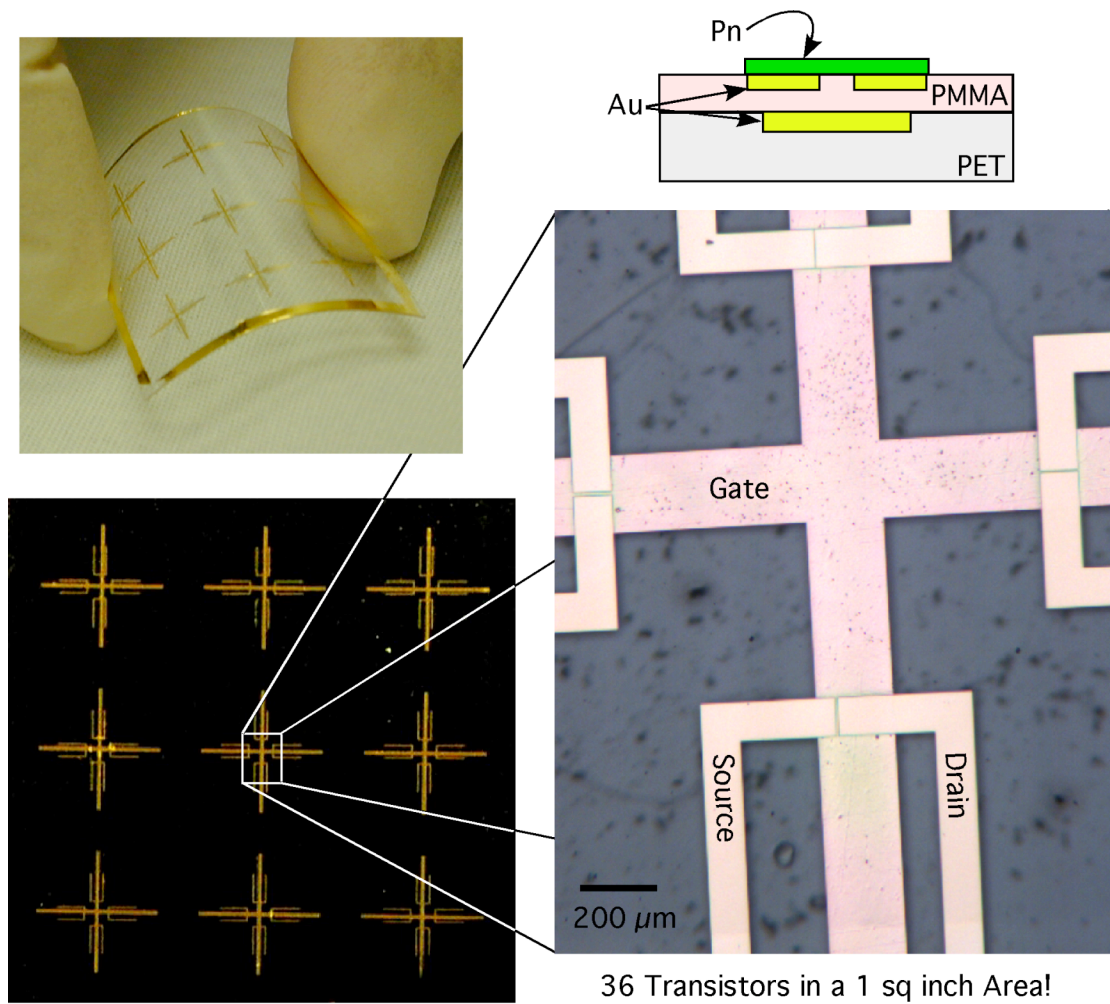


Figure 9.7: Optical images of a set of 36 OTFTs transfer printed onto a 1" square PET substrate.¹⁴⁶

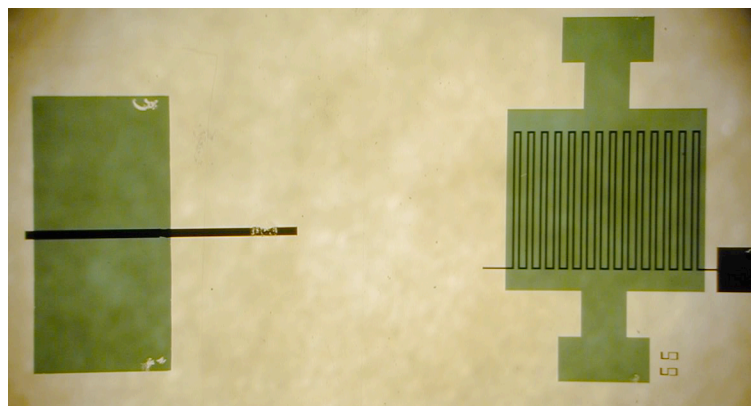


Figure 9.8: Optical image of two transfer printed OTFTs devices on the same PET substrate. These devices can be electrically connected to make an inverter circuit.

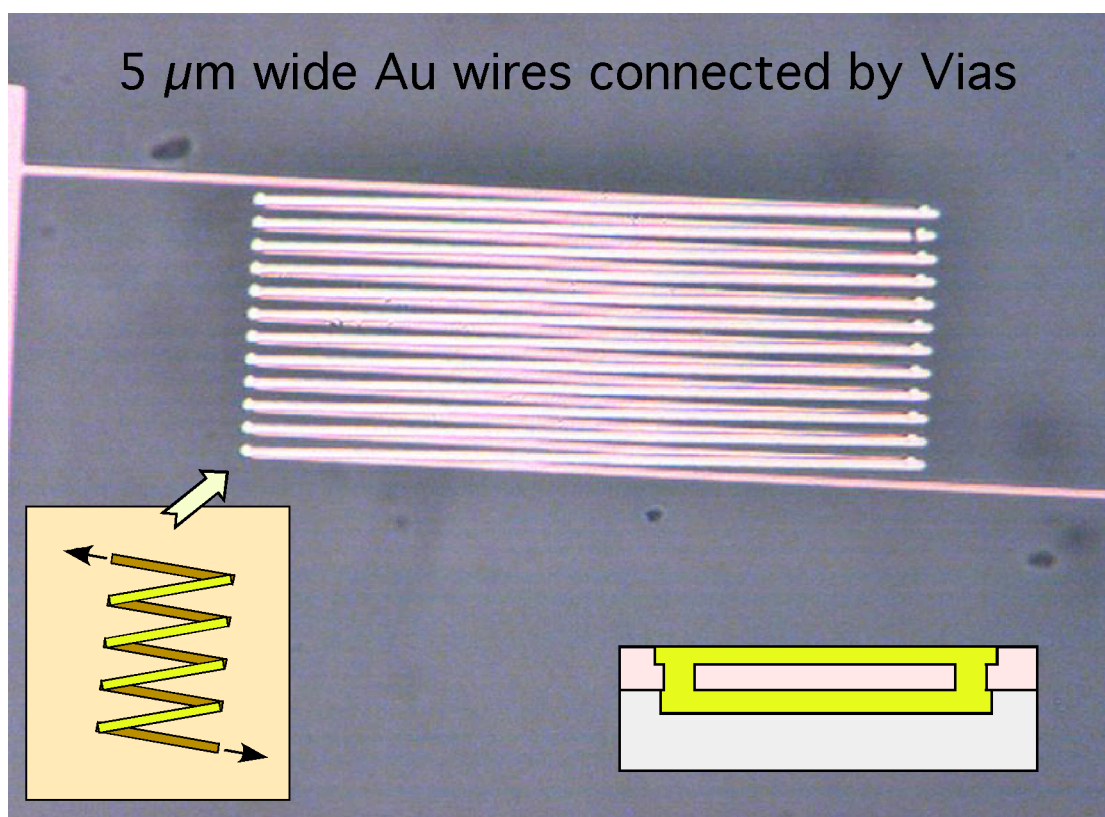


Figure 9.9: Optical image of a solenoid fabricated using sequential transfer printing steps onto a PET substrate. The bottom set of Au lines are connected to the top set of Au lines by printed vias.¹⁴⁶

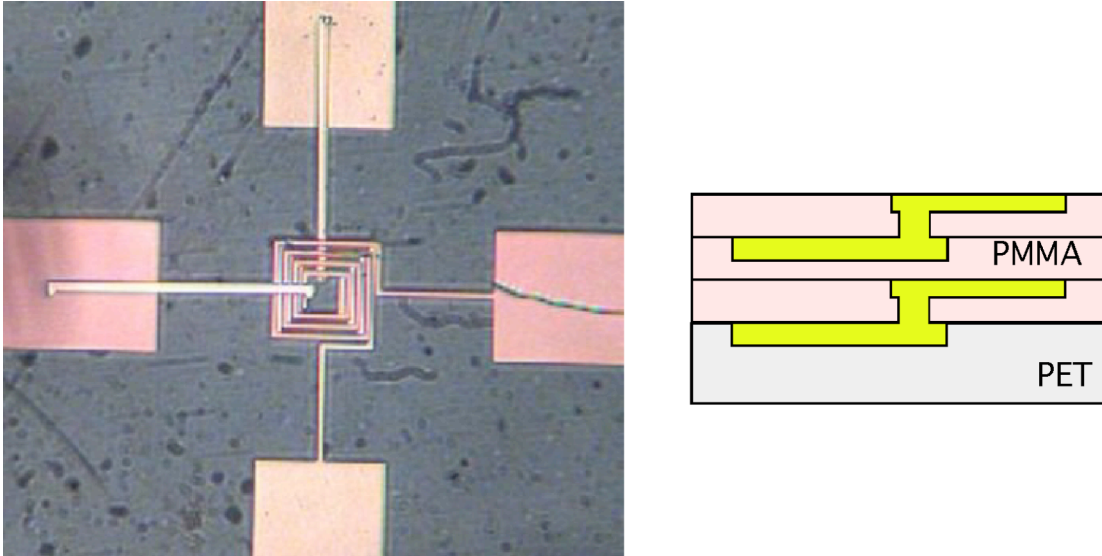
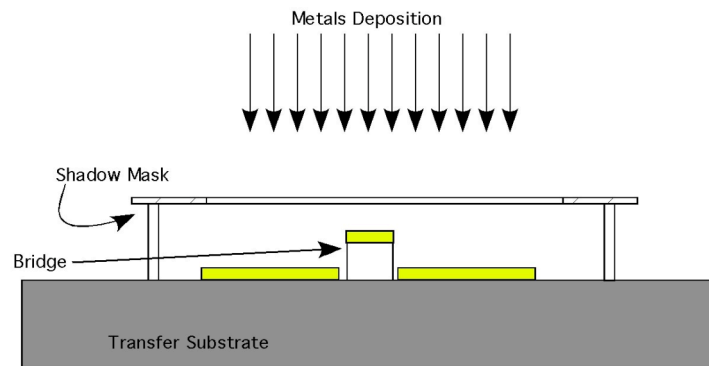


Figure 9.10: Optical image of transformer printed onto PET substrate. The device was constructed from the sequential printing of Au lines and vias. (Courtesy of A. Tunnell, UMD)

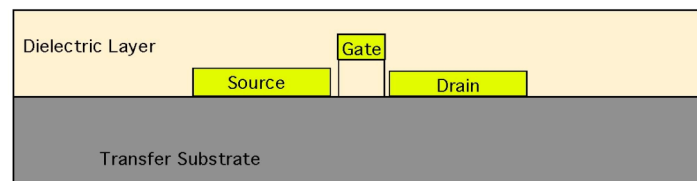
9.7 Self-Aligned Electrode Subassemblies

Figure 9.11 illustrates a concept that might make it possible to print self-aligned electrode subassemblies. The concept is based on work established by Professor John Fourkas of UMD which uses a two photopolymerization process to fabricate 3D structures on a substrate.¹⁸⁵ A bridge and associated shadow mask could be fabricated onto a substrate. A metallic film could be deposited through the shadow mask such that the metal coated the bridge and is shadowed by the bridge. The metal coated bridge becomes the gate electrode and the disconnected two metal features become the S/D electrodes. The width and length of the bridge define the channel length L and width W of the electrode subassembly. The height of the bridge defines the dielectric thickness. The shadow mask can then be removed and a polymer dielectric spin coated onto the substrate surface. This can all be transfer printed over to a flexible device substrate to create an electrode subassembly that has been self-

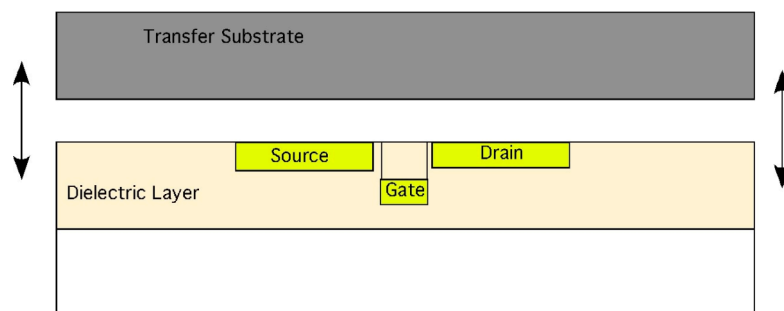
aligned and has a polymer dielectric layer. The printing of a semiconducting film would then complete the fabrication.



(a) Metals Deposition



(b) Spin coat dielectric layer



(c) Transfer Print

Figure 9.11: Conceptual illustration of a self-aligned electrode subassembly created using a two-photo polymerization technique.

9.8 Summary

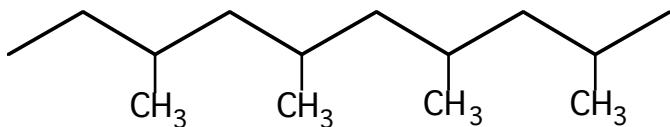
The research reported here provides a broad overview of materials issues and potential applications for transfer printing. Specifically, this method has been developed 1) for the placement of organic, inorganic and nanoscale materials and 2) for the sequential assembly of dissimilar materials all onto plastic substrates. The transfer printing method was expanded to the fabrication of high quality TFTs onto plastic substrates.

Because of their sensitivity to environmental and processing conditions, the emphasis on organic semiconductor materials has provided an excellent metric by which to highlight the advantages and potentials of transfer printing. Continuing research into materials adhesion, size scaling and multi-step fabrication for complex printed circuits is expected to lead to further advances toward low-cost, flexible electronics.

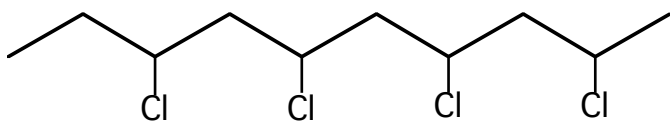
Appendix A Chemical Structures of Polymers



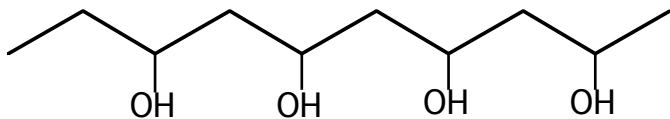
Polyethylene (PE) $T_g = -120\text{ }^\circ\text{C}$



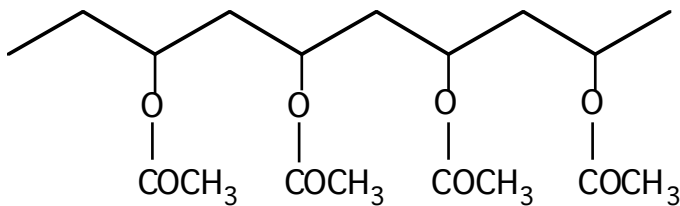
Polypropylene (PP) $T_g = -20\text{ }^\circ\text{C}$.



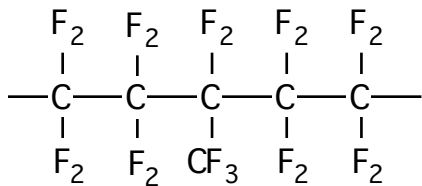
Polyvinylchloride (PVC) $T_g = 81\text{ }^\circ\text{C}$.



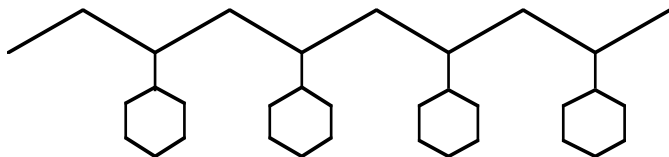
Polyvinylalcohol (PVA) $T_g = 49\text{ }^\circ\text{C}$.



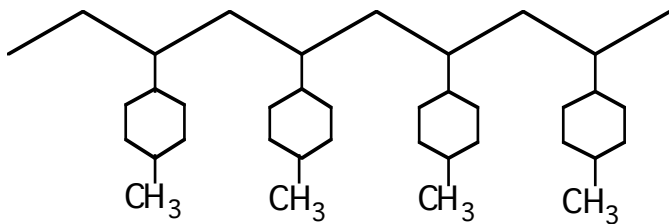
Polyvinylacetate (PVAc) $T_g = 28\text{ }^\circ\text{C}$.



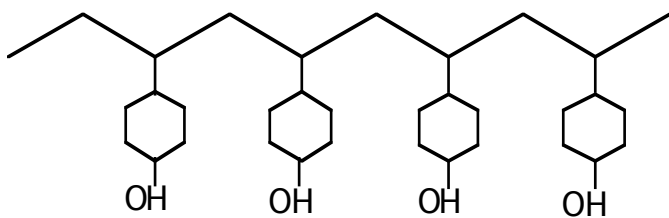
Fluorinated Ethylene Propylene (FEP) commonly referred to as Teflon. $T_g = 225\text{ }^\circ\text{C}$.



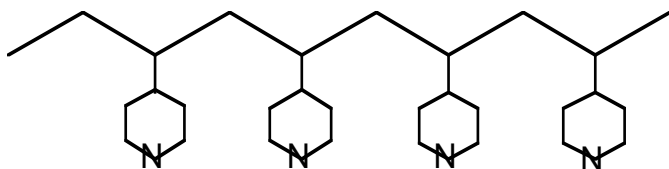
Polystyrene (PS) $T_g = 100\text{ }^\circ\text{C}$.



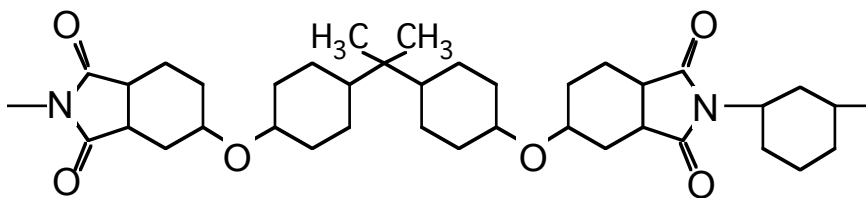
Poly(α -methylstyrene) (P α MS) $T_g = 106\text{ }^\circ\text{C}$.



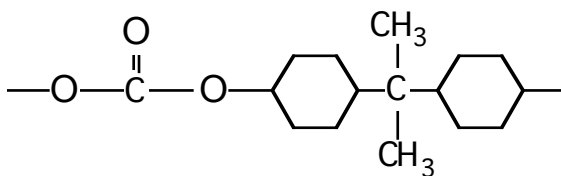
Poly(hydroxystyrene) (PHS) $T_g = 167\text{ }^\circ\text{C}$



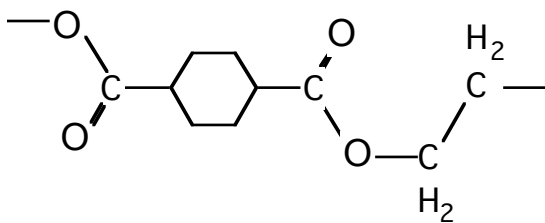
Poly(vinylpyridine) (PVPy) $T_g = 142\text{ }^{\circ}\text{C}$.



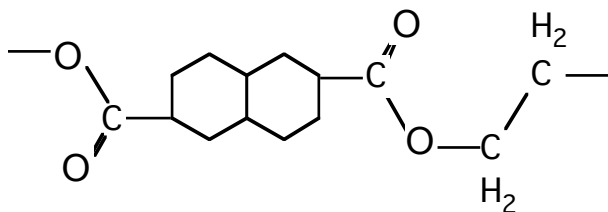
Polyimide (PI) commonly referred to as Kapton. $T_g = 385\text{ }^{\circ}\text{C}$



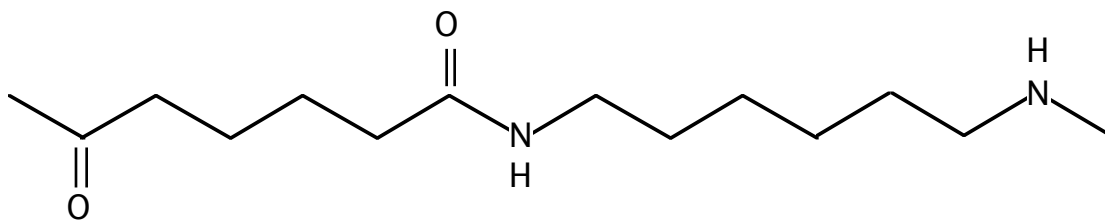
Polycarbonate (PC) $T_g = 150\text{ }^{\circ}\text{C}$.



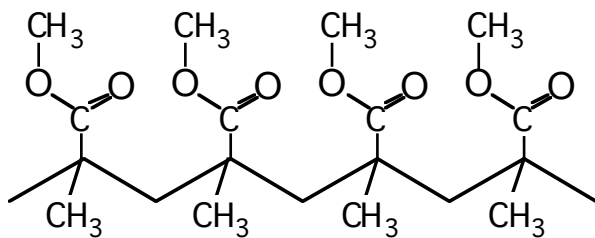
Polyethylene Terephthalate (PET) $T_g = 85\text{ }^{\circ}\text{C}$.



Polyethylene Naphthalene (PEN) $T_g = 125\text{ }^{\circ}\text{C}$.



Nylon 6,6 $T_g = 45\text{ }^{\circ}\text{C}$.



Polymethylmethacrylate (PMMA) $T_g = 105\text{ }^{\circ}\text{C}$.

References

- 1 D. R. Gamota, P. Brazis, K. Kalyanasundaram, and J. Zhang, *Printed Organic and Molecular Electronics*. (Kluwer Academic Publishers, Boston, 2004).
- 2 G. H. Gelinck, H. E. A. Huitema, E. V. Veenendaal, E. Cantatore, L. Schrijnemakers, J. B. P. H. V. D. Putten, T. C. T. Geuns, M. Beenhakkers, J. B. Giesbers, B.-H. Huisman, E. J. Meijer, E. M. Benito, F. J. Touwslager, A. W. Marsman, B. J. E. V. Rens, and D. M. D. Leeuw, "Flexible Active-Matrix Displays and Shift Registers Based on Solution-Processed Organic Transistors," *Nat. Mater.* **3**, 106 (2004).
- 3 T. W. Kelley, P. F. Baude, C. Gerlach, D. E. Ender, D. Muyres, M. A. Haase, D. E. Vogel, and S. D. Theiss, "Recent Progress in Organic Electronics: Materials, Devices, and Processes," *Chem. Mater.* **16**, 4413-4422 (2004).
- 4 J. B. Lee and V. Subramanian, "Weave Patterned Organic Transistors on Fiber for E-Textiles," *IEEE Trans. on Electron. Devices* **52** (2), 269 (2005).
- 5 J. T. Mabeck and G. G. Malliaras, "Chemical and Biological Sensors Based on Organic Thin-Film Transistors," *Anal. Bioanal. Chem.* **384**, 343-353 (2006).
- 6 M. Alpert, in *Scientific American* (2005), Vol. 292, pp. 94-96.
- 7 S. R. Forrest, "The Path to Ubiquitous and Low-Cost Organic Electronic Appliances on Plastic," *Nature* **428**, 911 (2004).
- 8 E. Reichmanis, H. Katz, C. Kloc, and A. Maliakal, "Plastic Electronic Devices: From Materials Design to Device Applications," *Proc. IEEE* **10** (3), 87-105 (2005).
- 9 J. W. P. Hsu, "Soft Lithography: Contacts to Organics," *Materials Today* **July/August**, 42-54 (2005).
- 10 Y. Xia and G. M. Whitesides, "Soft Lithography Review," *Angew. Chem. Int. Ed.* **37**, 550-575 (1998).
- 11 Y.-L. Loo, R. L. Willett, K. W. Baldwin, and J. A. Rogers, "Interfacial Chemistries for Nanoscale Transfer Printing," *J. Am. Chem. Soc.* **124**, 7654-7658 (2002).
- 12 K. J. Lee, M. J. Motala, M. A. Meitl, W. R. Childs, R. Menard, A. K. Shim, J. A. Rogers, and R. G. Nuzzo, "Large-Are, Selective Transfer of Microstructured Silicon: A Printing-Based Approach to High-Performance Thin-Film Transistors Supported on Flexible Substrates," *Adv. Mater.* **17**, 2332-2336 (2005).
- 13 A. Kumar and G. M. Whitesides, "Features of Gold Having Micrometer to Centimeter Dimensions Can Be Formed through a Combination of Stamping with an Elastomeric Stamp and an Alkanethiol "Ink" Followed by Chemical Etching," *Appl. Phys. Lett.* **63**, 2002-2004 (1993).
- 14 H. A. Biebuyck and N. B. Larsen, "Lithography Beyond Light: Microcontact Printing with Monolayer Resists," *IBM J. of Res. & Dev.* **41**, 159 (1997).
- 15 P. Calvert, "Inkjet Printing for Materials and Devices," *Chem. Mater* **13**, 3299-3305 (2001).

- 16 S. Y. Chou, P. R. Krauss, and P. J. Renstrom, "Imprint Lithography with 25-
Nanometer Resolution," *Science* **272**, 85-87 (1996).
- 17 B. H. Hamadani and D. Natelson, "Extracting Contact Effects in Organic
Fets," *Proc. IEEE* **93** (7), 1306-1311 (2005).
- 18 J. N. Israelachvili, *Intermolecular and Surface Forces*. (Academic Press,
London, 1991).
- 19 R. J. Good, "Contact Angle, Wetting and Adhesion: A Critical Review," *J.*
Adhesion Sci. **6** (12), 1269-1302 (1992).
- 20 H.-C. Scheer and H. Schulz, "A Contribution to the Flow Behaviour of Thin
Polymer Films During Hot Embossing Lithography," *Microelectron. Eng.* **56**,
311-332 (2001).
- 21 D. R. Hines, S. Mezheny, M. Breban, E. D. Williams, V. W. Ballarotto, G.
Esen, A. Southard, and M. S. Fuhrer, "Nanotransfer Printing of Organic and
Carbon Nanotube Thin-Film Transistors on Plastic Substrates," *Appl. Phys.*
Lett. **86**, 163101-163103 (2005).
- 22 D. R. Hines, V. W. Ballarotto, E. D. Williams, Y. Shao, and S. A. Solin,
"Transfer Printing Methods for the Fabrication of Flexible Organic
Electronics," *J. Appl. Phys.* **101**, 24503 (2007).
- 23 Y. Shao, S. A. Solin, D. R. Hines, and E. D. Williams, "The Effect of Transfer
Printing on Pentacene Thin-Film Crystal Structure," *J. Appl. Phys.* **100**,
044512 (2006).
- 24 A. J. Tunnell, D. R. Hines, E. Gomar-Nadal, and E. D. Williams, "Printing-
Induced Improvements of Organic Thin-Film Transistors," *Org. Electron.*
(Submitted 2007).
- 25 D. R. Hines, A. Southard, M. S. Fuhrer, and E. D. Williams, "P3ht Otft
Devices on Flexible Substrates," In Preperation (2007).
- 26 S. E. Fritz, T. W. Kelley, and C. D. Frisbie, "Effect of Dielectric Roughness
on Performance of Pentacene Tfts and Restoration of Performance with a
Polymeric Smoothing Layer," *J. Phys. Chem. B* **109**, 10574-10577 (2005).
- 27 F. Garnier, A. Yassar, R. Hajlaoui, G. Horowitz, F. Deloffre, B. Servet, S.
Ries, and P. Alnot, "Molecular Engineering of Organic Semiconductors:
Design of Self-Assembly Properties in Conjugated Thiophene Oligomers," *J.*
Am. Chem. Soc. **115**, 8716-8721 (1993).
- 28 J. G. Laquindanum, H. E. Katz, A. Dodabalapur, and A. J. Lovinger, "N-
Channel Organic Transistor Materials Based on Naphthalene Frameworks," *J.*
Am. Chem. Soc. **118**, 11331-11332 (1996).
- 29 D. L. Keeling, N. S. Oxtoby, C. Wilson, M. J. Humphry, N. R. Champness,
and P. H. Beton, "Assembly and Processing of Hydrogen Bond Induced
Supramolecular Nanostructures," *Nano Lett.* **3**, 9-12 (2003).
- 30 H. Sirringhaus, P. J. Brown, R. H. Friend, M. M. Nielsen, K. Bechgaard, B.
M. W. Langeveld-Voss, A. J. H. Spiering, R. A. J. Janssen, E. W. Meijer, P.
Herwig, and D. M. D. Leeuw, "Two-Dimensional Charge Transport in Self-
Organized, High-Mobility Conjugated Polymers," *Nature* **104**, 685 (1999).
- 31 B. Groenendaal, F. Jonas, D. Freitag, H. Pielartzik, and J. R. Reynolds,
"Poly(3,4-Ethylenedioxythiophene) and Its Derivatives: Past, Present, and
Future," *Adv. Mater.* **12**, 481 (2000).

- 32 H. Sirringhaus, T. Kawase, R. H. Friend, T. Shimoda, M. Inbasekaran, W.
Wu, and E. P. Woo, "High-Resolution Inkjet Printing of All-Polymer
Transistor Circuits," *Science* **290**, 2123 (2000).
- 33 T. Granlund, T. Nyberg, L. S. Roman, M. Svensson, and O. Inganäs,
"Patterning of Polymer Light-Emitting Diodes with Soft Lithography," *Adv.*
Mater. **12**, 269 (2000).
- 34 C. J. Drury, C. M. J. Mutsaers, C. M. Hart, M. Matters, and D. M. D. Leeuw,
"Low-Cost All-Polymer Integrated Circuits," *Appl. Phys. Lett.* **73**, 108
(1998).
- 35 T. Durkop, S. A. Grtty, E. Cobas, and M. S. Fuhrer, "Extrodinary Mobility in
Semiconducting Carbon Nanotubes," *Nano Lett.* **4**, 35-39 (2004).
- 36 D. B. Mitzi, K. Chondroudís, and C. R. Kagan, "Organic-Inorganic
Electronics," *IBM J. Res. & Dev.* **45**, 29-45 (2001).
- 37 A. Dodabalapur, L. Torsi, and H. E. Katz, "Organic Transistors: Two-
Dimensional Transport and Improved Electrical Characteristics," *Science* **268**,
270-271 (1995).
- 38 E. L. Granstrom and C. D. Frisbie, "Field Effect Conductance Measurements
on Thin Crystals of Sexithiophene," *J. Phys. Chem. B* **103**, 8842-8849 (1999).
- 39 B. H. Hamadani and D. Natelson, "Temperature-Dependent Contact
Resistances in High-Quality Polymer Field-Effect Transistors," *Appl. Phys.*
Lett. **84** (3), 443-445 (2004).
- 40 C. D. Dimitrakopoulos and D. J. Masearo, "Organic Thin-Film Transistors: A
Review of Recent Advances," *IBM J. of Res. and Dev.* **45** (1), 11-27 (2001).
- 41 C. D. Dimitrakopoulos and P. R. L. Malenfant, "Organic Thin Film
Transistors for Large Area Electronics," *Adv. Mater.* **14**, 99-117 (2002).
- 42 D. Knipp, R. A. Street, A. Volkel, and J. Ho, "Pentacene Thin Film
Transistors on Inorganic Dielectrics: Morphology, Structural Properties, and
Electronic Transport," *J. Appl. Phys.* **93** (1), 347-355 (2003).
- 43 D. Knipp, R. A. Street, and A. R. Völkel, "Morphology and Electronic
Transport of Polycrystalline Pentacene Thin-Film Transistors," *Appl. Phys.*
Lett. **82**, 3907-3909 (2003).
- 44 D. Knipp, R. A. Street, B. Krusor, J. Ho, and R. B. Apte, "Influence of the
Dielectric on the Growth and Performance of Pentacene Thin Film
Transistors," *Mat. Res. Soc. Symp. Proc.* **708**, BB8.10.11-16 (2002).
- 45 J. Veres, S. Ogier, and G. Lloyd, "Gate Insulators in Organic Field-Effect
Transistors," *Chem. Mater.* **16**, 4543-4555 (2004).
- 46 D. J. Gundlach, T. N. Jackson, D. G. Schlom, and S. F. Nelson, "Solvent-
Induced Phase Transition in Thermally Evaporated Pentacene Films," *Appl.*
Phys. Lett. **74**, 3302-3304 (1999).
- 47 I. P. M. Bouchoms, W. A. Schoonveld, J. Vrijmoeth, and T. M. Klapwijk,
"Morphology Identification of the Thin Film Phases of Vacuum Evaporated
Pentacene on SiO₂ Substrates," *Synth. Met.* **104**, 175-178 (1999).
- 48 M. Tejima, K. Kita, K. Kyuno, and A. Toriumi, "Study on the Growth
Mechanism of Pentacene Thin Films by the Analysis of Island Density and
Island Size Distribution," *Appl. Phys. Lett.* **85**, 3746-3748 (2004).

49 C. D. Dimitrakopoulos, A. R. Brown, and A. Pomp, "Molecular Beam
Deposited Thin Films of Pentacene for Organic Field Effect Transistor
Applications," *J. Appl. Phys.* **80** (4), 2501-2508 (1996).

50 Y.-Y. Lin, D. J. Gundlach, S. F. Nelson, and T. N. Jackson, "Stacked
Pentacene Layer Organic Thin-Film Transistors with Improved
Characteristics," *IEEE Electron Device Lett.* **18**, 606-608 (1997).

51 J. Collet, O. Tharaud, C. Legrand, A. Chapoton, and D. Vuillaume.,
"Performances of Sexithiophene Based Thin-Film Transistors Using Self-
Assembled Monolayers.," *Mat. Res. Soc. Symp. Proc.* **488**, 407-412 (1998).

52 L. L. Kosbar, C. D. Dimitrakopoulos, and D. J. Masearo, "The Effect of
Surface Preparation on the Structure and Electrical Transport in an Organic
Semiconductor," *Mat. Res. Soc. Symp. Proc.* **665**, C.10.16.11-16 (2001).

53 D. J. Gundlach, C.-C. S. Kuo, C. D. Sheraw, J. A. Nichols, and T. N. Jackson,
"Improved Organic Thin Film Transistor Performance Using Chemically
Modified Gate Dielectrics," *Proc. of SPIE* **4466**, 54-64 (2001).

54 M. Shtein, J. Mapel, J. B. Benziger, and S. R. Forrest, "Effects of Film
Morphology and Gate Dielectric Surface Preparation on the Electrical
Characteristics of Organic-Vapor-Phase-Deposited Pentacene Thin-Film
Transistors," *Appl. Phys. Lett.* **81**, 268-270 (2002).

55 A. Salleo, M. L. Chabinyc, M. S. Yang, and R. A. Street, "Polymer Thin-Film
Transistors with Chemically Modified Dielectric Interfaces," *Appl. Phys. Lett.*
81, 4383-4385 (2002).

56 J. Lee, K. Kim, J. H. Kim, S. Im, and D.-Y. Jung, "Optimum Channel
Thickness in Pentacene-Based Thin-Film Transistors," *Appl. Phys. Lett.* **82**,
4169-4171 (2003).

57 H. Sirringhaus, N. Tessler, and R. H. Friend, "Integrated Optoelectronic
Devices Based on Conjugated Polymers," *Science* **280**, 1741-1744 (1998).

58 H. Yang, S. H. Kim, L. Yang, S. Y. Yang, and C. E. Park, "Pentacene
Nanostructures on Surface-Hydrophobicity-Controlled Polymer/SiO₂ Bilayer
Gate-Dielectrics," *Adv. Mater.* **19**, 2868-2872 (2007).

59 G. Nunes Jr., S. G. Zane, and J. S. Meth, "Styrenic Polymers as Gate
Dielectrics for Pentacene Field-Effect Transistors," *J. Appl. Phys.* **98**, 104503
(2005).

60 T. W. Kelley, D. V. Muyres, P. F. Baude, T. P. Smith, and T. D. Jones, "High
Performance Organic Thin Film Transistors," *Mat. Res. Soc. Symp. Proc.* **771**,
L6.5.1-11 (2003).

61 C. Kim, A. Facchetti, and T. J. Marks, "Gate Dielectric Microstructural
Control of Pentacene Film Growth Mode and Field-Effect Transistor
Performance," *Adv. Mater.* (2007).

62 J. Puigdollers, C. Voz, I. Martin, A. Orpella, M. Vetter, and R. Alcubilla,
"Pentacene Thin-Film Transistors on Polymeric Gate Dielectric: Device
Fabrication and Electrical Characterization," *J. Non-Crystal. Solids* **338-340**,
617-621 (2004).

63 J. Veres, "Interface Effects in Organic Field Effect Transistors. ," *MRS Fall
Meeting*, K8.7 (2003).

- 64 Y. Hong, F. Yan, P. Migliorato, S. H. Han, and J. Jang, "Injection-Limited
Contact in Bottom-Contact Pentacene Organic Thin-Film Transistors," *Thin
Solid Films* **515**, 4032-4035 (2007).
- 65 D. J. Gundlach, L. Zhou, J. A. Nichols, and T. N. Jackson, "An Experimental
Study of Contact Effects in Organic Thin-Film Transistors," *J. Appl. Phys.*
100, 024509 (2006).
- 66 M. Kymissis, C. D. Dimitrakopoulos, and S. Purushothaman,
"Highperformance Bottom Electrode Organic Thin-Film Transistors," *IEEE
Trans. on Electron. Devices* **48** (6), 1060-1064 (2001).
- 67 C. K. Chiang, J. C. R. Fincher, Y. W. Park, A. J. Heeger, H. Shirakawa, E. J.
Louis, S. C. Gau, and A. G. Macdiarmid, "Electrical Conductivity in Doped
Polyacetylene," *Phys. Rev. Lett.* **39**, 1098 (1977).
- 68 F. Ebisawa, T. Kurokawa, and S. Nara, "Electrical Properties of
Polyacetylene/Polysiloxane Interface," *J. Appl. Phys.* **54**, 3255 (1983).
- 69 A. Assadi, C. Svensson, M. Willander, and O. Inganäs, "Field-Effect Mobility
of Poly(3-Hexylthiophene)," *Appl. Phys. Lett.* **53**, 195 (1988).
- 70 G. Horowitz, D. Fichou, X. Peng, Z. Xu, and F. Garnier, "A Field-Effect
Transistor Based on Conjugated Alpha-Sexithienyl," *Solid State Commun.* **72**,
381 (1989).
- 71 G. Horowitz, X. Z. Peng, D. Fichou, and F. Garnier, "Organic Thin-Film
Transistors Using Pi-Conjugated Oligomers - Influence of the Chain-Length,"
J. Mol. Electron. **7**, 85-89 (1991).
- 72 G. Horowitz, D. Fichou, X. Z. Peng, and F. Garnier, "Thin-Film Transistors
Based on Alpha-Conjugated Oligomers," *Synth. Met.* **41**, 1127-1130 (1991).
- 73 A. R. Brown, A. Pomp, C. M. Hart, and D. M. D. Leeuw, "Logic Gates Made
from Polymer Transistors and Their Use in Ring Oscillators," *Science* **270**,
972-974 (1995).
- 74 G. H. Gelinck, T. C. T. Geuns, and D. M. D. Leeuw, "High-Performance All-
Polymer Integrated Circuits," *Appl. Phys. Lett.* **77**, 1487 (2000).
- 75 J. Needham, *Science and Civilization in China; Vol 5, Pt 1 Paper and
Printing*. (Cambridge [Eng.] University Press).
- 76 K. Doo-Jong, "History of Korean Printing," *Korea Journal* **3**, 22 (1963).
- 77 P. E. J. Legierse and J. H. T. Pasman, *Polymers in Information Storage
Technology*. (Plenum, New York, 1989).
- 78 W. Michaeli and R. Bieleser, "Metal Injection Molding: Shaping Sintered
Metal Parts," *Adv. Mater.* **3**, 260-262 (1991).
- 79 T. E. Huber and L. Luo, "Far-Infrared Propagation in Metal Wire
Microstructures," *Appl. Phys. Lett.* **70**, 2502-2504 (1997).
- 80 P. Hoyer, N. Baba, and H. Masuda, "Small Quantum-Sized Cds Particles
Assembled to Form a Regularly Nanostructured Porous Film," *Appl. Phys.*
Lett. **66**, 2700-2702 (1995).
- 81 H. Masuda and K. Fukuda, "Ordered Metal Nanohole Arrays Made by a Two-
Step Replication of Honeycomb Structures of Anodic Alumina," *Science* **268**,
1466-1468 (1995).
- 82 P. Hoyer, "Semiconductor Nanotube Formation by a Two-Step Template
Process," *Adv. Mater.* **8**, 857-859 (1996).

- 83 J. S. Winslow, "Mastering and Replication of Reflective Videodiscs," IEEE
Trans. Consumer Electron **22**, 318-326 (1976).
- 84 H. W. Lehmann, R. Widmer, M. Ebnoether, A. Wokaun, M. Meier, and S. K.
Miller, "Fabrication of Sub-Micron Crossed Square-Wave Gratings by Dry
Etching and Thermoplastic Replication Techniques " J. Vac. Sci. Technol. B
1, 1207-1210 (1983).
- 85 C. M. Rodia, "Precision Electroforming for Optical Disk Manufacturing,"
Proc. SPIE Int. Soc. Opt. Eng. **529**, 69-75 (1985).
- 86 K.-H. Schlereth and H. Böttcher, "Embossed Grating Lead Chalcogenide
Distributed-Feedback Lasers," J. Vac. Sci. Technol. B **10**, 114-117 (1992).
- 87 M. Emmelius, G. Pawlowski, and H. W. Vollmann, "Materialien Für Die
Optische Datenspeicherung," Angew. Chem. Int. Ed. Engl **101**, 1475-1501
(1989).
- 88 F. P. Shvartsman, *Diffraction and Miniaturized Optics*. (SPIE Optical
Engineering Press, Bellingham, WA, 1993), pp.165-186.
- 89 S. Y. Chou, P. R. Krauss, and P. J. Renstrom, "Imprint of Sub-25 Nm Vias
and Trenches in Polymers," Appl. Phys. Lett. **67**, 3114-3116 (1995).
- 90 S. Y. Chou, P. R. Krauss, and P. J. Renstrom, "Imprint Lithography with 25-
Nanometer Resolution," Science **272**, 85-87 (1996).
- 91 M. T. Gale, *Micro-Optics: Elements, Systems and Applications*. (Taylor &
Francis, London, 1997), pp.153-179.
- 92 H. C. H. V. Rijsewijk, P. E. J. Legierse, and G. E. Thomas, Philips Tech.
Rev. **40**, 287-297 (1982).
- 93 J. G. Kloosterboer, G. J. M. Lippits, and H. C. Meinders, Philips Tech. Rev.
40, 198-309 (1982).
- 94 B. D. Terris, H. J. Mamin, M. E. Best, and J. A. L. Rugar, "Nanoscale
Replication for Scanning Probe Data Storage," Appl. Phys. Lett. **69**, 4262-
4264 (1996).
- 95 U. Reblan, H. Endert, and G. Zaal, Laser Focus World **30**, 91-96 (1994).
- 96 S. A. Weiss, "Think Small - Lasers Compete in Micromachining " Photonics
Spectra **29** (10), 108-114 (1995).
- 97 M. A. Roberts, J. S. Rossier, P. Bercier, and H. Giault, "Uv Laser Machined
Polymer Substrates for the Development of Microdiagnostic Systems," Anal.
Chem. **69**, 2035-2042 (1997).
- 98 D. Y. Kim, S. K. Tripathy, L. Li, and J. Kumar, "Laser-Induced Holographic
Surface Relief Gratings on Nonlinear Optical Polymer Films," Appl. Phys.
Lett. **66**, 1166-1168 (1995).
- 99 M. Müllenborn, H. Dirac, and J. W. Peterson, "Silicon Nanostructures
Produced by Laser Direct Etching," Appl. Phys. Lett. **66**, 3001-3003 (1995).
- 100 N. Kramer, M. Niesten, and C. Schönenberger, "Resistless High Resolution
Optical Lithography on Silicon," Appl. Phys. Lett. **67**, 2989-2991 (1995).
- 101 N. L. Abbott, A. Kumar, and G. M. Whitesides, "Using Micromachining,
Molecular Self-Assembly, and Wet Etching to Fabricate 0.1-1-.Mu.M Scale
Structures of Gold and Silicon," Chem. Mater. **6**, 596-602 (1994).

- 102 T. J. Hirsch, R. F. Miracky, and C. Lin, "Selective-Area Electroless Copper
Plating on Polyimide Employing Laser Patterning of a Catalytic Film," *Appl.*
Phys. Lett. **57**, 1357-1359 (1990).
- 103 V. Malba and A. F. Bernhardt, "Laser Surface Modification for Selective
Electroplating of Metal: A 2.5 M/S Laser Direct Write Process," *Appl. Phys.*
Lett. **60**, 909-911 (1992).
- 104 A. Miehr, R. A. Fisher, O. Lehmann, and M. Stuke, "Laser Direct Writing of
Beta-Co/Ga and Mn/Ga Alloy Microstructures from Organometallic Single-
Source Precursors," *Adv. Mater. Opt. Electron.* **6**, 27-32 (1996).
- 105 M. Datta, "Fabrication of an Array of Precision Nozzles by through-Mask
Electrochemical Micromachining," *J. Electrochem. Soc.* **142**, 3801-3805
(1995).
- 106 H. Tabei, S. Nara, and K. Matsuyama, "Method for Forming a Printed Circuit
by Photolysis of Silver Salt of Organic Acid," *J. Electrochem. Soc.* **121**, 67-69
(1974).
- 107 A. Rose and P. K. Weimer, "Physical Limits to the Performance of Imaging-
Systems," *Physics Today* **42** (9), 24-32 (1989).
- 108 M. R. V. Sahyun, "Secrecies of Photographic Development Revealed!," *Chem*
Tech **22** (7), 418-424 (1992).
- 109 S. Leppävuori, J. Väänänen, M. Lothi, J. Remes, and A. Uusimäki, "A Novel
Thick-Film Technique, Gravure Offset Printing, for the Realization of Fine-
Line Sensor Structures," *Sens. Actuators A* **42**, 593-596 (1994).
- 110 H. Moilanen, J. Lappalainen, and S. Leppävuori, "Development of
Piezoelectric Micromovement Actuator Fabrication Using a Thick-Film
Double-Paste Printing Method," *Sens. Actuators A* **43**, 357-365 (1994).
- 111 M. Döring, *Philips Tech. Rev.* **40**, 192-198 (1982).
- 112 E. Anczurowski, J. Oliver, and R. H. Marchessault, "New Papers for New
Printers," *Chem. Tech.* **16** (5), 304-310 (1986).
- 113 C. Wu, "Ink Jets Not Just for the Printed Page," *Sci. News* **151**, 205 (1997).
- 114 A. P. Blanchard, R. J. Kaiser, and L. E. Hood, "High-Density Oligonucleotide
Arrays," *Biosens. Bioelectron.* **11**, 687-690 (1996).
- 115 A. V. Lemmo, J. T. Fisher, H. M. Geysen, and D. J. Rose, "Characterization
of an Inkjet Chemical Microdispenser for Combinatorial Library Synthesis,"
Anal. Chem. **69**, 543-551 (1997).
- 116 M. Stolka, *Chem Tech* **19** (8), 487-495 (1989).
- 117 Q. M. Pai and B. E. Springett, "Physics of Electrophotography " *Rev. Mod.*
Phys. **65**, 163-211 (1993).
- 118 D. C. Neckers, "Stereolithography - an Introduction," *Chem Tech* **20** (10),
615-619 (1990).
- 119 T. M. Bloomstein and D. J. Ehrlich, "Stereo Laser Micromachining of
Silicon," *Appl. Phys. Lett.* **61**, 708-781 (1992).
- 120 F. T. Wallenberger, "Rapid Prototyping Directly from the Vapor Phase,"
Science **267**, 1274-1275 (1995).
- 121 O. Lehmann and M. Stuke, "Laser-Driven Movement of Three-Dimensional
Microstructures Generated by Laser Rapid Prototyping," *Science* **270**, 1644-
1646 (1995).

- 122 Y. Xia, Harvard University, 1996.
- 123 X.-M. Zhao, Y. Xia, and G. M. Whitesides, "Soft Lithographic Methods for Nano-Fabrication," *J. Mater. Chem.* **7**, 1069-1074 (1997).
- 124 D. Qin, Y. Xia, J. A. Rogers, R. J. Jackman, X.-M. Zhao, and G. M. Whitesides, "Microfabrication, Microstructures and Microsystems," *Top. Curr. Chem.* **194**, 1-20 (1998).
- 125 G. M. Whitesides and Y. Xia, "Soft Lithography," *Annu. Rev. Mater. Sci.* **28**, 153-184 (1998).
- 126 Y. Xia, E. Kim, X.-M. Zhao, J. A. Rogers, M. Prentiss, and G. M. Whitesides, "Complex Optical Surfaces Formed by Replica Molding against Elastomeric Masters," *Science* **273**, 347-349 (1996).
- 127 X.-M. Zhao, Y. Xia, and G. M. Whitesides, "Fabrication of Three-Dimensional Micro-Structures: Microtransfer Molding," *Adv. Mater.* **8**, 837-840 (1996).
- 128 E. Kim, Y. Xia, and G. M. Whitesides, "Polymer Microstructures Formed by Moulding in Capillaries," *Nature* **376**, 581-584 (1995).
- 129 E. King, Y. Xia, X.-M. Zhao, and G. M. Whitesides, "Solvent-Assisted Microcontact Molding: A Convenient Method for Fabricating Three-Dimensional Structures on Surfaces of Polymers," *Adv. Mater.* **9**, 651-654 (1997).
- 130 J. Kohler, in *Printed Organic and Molecular Electronics*, edited by D. R. Gamota, P. Brazis, K. Kalyanasundaram et al. (Kluwer Academic Publishers, Boston, 2004), pp. 193-245.
- 131 A. Afzali, C. D. Dimitrakopoulos, and T. L. Breen, "High-Performance, Solution-Processed Organic Thin Film Transistors from a Novel Pentacene Precursor," *J. Am. Chem. Soc.* **124**, 8812 (2002).
- 132 J.-F. Chang, B. Sun, D. W. Breiby, M. M. Nielsen, T. I. Sölling, M. G. McCulloch, and H. Sirringhaus, "Enhanced Mobility of Poly(3-Hexylthiophene) Transistors by Spin-Coating from High-Boiling-Point Solvents," *Chem. Mater.* **16**, 4772-4776 (2004).
- 133 K. Murata, presented at the Proc. of the Int. Conf. on MEMS, NANO and Smart Systems, Los Alamitos, CA, 2003 (unpublished).
- 134 C. W. Sele, T. V. Werne, R. H. Friend, and H. Sirringhaus, "Lithography-Free, Self-Aligned Inkjet Printing with Sub-Hundred-Nanometer Resolution," *Adv. Mater.* **17**, 997 (2005).
- 135 Y.-L. Loo, J. W. P. Hsu, R. L. Willett, K. W. Baldwin, K. W. West, and J. A. Rogers, "High-Resolution Transfer Printing on Gaas Surfaces Using Alkane Dithiolmonolayers," *J. Vac. Sci. Technol. B* **20**, 2853 (2002).
- 136 W. R. Childs and R. G. Nuzzo, "Decal Transfer Microlithography: A New Soft-Lithographic patterning Method," *J. Am. Chem. Soc.* **124**, 13583 (2002).
- 137 M. Colburn, S. Johnson, M. Stewart, S. Damle, T. Bailey, B. J. Choi, M. Wedlake, T. Michaelson, S. V. Sreenivasan, J. Ekerdt, and C. G. Willson, presented at the SPIE's 24th International Symposium on Microlithography: Emerging Lithographic Technologies III, Santa Clara, CA, 1999 (unpublished).

- 138 P. S. Hong, J. Kim, and H. H. Lee, "Contrast Modified Room-Temperature
Imprint Lithography," *Appl. Phys. Lett.* **88**, 173105 (2006).
- 139 H. Lee and G.-Y. Jung, "Wafer to Wafer Nano-Imprinting Lithography with
Monomer Based Thermally Curable Resin," *Microelectron. Eng.* **77**, 168-174
(2005).
- 140 S. Y. Chou, C. Keimel, and J. Gu, "Ultrafast and Direct Imprint of
Nanostructures in Silicon," *Nature* **417**, 835 (2002).
- 141 H. W. Ro, R. L. Jones, H. Peng, D. R. Hines, H.-J. Lee, Eric K. Lin, A.
Karim, D. Y. Yoon, D. W. Gidley, and C. L. Soles, "The Direct Patterning of
Nanoporous Interlayer Dielectric Insulator Films by Nanoimprint
Lithography," *Adv. Mater.* **19**, 2919-2924 (2007).
- 142 S. Y. Chou, P. R. Krauss, W. Zhang, L. Guo, and L. Zhuang, "Sub-10 Nm
Imprint Lithography and Applications," *J. Vac. Sci. Technol. B* **15**, 2897
(1997).
- 143 A. C. Arias, S. E. Ready, R. Lujan, W. S. Wong, K. E. Paul, A. Salleo, M. L.
Chabinyc, R. Apte, R. A. Street, Y. Wu, P. Liu, and B. Ong, "All Jet-Printed
Polymer Thin-Film Transistor Active-Matrix Backplanes," *Appl. Phys. Lett.*
85 (15), 3304-3306 (2004).
- 144 A. Kumar and G. M. Whitesides, "Features of Gold Having Micrometer to
Centimeter Dimensions Can Be Formed through a Combination of Stamping
with an Elastomeric Stamp and an Alkanethiol "Ink" Followed by Chemical
Etching," *Appl. Phys. Lett.* **63** (14), 2002-2004 (1993).
- 145 R. Parashkov, E. Becker, T. Riedl, H.-H. Johannes, and W. Kowalsky,
"Microcontact Printing as a Versatile Tool for Patterning Organic Field-
Effect Transistors," *Adv. Mater.* **17**, 1523-1527 (2005).
- 146 D. R. Hines, A. E. Southard, A. Tunnell, V. Sangwan, T. Moore, J.-H. Chen,
M. S. Fuhrer, and E. D. Williams, "Transfer Printing as a Method for
Fabricating Hybrid Devices on Flexible Substrates," *Proceedings of the SPIE*
Accepted (2007).
- 147 M. W. Pruessner, N. Siwak, K. Amarnath, S. Kanakaraju, W.-H. Chuang, and
R. Ghodssi, "End-Coupled Optical Waveguide Mems Devices in the Indium
Phosphide Material System," *J. Micromech. Microeng.* **16**, 832-842 (2006).
- 148 M. A. Meitz, Z.-T. Zhu, V. Kumar, K. J. Lee, X. Feng, Y. Y. Huang, I.
Adesida, R. G. Nuzzo, and J. A. Rogers, "Transfer Printing by Kinetic Control
of Adhesion to an Elastomeric Stamp," *Nat. Mater.* **5**, 33-38 (2006).
- 149 S. W. Lee, D. S. Lee, H. Y. Yu, E. E. B. Campbell, and Y. W. Park,
"Production of Individual Suspended Single-Walled Carbon Nanotubes Using
the Ac Electrophoresis Technique," *Appl. Phys. A* **78**, 283-286 (2004).
- 150 S. Ju, A. Facchetti, Y. Xuan, J. Liu, F. Ishikawa, P. Ye, C. Zhou, T. J. Marks,
and D. B. Janes, "Fabrication of Fully Transparent Nanowire Transistors for
Transparent and Flexible Electronics," *Nat. Nanotechnol.* **2**, 378-384 (2007).
- 151 T. L. Moore, D. R. Hines, S. Cho, S. B. Lee, and E. D. Williams, "Nanowire
Networks for Use as Printed Electrodes on Flexible Substates," *In Preparation*
(2007).
- 152 J. H. Chen, M. Ishigami, C. Jang, D. R. Hines, M. S. Fuhrer, and E. D.
Williams, "Printed Graphene Circuits," *Adv. Mater.* **In Press** (2007).

- 153 W. Kim, H.-C. Choi, M. Shim, Y. Li, D. Wang, and H. Dai, "Synthesis of
Ultralong and High Percentage of Semiconducting Single-Walled Carbon
Nanotubes," *Nano Lett.* **2**, 703-708 (2002).
- 154 H. Dallaporta and A. Cros, "Influence of Low-Energy Electron Irradiation on
the Adhesion of Gold Films on a Silicon Substrate.," *Appl. Phys. Lett.* **48**
(20), 1357-1359 (1986).
- 155 D. J. Resnick, D. P. Mancini, S. V. Sreenivasan, and C. G. Willson, "Release
Layers for Contact and Imprint Lithography," *Semicon. Int.* **June**, 71-79
(2002).
- 156 T. Bailey, B. J. Choi, M. Colburn, M. Meissl, S. Shaya, J. G. Ekerdt, S. V.
Sreenivasan, and C. G. Willson, "Step and Flash Imprint Lithography:
Template Surface Treatment and Defect Analysis," *J. Vac. Sci. Technol. B* **18**,
3572-3577 (2002).
- 157 R. Schroeder, L. A. Majewski, and M. Grell, "A Study of the Threshold
Voltage in Pentacene Organic Field-Effect Transistors," *Appl. Phys. Lett.* **83**
(15), 3201-3203 (2003).
- 158 R. R. Deshmukh and A. S. Shetty, "Surface Characterization of Polyethylene
Films Modified by Gaseous Plasma," *J. Appl. Poly. Sci.* **104**, 449-457 (2007).
- 159 C. C. Cedeno, J. S. P. Kam, T. Hoffmann, S. Zankovych, C. M. S. Torres, C.
Menozzi, M. Cavallini, M. Murgia, G. Ruani, F. Biscarini, M. Behl, R. Zentel,
and J. Ahopelto, "Nanoimprint Lithography for Organic Electronics,"
Microelectron. Eng. **61-62**, 25-31 (2002).
- 160 A. Dodabalapur, H. E. Katz, L. Torsi, and R. C. Haddon, "Organic
Heterostructure Field-Effect Transistors," *Science* **269** (5230), 1560-1562
(1995).
- 161 R. Ruiz, D. Choudhary, B. Nickel, T. Toccoli, K. C. Chang, A. C. Mayer, P.
Clancy, J. M. Blakely, R. L. Headrick, S. Iannotta, and G. G. Malliaras,
"Pentacene Thin Film Growth," *Chem. Mater.* **16** (23), 4497-4508 (2004).
- 162 A. D. Carlo, F. Piacenza, A. Bolognesi, B. Stadlober, and H. Maresch,
"Influence of Grain Sizes on the Mobility of Organic Thin-Film Transistors,"
Appl. Phys. Lett. **86** (263501) (2005).
- 163 F. Eder, H. Klauk, M. Halik, U. Zschieschang, G. Schmid, and C. Dehm,
"Organic Electronics on Paper," *Appl. Phys. Lett.* **84** (14), 2673-2675 (2004).
- 164 G. Wang, Y. Luo, and P. H. Beton, "High Mobility Organic Transistors
Fabricated from Single Pentacene Microcrystals Grown on a Polymer Film,"
Appl. Phys. Lett. **83** (15), 3108-3110 (2003).
- 165 D. J. Gundlach, L. Jia, and T. N. Jackson, "Pentacene Tft with Improved
Linear Region Characteristics Using Chemically Modified Source and Drain
Electrodes," *IEEE Electron Device Lett.* **22**, 571 (2001).
- 166 R. Ruiz, A. Papadimitratos, A. C. Mayer, and G. G. Malliaras, "Thickness
Dependence of Mobility in Pentacene Thin-Film Transistors," *Adv. Mater.* **17**,
1795-1798 (2005).
- 167 P.-Y. Lo, Z.-W. Pei, and J.-J. Hwang, "Study of Carrier Transport by
Pentacene Thin-Film Transistors at High Temperatures," *Jpn. J. Appl. Phys.,
Pt 1* **45** (4B), 3704-3707 (2006).

- 168 P. V. Necliudov, M. S. Shur, D. J. Gundlach, and T. N. Jackson, "Modeling of
Organic Thin Film Transistors of Different Designs," J. Appl. Phys. **88** (11),
6594-6597 (2000).
- 169 J. Zaumseil, T. Someya, Z. Bao, Y.-L. Loo, R. Cirelli, and J. A. Rogers,
"Nanoscale Organic Transistors That Use Source-drain Electrodes Supported
by High Resolution Rubber Stamps," Appl. Phys. Lett. **82**, 793-795 (2003).
- 170 I. Yagi, K. Tsukagoshi, and Y. Aoyagi, "Direct Observation of Contact and
Channel Resistance in Pentacene Four-Terminal Thin-Film Transistor
Patterned by Laser Ablation Method," Appl. Phys. Lett. **84** (5), 813-815
(2004).
- 171 A. C. Mayer, Ricardo Ruiz, H. Zhou, R. L. Headrick, A. Kazimirov, and G. G.
Malliaras, "Growth Dynamics of Pentacene Thin Films: Real-Time
Synchrotron X-Ray Scattering Study," Phys. Rev. B **73**, 205307 (2006).
- 172 T. Brintlinger, Y.-F. Chen, T. Dürkop, E. Cobas, and M. S. Fuhrer, "Rapid
Imaging of Nanotubes on Insulating Substrates," Appl. Phys. Lett. **81**, 2425
(2002).
- 173 K. Bradley, J.-C. P. Gabriel, and G. Gruner, "Flexible Nanotube Electronics,"
Nano Lett. **3**, 135 (2002).
- 174 E. S. Snow, J. P. Novak, P. M. Campbell, and D. Park, "Random Networks of
Carbon Nanotubes as an Electronic Material," Appl. Phys. Lett. **82** (13), 2145
(2003).
- 175 M. S. Fuhrer, B. M. Kim, T. Dürkop, and T. Brintlinger, "High-Mobility
Nanotube Transistor Memory," Nano Lett. **2**, 755 (2002).
- 176 M. Radosavljevic, M. Freitag, K. V. Thadani, and A. T. Johnson, "Nonvolatile
Molecular Memory Elements Based on Ambipolar Nanotube Field Effect
Transistors," Nano Lett. **2**, 761 (2002).
- 177 V. K. Sangwan, D. R. Hines, V. W. Ballarotto, G. Esen, M. S. Fuhrer, and E.
D. Williams, "Patterned Carbon Nanotube Thin-Film Transistors with
Transfer-Print Assembly " Mater. Res. Soc. Symp. Proc. **963**, 0963-Q0910-
0957 (2007).
- 178 K. S. Novoselov, "Electric Field Effect in Atomically Thin Carbon Films,"
Science **306**, 666-669 (2004).
- 179 K. S. E. A. Novoselov, "Two-Dimensional Gas of Massless Dirac Fermions in
Graphene," Nature **438**, 197-200 (2005).
- 180 Y. Zhang, J. W. Tan, H. L. Stormer, and P. Kim, "Experimental Observation
of the Quantum Hall Effect and Berry's Phase in Graphene," Nature **438**, 201-
204 (2005).
- 181 I. R. Peterson, "Towards a Theory of Adhesion with Predictive Power," Surfa.
Coati. Int., Part B: Coating Transactions **88**, 1-8 (2005).
- 182 A. J. Kinloch, *Polymer Surfaces and Interfaces*. (John Wiley and Sons,
Chichester, 1987), pp.75-97.
- 183 B. Janocha, University of Tübingen, 1998.
- 184 L. J. Norton, V. Smigolova, M. U. Pralle, A. Hubenko, K. H. Dai, and E. J.
Kramer, "Effect of End-Anchored Chains on the Adhesion at a Thermoset-
Thermoplastic Interface," Macromolecules **28**, 1999-1208 (1995).

- ¹⁸⁵ T. Baldacchini, C. N. Lafratta, R. A. Farrer, M. C. Teich, B. E. A. Saleh, M. J. Naughton, and J. T. Fourkas, "Acrylic-Based Resin with Favorable Properties for Three-Dimensional Two-Photon Polymerization," *J. Appl. Phys.* **95**, 6072-6076 (2004).